INFORMATION TO USERS

This manuscript has been reproduced from the microfilm master. UMI films the text directly from the original or copy submitted. Thus, some thesis and dissertation copies are in typewriter face, while others may be from any type of computer printer.

The quality of this reproduction is dependent upon the quality of the copy submitted. Broken or indistinct print, colored or poor quality illustrations and photographs, print bleedthrough, substandard margins, and improper alignment can adversely affect reproduction.

In the unlikely event that the author did not send UMI a complete manuscript and there are missing pages, these will be noted. Also, if unauthorized copyright material had to be removed, a note will indicate the deletion.

Oversize materials (e.g., maps, drawings, charts) are reproduced by sectioning the original, beginning at the upper left-hand corner and continuing from left to right in equal sections with small overlaps.

ProQuest Information and Learning
300 North Zeeb Road, Ann Arbor, MI 48106-1346 USA
800-521-0600

APPLICATION OF MOLECULAR-SCALE SPECTROSCOPIC STUDIES TO PROBE OXYANION REACTIVITY IN SOILS.

by

Derek Peak

A dissertation submitted to the Faculty of the University of Delaware in partial fulfillment of the requirements for the degree of Doctor of Philosophy in Plant and Soil Sciences

Summer 2002

ProQuest Information and Learning Company
300 North Zeeb Road
P.O. Box 1346
Ann Arbor, MI 48106-1346

APPLICATION OF MOLECULAR SCALE

SPECTROSCOPIC STUDIES TO PROBE OXYANION REACTIVITY IN SOILS.

by

Derek Peak

Approved: Donald L. Sparks

Donald L. Sparks, Ph.D.
Chair of the Department of Plant and Soil Sciences

Approved: Robin W. Morgan

Robin Morgan, Ph.D.
Dean of the College of Agriculture and Natural Resources

Approved:

Conrado M. Gempesaw II, Ph.D.
Vice Provost for Academic Programs and Planning

I certify that I have read this dissertation and that in my opinion it meets the academic and professional standard required by the University as a dissertation for the degree of Doctor of Philosophy.

Signed: _____

Donald L. Sparks, Ph.D.
Professor in charge of dissertation

I certify that I have read this dissertation and that in my opinion it meets the academic and professional standard required by the University as a dissertation for the degree of Doctor of Philosophy.

Signed: _____

Steve Dentel, Ph.D.
Member of dissertation committee

I certify that I have read this dissertation and that in my opinion it meets the academic and professional standard required by the University as a dissertation for the degree of Doctor of Philosophy.

Signed: _____

George W. Luther III, Ph.D.
Member of dissertation committee

I certify that I have read this dissertation and that in my opinion it meets the academic and professional standard required by the University as a dissertation for the degree of Doctor of Philosophy.

Signed: _____

J.T. Sims, Ph.D.
Member of dissertation committee

ACKNOWLEDGMENTS

I remember in 1997 when I was moving to Newark for graduate school that the comments from family and friends were consistently stated as "Why Delaware?" After completing my dissertation almost exactly five years later, I find myself recommending the program to other prospective doctoral students not because of the location or the campus, but because of the people that I have gotten the opportunity to work with. First and foremost, I owe a great debt to my advisor Dr. Sparks. He has constantly provided the freedom that I needed to mature as a scientist, always been willing to take chances on new equipment and ideas, and offered access to world class research facilities. Although Dr. Sparks was instrumental in the theme and hypotheses of the projects that I completed during my degree, he always sent me in person to meetings to present the research findings and encouraged me to write publications for peer-reviewed journals and to seek out competitive fellowships to fund my education. I feel that I am well prepared for a scientific career now, and that I owe to Dr. Sparks. I also learned quite a bit from Dr. Sparks that was not purely scientific: his professional ethics and integrity are a model that I hope I can live up to in my career.

I also owe a debt of gratitude to the soil chemistry research group. In particular, I recall many enlightening and lively conversations in the trailer (RIP) with post docs (Robert and Andreas), other graduate students (Eef, Chris, Yuji, Erin, Dan, and Kirk) and with visiting scientists (Lynn and Noriko) that were of great value to a

new graduate student. After the untimely demise of the trailer and our relocation to our new offices, many faces changed but the group remained a fine source of support and critiques of papers and theories. Thanks to Maarten, Stefan, and Markus for taking the time to talk science (or nonsense) from time to time.

I would also like to thank the beamline scientists and support staff at all the beam lines I have worked at while at Delaware. I know that a few of them have gotten late night calls and had to deal with some rather difficult experimental setups, and they have always made the protracted stays at synchrotrons as painless as possible.

While Dr. Sparks and the soil chemistry group provided a truly exceptional environment for conducting research, this dissertation also couldn't have been completed without the support of my wife Jennifer at home. She has taken jobs that she couldn't stand so that I could afford to finish my degree, dealt with my incredibly odd work schedules, put up with my frantic scrambling to meet deadlines for meetings and NSLS trips, rescheduled countless appointments because I was out of town at Brookhaven or at meetings, and been inconvenienced in many other ways. Completing a doctoral degree places a strain upon a marriage, but we made it through with flying colors. That is a good thing because I truly would be lost without her.

TABLE OF CONTENTS

LIST OF TABLES

LIST OF FIGURES

ABSTRACT

Oxyanions such as sulfate, selenate, boric acid, and phosphate are important to soil chemists for both environmental and agronomic reasons. Therefore, a clear understanding of the reactions that these oxyanions undergo with mineral phases is crucial to predicting their availability, toxicity, and mobility in natural systems. A variety of molecular scale techniques, such as Attenuated Total Reflectance Fourier Transform Infrared (ATR-FTIR), Extended X-ray Absorption Fine Structure (EXAFS), and X-ray Absorption Near Edge Structure (XANES) spectroscopy were employed to probe the bonding mechanisms of oxyanions on common soil components and in natural systems. The experimental systems chosen for study were: sulfate and selenate adsorption mechanisms on goethite, hematite, and amorphous iron hydroxide; boric acid adsorption on amorphous iron hydroxide; effects of sulfate on lead adsorption and desorption on goethite; and effects of alum addition on phosphate speciation in poultry litter. It was found that sulfate, selenate, and boric acid all form a mixture of outer-sphere and inner-sphere surface complexes on iron oxides, with solution pH, ionic strength, and the iron oxide chosen affecting the amount of inner-sphere vs. outer-sphere complexation.

The above studies were all conducted with model components and a single oxyanion in suspensions with sodium chloride as an electrolyte. In natural systems, many other ions such as metals, other oxyanions, organic ligands are present that may interact with oxyanions at the mineral/water interface. The effects that sulfate has on lead adsorption and desorption on goethite was studied to better understand how

oxyanion chemistry may affect metal reactivity in natural systems. The overall findings were that ternary complex formation between lead and sulfate can significantly change the amount, rate, and stability of lead adsorption onto an iron oxide surface. It is also possible to utilize molecular-scale approaches to directly speciate oxyanions in soils. One such example is the study of how speciation of phosphate is affected by the addition of aluminum sulfate (alum) using XANES spectroscopy. It was learned that alum addition resulted in precipitation of aluminum hydroxides followed by adsorption of phosphates to these phases.

INTRODUCTION

An oxyanion (or alternatively oxoanion) can be defined as a negatively charged (anionic) inorganic molecule with a positive metal center surrounded by multiple oxygen atoms. The tendency of a metal or metalloid to form an oxyanion rather than a hydrated cation is favored by a high oxidation state and a high pH (Shriver et al. 1994).

Many different oxyanions are found in the soil environment, and the chemistry of these oxyanions is quite varied. Some oxyanions such as phosphate and sulfate are essential nutrients for plant growth and are found in relatively high concentrations in soils. Other oxyanions, including borate and molybdate, are micronutrients. They are essential for plant growth at low concentrations but become toxic at higher concentrations. The range between deficiency symptoms and toxicity is usually quite narrow. A third group of oxyanions, such as arsenate, arsenite, selenate, selenite, and chromate are frequently studied because they have little agronomic use and are instead detrimental to human health.

Much of the foundation for understanding reactions that occur at the soil mineral/water interface comes from the pioneering work of Dr. Werner Stumm. While concepts of

soil chemistry certainly had been studied long before Stumm's work in aquatic environmental chemistry, he provided the foundation of the concepts of surface complexation and much of the vocabulary that is used by soil chemists to discuss soil chemical reactions today. It is not too surprising that a strong connection exists between aquatic chemistry and soil chemistry; almost all of the chemistry of ions in soils occurs either in the soil solution or at the interface between solid phases and the solution. This fact makes the surface properties of soil components more representative of their reactivity than are their bulk mineralogical properties.

The chemistry of oxyanions in soils can be divided into three principal components: polymerization, sorption, and release. Polymerization reactions produce soluble multinuclear complexes of the reactant. Chemical properties such as solubility, protonation, redox activity, and adsorption behavior can all be changed considerably by polymerization of the reactant. Polymers sometimes form in bulk solution, and polymerization can also be catalyzed at the surface of solid phases. Sorption is a general term that can be defined as the accumulation of a material at an interface. Sorption can also be thought of as the removal of a material from the soil solution. Sorption encompasses both adsorption and precipitation processes. Release is another general term that refers to the depletion of a material from an interface. This release from the sorbent is accompanied by an increase of that material in solution. Release includes desorption of adsorbed materials and dissolution of solid phases such as

minerals and precipitates (Sparks 1995). Both sorption and release are usually somewhat reversible, and the soil environment is best thought of as being in a dynamic equilibrium that is affected by solution conditions and reaction time.

Adsorption reactions of oxyanions at the mineral/water interface occur via either electrostatic interaction (outer-sphere complexation) or chemical interaction (inner-sphere complexation). Initially, researchers tended to label reactions as occurring by either one mechanism or the other, but more recently it has been shown (Perrson et al. 1998, Peak et al. 1999) that both mechanisms can be operational simultaneously and that a continuum of adsorption processes exists. In addition, many ions exist as more than one species depending on pH. It is possible that speciation at the surface is quite different from speciation in the bulk solution. Determining the species involved in adsorption and the type of adsorption complex that is forming is crucial to understanding the behavior of a species in the soil environment.

Precipitation reactions involve the depletion of ions from solution via the formation of a solid phase. Precipitation can occur in solution as the result of oversaturation, or the presence of compounds at higher levels than the solubility of their products. Precipitates can also form on the surface of sorbents as either a pure secondary phase, or they can incorporate ions from the sorbent to form secondary precipitates (Sparks 1995). Precipitation of trace metals with oxyanions is important in controlling the fate

and mobility of contaminants, as metal-oxyanion precipitates usually are very insoluble and form readily in soils.

As mentioned earlier, most soil chemical reactions are at least partially reversible and are affected by solution equilibrium. If the concentration of an adsorbed ion is depleted in solution by transport processes or plant or microbial uptake then desorption of the adsorbed ion can occur to maintain equilibrium with solution. Dissolution of precipitate phases and minerals can also replace ions lost from solution. It is important to visualize all of these processes as occurring simultaneously and forming a continuum of adsorption processes. For example, adsorption and precipitation can occur on the same time scales (Sheiddeger et al. 1998), and competition between adsorption and precipitation has been seen in the case of mixed metal precipitate formation (Elzinga 2000) on some clay minerals.

Understanding the nature of sorption in soils can be quite difficult. The macroscopic adsorption data may look quite similar even when very different sorption mechanisms are present (Ford). To assess different adsorption mechanisms and determine their importance in soils, it is necessary to use *in situ* spectroscopy. With spectroscopic techniques that are available today, it is possible to distinguish between outer-sphere and inner-sphere adsorption mechanisms as well as differentiating between adsorption

and precipitation. In many cases it is possible to estimate the distribution of complexes when multiple mechanisms are occurring simultaneously.

Objectives of Dissertation Research

The goal of this research my dissertation research was to gain a fundamental understanding of the reactions that oxyanions undergo in soils. The overall strategy for this research was to combine macroscopic adsorption experiments with *in situ* spectroscopic techniques to gain molecular-scale insight into sorption mechanisms. Emphasis was placed on experimental systems where there is disagreement in the soil chemistry literature about the sorption mechanisms for an oxyanion. Specifically, this project studied sulfate and selenate adsorption mechanisms on iron oxides and hydroxides, boric acid sorption mechanisms on amorphous iron hydroxide, and ternary lead-sulfate-goethite adsorption reactions. While these projects may all seem quite different, they all serve to illustrate a greater point about oxyanion sorption mechanisms in soils. It is my hypothesis that oxyanions often sorb on mineral surfaces via several co-occurring mechanisms, and depending on reaction conditions one mechanism will be dominant. Therefore, my general approach is to examine samples at a wide range of pH, reactant concentration, and ionic strength to obtain a clear picture of how reaction conditions affect the continuum of sorption processes in the soil environment. One may also notice that the complexity of the systems to be studied increases throughout the work, and that several different spectroscopic

techniques were employed to probe different reactions. The goal of my laboratory research was to gain a fundamental insight into oxyanion reactivity with relatively simple model systems (sulfate and selenate) and then to see how adding complications such as more than one chemical species (boric acid and borate) or co-occurring ions (lead and sulfate) would affect both the reactivity of oxyanions and the ability to probe their reactivity at the molecular scale. The final goal of all laboratory studies should be to gain knowledge that is applicable to the natural world and to push the envelope of what is possible with current spectroscopic tools. To this end, my final project uses spectroscopy to perform direct speciation of phosphate in poultry litter and to determine how addition of aluminum sulfate affects phosphate speciation.

Chapter 1

SULFATE ADSORPTION MECHANISMS ON IRON (III) OXIDES AND HYDROXIDES: RESULTS FROM ATR-FTIR SPECTROSCOPY

Sulfate ($SO_4^{2-}{}_{aq}$) is a weakly basic Group VI oxyanion with a metal center that has a charge of +6. In aqueous solution it exists as either as the fully-deprotonated form, or as the singly-protonated bisulfate ($HSO_4^-{}_{aq}$) ion (Stumm and Morgan 1991). The pK_a for the protonation reaction is ~1.9, making the fully-deprotonated form the dominant ion under normal soil conditions. Sulfate ions have a hydrated radius of about 4 Å. At present time, the chemistry of sulfate in the soil environment is still poorly understood. In fact, the mechanisms of sulfate sorption have often been the subject of debate, both historically and in the current scientific literature. Sulfate is of interest to soil chemists for both environmental and agronomic reasons. It is an essential micronutrient for plant growth. Neither deficiency nor toxicity symptoms are commonly seen in cultivated soils, but sulfate can occur in extremely high levels near sites of mine waste deposition as a result of hydrogen sulfide oxidation (Persson and Lövgren 1996). Sulfate is a product in the geochemical cycling of pyrite and therefore plays an important role in marine sediment chemistry.

Macroscopic studies of sulfate sorption have suggested that sulfate adsorbs via an outer-sphere (electrostatic) adsorption mechanism on both soils and reference minerals

(Charlet et al. 1993). This conclusion is supported primarily by two observations: (i) ionic strength has a large effect on the amount of sulfate that is adsorbed, with increasing adsorption as ionic strength decreases, and (ii) no adsorption of sulfate is usually seen above the point of zero charge of the mineral. This fact potentially makes iron and aluminum oxides important sites for sulfate adsorption in soils, since these components have high points of zero charge and are commonly found in soils.

He and colleagues (1996) studied the stoichiometry of hydroxyl-sulfate exchange on gamma aluminum oxide and kaolinite using a back-titration technique. Combining a thermodynamic approach with their data, they suggested that the observed hydroxyl release upon sulfate adsorption need not be associated with a ligand-exchange mechanism. Instead, they suggested a mechanism consisting initially of surface site protonation and generation of a hydroxyl in solution via a reaction such as $Al–OH^0 + H_2O \rightarrow Al–OH_2^+ + OH^-$. They proposed that this protonation was then followed by the formation of an outer-sphere surface complex: $Al–OH_2^+SO_4^{2-}$. This mechanism accounts for the observed proton consumption to maintain pH (neutralizing the hydroxyl generated) without requiring an inner-sphere surface complex.

It has also been shown that the rate of gibbsite dissolution in the presence of sulfate is more rapid than in the presence of chloride (Ridley et al. 1997). While an enhancement of dissolution in the presence of ligands is often attributed to inner-

sphere surface complex formation, the explanation for this observed effect was the formation of aluminum-sulfate complexes in solution that enhance mineral solubility. These aluminum-sulfate complexes result in more aluminum being released from the surface because they keep the free aluminum concentration in solution much lower than when only chloride is present.

Sposito (1984) suggested that sulfate adsorption might be of an intermediate nature, sometimes sorbing as an outer-sphere complex and sometimes as an inner-sphere complex via a ligand exchange mechanism. This concept was supported by the observations of Yates and Healy (1975) who investigated sulfate adsorption on both α-FeOOH and α-Cr_2O_3. Although the rates of hydroxyl exchange for the two sorbents are markedly different, the rate and extent of sulfate adsorption was very similar implying an outer-sphere complexation mechanism. However, sulfate adsorption also shifts the point of zero charge to higher values on both α-FeOOH and α-Cr_2O_3, which is consistent with inner-sphere complexation.

Many research groups have modeled sulfate adsorption on both soils and pure mineral components, with differing results. He and co-workers (1997) utilized the triple layer model with outer-sphere surface complex formation to describe sulfate adsorption on γ-alumina and kaolinite. Charlet and co-workers (1993) modeled the adsorption of sulfate on an aluminum-coated TiO_2, δ-Al_2O_3, and an acidic forest soil. They found

that outer-sphere complexation described the data well. Sulfate adsorption on goethite has been modeled using several different approaches. Zhang and Sparks (1990a) modeled sulfate adsorption on goethite using the triple-layer model and an outer-sphere surface complex. Davis and Leckie (1980) employed a modified triple-layer model to represent sulfate adsorption on goethite. They determined that a mixture of outer-sphere and inner-sphere sulfate surface complexes best described their data. The charge-distribution multi-site complexation approach (CD-Music) has been used by several researchers to model sulfate adsorption on goethite. Geelhoed and colleagues (1997) described sulfate complexation using an inner-sphere bidentate binuclear surface complex, while Rietra and co-workers (1999) used an inner-sphere monodentate surface complex. Persson and Lovgren (1996) utilized an extended double-layer model to describe their experimental data and concluded that an outer-sphere surface complex was most likely. Ali and Dzombak (1996) modeled adsorption of sulfate on goethite in both the absence and presence of simple organic acids using a generalized two-layer model. Three different inner-sphere surface complexes of sulfate were required to describe the experimental data.

There are a few possible reasons that modelers have not completely agreed about the nature of sulfate–goethite complexation mechanisms. First of all, different synthesis methods and pretreatment techniques can result in goethite with quite different surface properties. If the morphology and crystallinity of the sorbent varies then the surface

chemistry can sometimes also be different. For example, Sujimoto and Wang (1997) found that hematite morphology had a significant effect on the mechanism of sulfate sorption. Another possible source of error is the fact that the design of some surface complexation models excludes some potential surface complexes. This could result in an incorrect assignment of sulfate surface-complexation mechanisms. For example, the original triple-layer model only considered outer-sphere complex formation and the CD-MUSIC model as currently implemented only describes inner-sphere complex formation. A third possibility is that none of the surface complexation models used are robust enough to converge only on one unique solution when several surface complexes are occurring simultaneously. Definitive mechanistic information from spectroscopy can constrain models to physically relevant complexes and can therefore improve model refinement.

Although somewhat contradictory to the macroscopic laboratory studies, there is microscopic and spectroscopic evidence of sulfate inner-sphere surface complexation. Transmission infrared spectroscopic studies of sulfate adsorption on goethite and hematite (Parfitt and Smart 1978; Turner and Kramer 1991) revealed the formation of sulfate bidentate binuclear surface complexes on both solids. XPS studies (Martin and Smart 1987) also validated this sorption mechanism. More recently, Persson and Lövgren (13) concluded that outer-sphere adsorption of sulfate on goethite was occurring based on results from diffuse reflectance infrared (DRIFT) spectroscopy.

However, these spectroscopic experiments all involved potential sample alteration via either drying, the application of heat and pressure, or dilution in a salt which could have modified the structure of the original sorption complex.

Due to the potential artifacts in *ex situ* spectroscopy, it is greatly preferable to conduct *in situ* experimentation to elucidate interactions that occur in aqueous suspensions. *In situ* experiments using Scanning Tunneling Microscopy (STM) (Eggleston et al. 1998) and ATR-FTIR spectroscopy (Eggleston et al. 1998, Hug 1997) to determine the adsorption mechanism of sulfate on hematite have more recently shown that inner-sphere monodentate surface complexes form at the hematite surface under aqueous conditions. Degenhardt and McQuillan (1999) found that sulfate forms primarily outer-sphere surface complexes on chromium (III) oxide hydroxide, with some splitting of infrared bands being observed and attributed to electrostatic forces. Peak et al. (1999) utilized ATR-FTIR to better understand the adsorption of sulfate on goethite. We determined that sulfate forms only outer-sphere surface complexes above pH 6.0, and that it forms a mixture of outer- and inner-sphere surface complexes at pH less than 6.0. This is quite significant, as it demonstrates a continuum between different adsorption mechanisms that can potentially explain the discrepancies in earlier macroscopic and surface complexation modeling research.

Hodges and Johnson (1987) used a miscible displacement technique to follow the kinetics of sulfate adsorption/desorption on goethite. They found that the reaction kinetics could best be described using diffusion-limited kinetics models. This is not surprising considering the nature of the miscible displacement technique. A miscible displacement setup is a continuous flow system where a small amount of sorbent is injected into a thin disk (usually a filter holder with filter paper). A dilute solution of the sorbate in a constant ionic strength background is flowed through this disk until equilibrium is reached. At this point the solution is changed to pure background electrolyte and the desorption reaction is monitored. The main problems with this experiment are that there is little mixing inside the thin disk and it is difficult to ensure that the sorbent is distributed evenly inside the thin disk without preferential flow pathways. Both these drawbacks tend to make diffusional forces extremely important in modeling the experimental results. Hodges and Johnson (1987) were unable to clearly determine whether sulfate adsorption was due to ligand exchange or electrostatic attraction in these studies. Pressure-jump chemical relaxation studies investigating sulfate adsorption on goethite (Zhang and Sparks 1990) suggested an outer-sphere complexation mechanism. This seems somewhat at odds with the recent observation that sulfate forms both outer-sphere and inner sphere complexes on goethite at pH below 6. However, pressure-jump studies cannot conclusively determine the mechanism by which a reaction proceeds. Instead they determine the number of reaction steps and the rate constants for those individual steps. This

information must then be coupled with an equilibrium model and/or spectroscopic studies to accurately assess the identity of these individual reaction products. Furthermore, if reactions are occurring simultaneously rather than sequentially, then a pressure-jump experiment may not distinguish them effectively if the time scales of the reactions are similar.

Infrared Theory. The relationship between the symmetry of sulfate complexes and their infrared spectra is well established (Nakamoto 1986), and it is possible to assign molecular symmetry based on the number and position of peaks that appear in the mid-infrared region. The relationship between the symmetry of surface complexes and the resulting infrared spectrum is summarized in Figure 1. With the Attenuated Total Reflectance (ATR) technique under aqueous conditions, there are two infrared sulfate vibrations that are accessible to spectroscopic investigation. They are the non-degenerate symmetric stretching ν_1, and the triply degenerate asymmetric stretching ν_3 bands (Perrson and Lövgren 1996). As a free anion in solution, sulfate has tetrahedral symmetry and belongs to the point group T_d. For this symmetry, only one broad peak at approximately 1100 cm^{-1} due to the triply degenerate ν_3 band is usually observed. In some cases the ν_1 band is also weakly active and appears at around 975 cm^{-1}. Since outer-sphere complexes retain their waters of hydration and form no chemical bonds, it is expected that the symmetry of outer-sphere sulfate complexes is similar to aqueous sulfate. However, distortion due to electrostatic effects could shift the ν_3 to higher

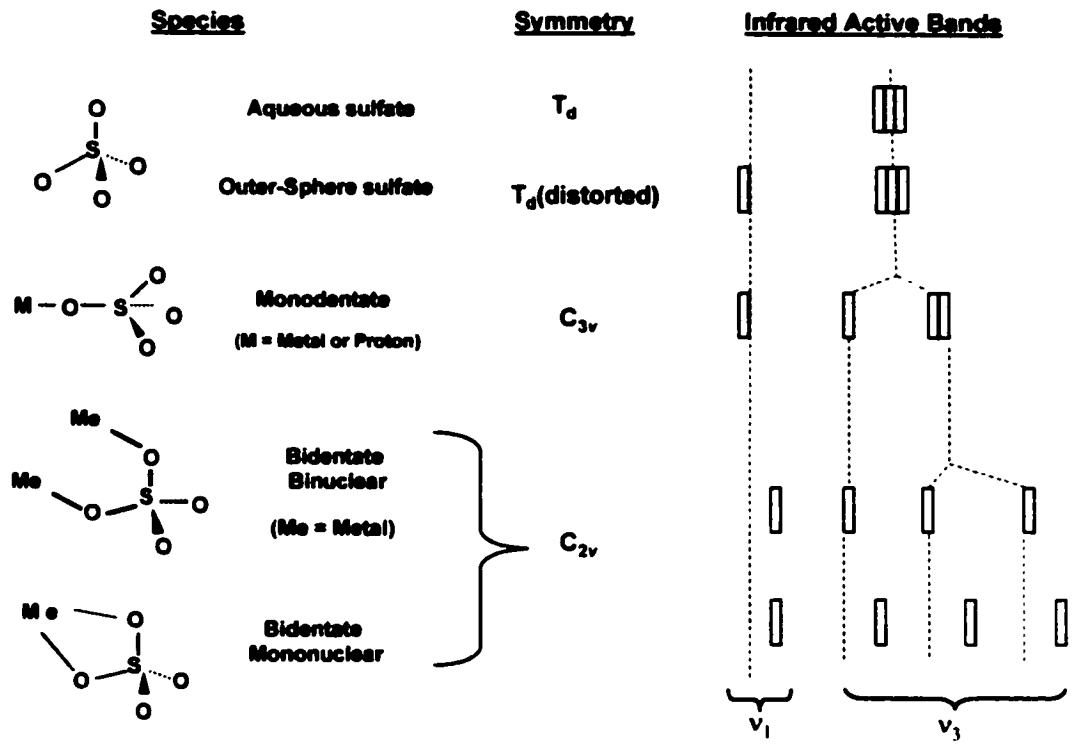

Figure 1.1 The relationship between the molecular symmetry of sulfate complexes and the observed infrared spectrum they produce. Adapted from Hug (1997).

wavenumber and cause the ν_1 band to become IR active. If sulfate is present as an inner-sphere complex, the symmetry is lowered. As a result, the ν_1 band becomes infrared active and the ν_3 band splits into more than one peak. In the case of a monodentate inner-sphere surface complex, such as observed for sulfate adsorption on hematite, C_{3v} symmetry results. The ν_3 band splits into two peaks, one at higher wavenumber and one at lower wavenumber, while the ν_1 band becomes fully active at about 975 cm^{-1} (Hug 1997, Nakamoto 1986). If sulfate forms a bidentate binuclear (bridging) surface complex, the symmetry is further lowered to C_{2v}, and the ν_3 band splits into three bands between 1050 and 1250 cm^{-1}, while the ν_1 band is shifted to around 1000 cm^{-1} (Nakamoto 1986). Figure 2 contains a table (adapted from Hug 1997) that details the positions of ν_1 and ν_3 sulfate bands reported in the literature for different molecular configurations.

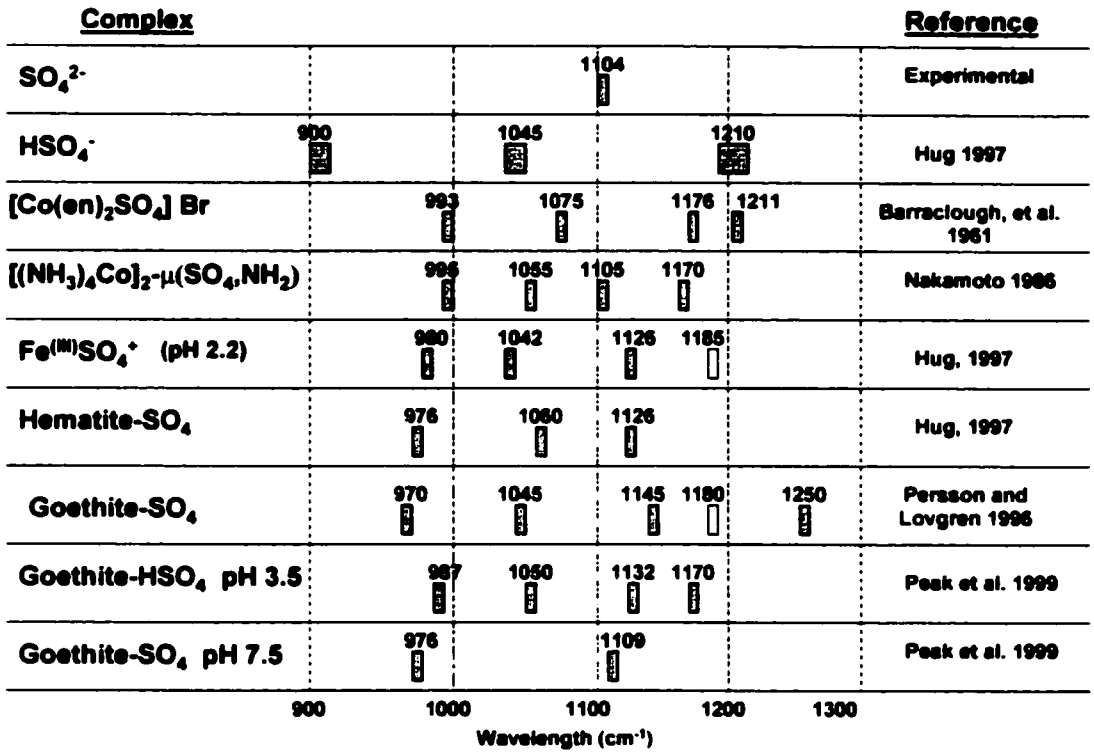

Figure 1.2 Table of infrared peak positions for relevant sulfate reference compounds in the literature. Adapted from Hug (1997)

OBJECTIVES

The purpose of this research was to investigate the mechanism of sulfate adsorption on goethite, hematite, and ferrihydrite as a function of pH. Additionally, the effects of surface loading and ionic strength on sulfate adsorption on goethite were studied. Understanding how adsorption mechanisms are affected by reaction conditions is of considerable interest to developers of surface complexation models as well as soil scientists, but there are few studies that use in situ spectroscopy to studies soil chemical reactions over a wide range of conditions.

MATERIALS AND METHODS

Mineral Synthesis. The goethite used in this study was synthesized using the method of Schwertmann et al. (1985). Initially, ferrihydrite was precipitated by adding 50 mL of 1 M ferric nitrate solution to 450 mL of 1 M KOH. This suspension of amorphous hydrous ferric oxide was then aged for 14 days at 25° C. The suspension was next washed via centrifugation, replacing the supernatant with doubly deionized water to remove residual KOH. The rinsed solid was then resuspended in 0.4 M HCl and shaken for two hours using a mechanical shaker. This treatment was used to remove any remaining ferrihydrite from the surface of the goethite. The acidified goethite suspension was again washed via centrifugation to remove both HCl and dissolved

iron. Finally, the goethite was dialyzed, frozen with liquid nitrogen, and freeze-dried. The solid was confirmed as goethite via infrared spectroscopy using both ATR and transmission mode KBr pellets. The external surface area determined from N_2 BET was 63.5 m^2g^{-1} and the point of zero salt effect was 8.4, as determined via potentiometric titration in 0.1, 0.01, and 0.005 M sodium perchlorate. The hematite used in these experiments was synthesized from ferric perchlorate using the method of Schwertmann and Cornell (1991). It was also acid-washed and dialyzed prior to freeze-drying, and had an N_2-BET surface area of 14 m^2g^{-1}. Ferrihydrite (6 line) was synthesized by titrating 1 M ferric chloride to pH 7.5 with 1 M KOH. This precipitate was washed 3 times with 0.1 M NaCl to remove any residual iron, washed once with deionized water, and then dialyzed for 3 days in deionized water.

Attenuated Total Reflectance (ATR-FTIR) Spectroscopy

Attenuated Total Reflectance Fourier Transform Infrared (ATR-FTIR) spectroscopy is ideally suited to probe sulfate adsorption mechanisms on iron oxides since there are no overlapping bands in the mid-infrared region. As described earlier, the relationship between symmetry and infrared spectra is well established for sulfate, so it is possible to identify surface complexes based on the number and position of peaks in the mid-IR range.

All FTIR experiments were conducted using a Perkin-Elmer 1720x spectrometer equipped with a purge gas generator and either a DTGS or MCT detector. A horizontal ATR accessory and flow cell (Spectra-Tech) were used for sampling. A flow-through system has been developed by our group (Peak et al. 1999) that greatly improves the applicability of ATR-FTIR spectroscopy to the study of interfacial chemistry. The sorbent phase was first deposited onto the 45° Zinc Selenide crystal using a modification of the method of Hug (1997). Once dry, the deposited metal oxide was rinsed with 0.01 N NaCl to remove any non-adhering sorbent, allowed to air-dry again, and the crystal was then placed into a flow cell. Once the crystal containing the deposited sorbent is placed into the flow cell, Tygon tubing connects the flow cell to a peristaltic pump that delivers solution at a constant flow rate from a reaction vessel containing water, sulfate, and an inert salt (NaCl) to maintain constant ionic strength. The reaction vessel was nitrogen purged and pH controlled. It is possible to conduct adsorption edges, adsorption isotherms, and kinetics experiments directly within the flow cell using this experimental setup. Figure 1.3 shows a schematic of the flow cell experimental setup.

The greatest advantage of this flow-through type experimental setup is that aqueous sulfate concentrations remain low throughout the experiment. In fact, even in isotherms where aqueous sulfate concentrations reached 500 uM, the absorbance accounts for less than 0.1% of the total infrared absorbance in the flow cell. The

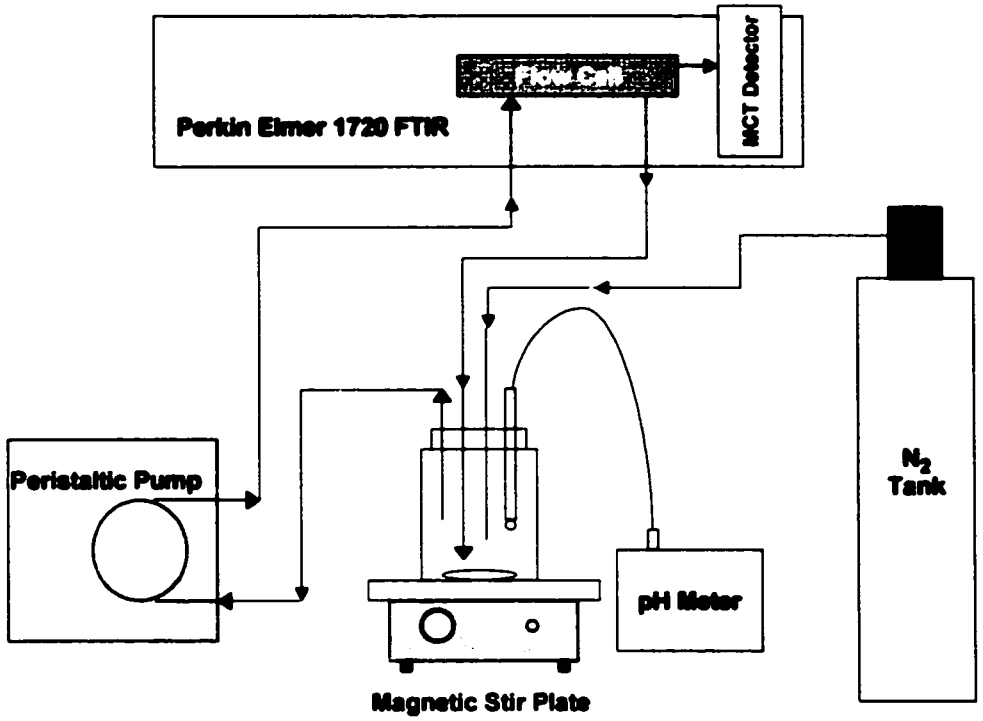

Figure 1.3 Experimental apparatus used for pH envelopes and adsorption isotherms

deposited sorbent concentrates the adsorbed sulfate in the path of the IR beam greatly because a large volume of low concentration reactant flows through it during the experiment. It is therefore possible to avoid many spectral subtractions of supernatants that are common when using pastes to analyze sorption samples with ATR-FTIR spectroscopy. This can be especially useful when outer-sphere complexation is occurring, because an outer-sphere complex may be difficult to separate from the non-adsorbing aqueous reactant. Another advantage is that a better subtraction of the background (sorbent and background electrolyte) is possible, and this leads to better data quality over a wider spectral range.

pH Envelopes. To generate pH envelopes, the outflow tube from the flow cell was connected to the reaction vessel containing background electrolyte solution at a pH where adsorption of the sulfate is very low (pH 9.0). Once a stable background was collected, sulfate was then added, and spectra were collected until there was no increase in the intensity of the spectra with time. This is operationally defined as an equilibrium state. At this point the pH was lowered so more adsorption occurs. Spectra were collected in this manner from pH 9 to pH 3.5.

Adsorption Isotherms. For the adsorption isotherms, the effluent from the flow cell is collected as waste instead of being circulated back to the reaction vessel. This was done to ensure that the equilibrium sulfate concentration (C_{eq}) can be determined.

When the sulfate initially enters the flow cell, it is rapidly adsorbed to the deposited goethite in the flow cell, and the sulfate concentration in the effluent will remain low. As the system approaches equilibrium, however, the effluent concentration rises until it equals the influent concentration. At this time the influent concentration is equal to C_{eq} and the system is at equilibrium.

For these experiments, equilibrium is again defined as the point where no further increase in the infrared spectra of the adsorbed reactant is observed. The amount of reactant needed to adjust the remaining volume to the next concentration can then be calculated using the flow rate of the pump and the time elapsed since the pump was started. The reactant concentration in the reaction vessel is then raised and allowed to reach a new equilibrium with the sorbent in the flow cell. This is repeated to generate spectra of adsorbed reactant as a function of equilibrium reactant concentration. The integrated absorbance of these samples is then plotted vs. C_{eq} as in a traditional isotherm.

Data analysis. Peak Solve for Windows (Galactus Industries) was used to fit a linear baseline to all spectra and also to fit peaks to these corrected spectra. It was determined that Gaussian peaks best described all of the raw sulfate spectra as well as the aqueous reference samples. When inner-sphere sulfate surface complexes were

isolated however (to be discussed in results) then Lorentzian peaks described the data better.

RESULTS

Changes in reaction conditions such as sorbent phase, pH, surface loading, and ionic strength all have a pronounced effect on sulfate adsorption mechanisms on iron oxides. Therefore the effects of changing these reaction parameters will all be discussed separately.

Influence of pH. On goethite (Figure 1.4a), sulfate adsorption mechanisms are highly pH dependent. As the pH is lowered from pH 9 to pH 6, sulfate adsorption increases, but in all cases only one broad peak (ν_3) at approximately 1108 cm^{-1} is present. This peak is consistent with outer-sphere sulfate surface complexes, since outer-sphere sulfate would be expected to retain its T_d symmetry. Also consistent with an outer-sphere complex is the appearance of a ν_1 peak at 975 cm^{-1} at pH 6.0 and the systematic shift of the ν_3 band to higher wavenumbers as pH decreases. This is typical of an electrostatic interaction, because as pH is decreased the surface charge of the surface becomes more positive, and increased distortion of the T_d symmetry is expected. As the pH is decreased below 6.0, splitting of the 1050-1200 cm^{-1} region into multiple peaks occurs, and the peak at 975 cm^{-1} becomes much larger, along with a smaller

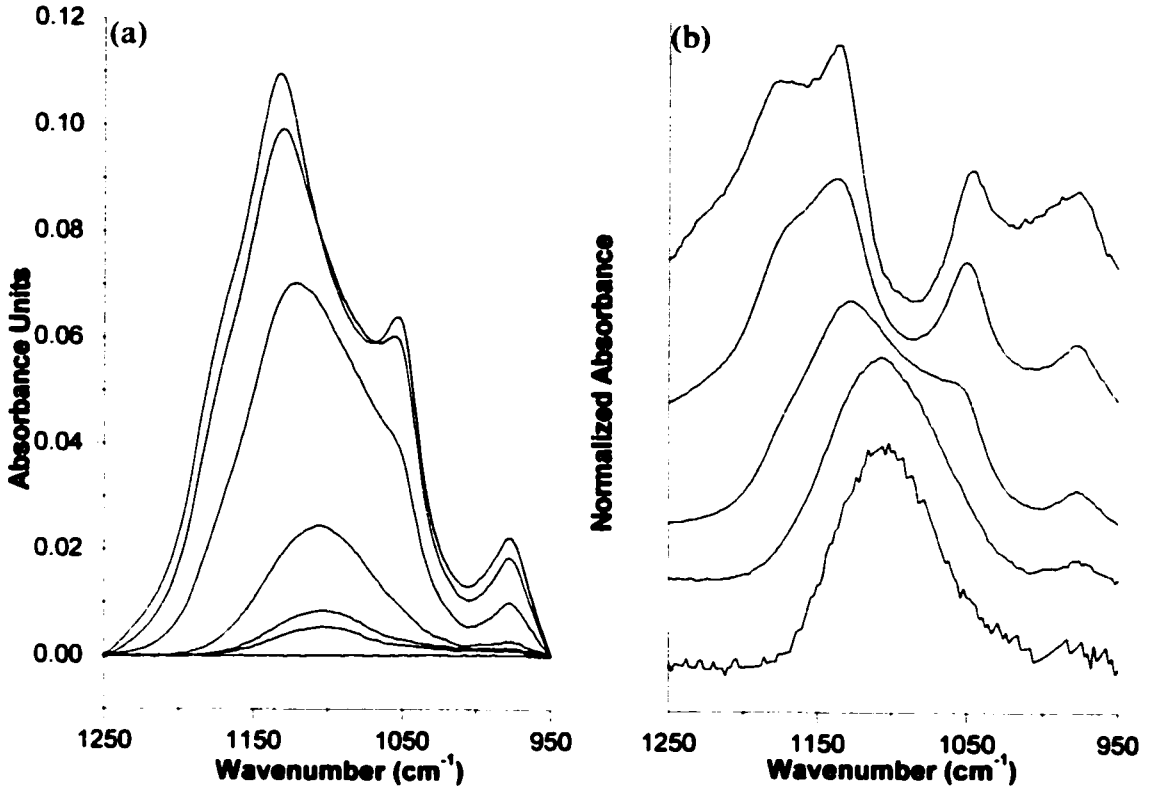

Figure 1.4 (1.4a) Spectra from a pH envelope of sulfate adsorbed on goethite. Reaction conditions were 0.01 N NaCl as background electrolyte, and 20 μM SO_4^{2-} added. The spectra were the result of 128 co-added scans at 4 cm^{-1} resolution. The spectra were collected at pH (from bottom): pH 8, 7, 6, 5, 4, and 3.5 (1.4b) Difference spectra obtained by subtracting pH 8.0, 7.0, 6.0, 5.0, and 4.0 spectra from the pH 7, 6, 5, 4, and 3.5 spectra (respectively) of Figure 1.4a.

peak at approximately 1000 cm^{-1}. This is strong evidence of an inner-sphere surface complex. In fact, peak-fitting revealed that there are two sulfate surface complexes at low pH. The inner-sphere complex of C_1 or possibly C_{2v} symmetry has three ν_3 bands that appear at 1170, 1134, and 1051 cm^{-1} and a ν_1 band occurring at 992 cm^{-1}. The outer-sphere complex also seen at high pH remains in the low pH samples, but the ν_3 band continues to shift to higher wavenumber as pH is lowered. At pH 3.5 this peak occurs at 1118 cm^{-1}, a shift of 14 cm^{-1} from the same 1104 cm^{-1} peak at pH 8.0.

These results suggest that rather than the outer-sphere sulfate converting to an inner-sphere complex at low pH, instead there is additional adsorption of an inner-sphere component. This is clearly demonstrated in Figure 1.4b, where the spectrum from pH 8, 7, 6, 5, and 4 are subtracted from pH 7, 6, 5, 4, and 3.5 respectively. These difference spectra are equal to spectra of the additional sulfate adsorption that occurs as pH is lowered. Using this method it can clearly be seen that above pH 6, all adsorption is due to outer-sphere complexation. However in the pH 5 minus pH 6 spectrum (c) it is clear that the additional adsorption has a large inner-sphere component. And in the pH 4 minus pH 5 spectrum (b) the additional adsorption can be described only with an inner-sphere complex. Interestingly, in the pH 3.5 minus pH 4 spectrum (a) the same inner-sphere peaks are seen as in (b) but with negative absorbance occurring in the 1050-1100 cm^{-1} range. This is due either to desorption of outer-sphere sulfate or to a transformation of some outer-sphere sulfate into an inner-

sphere complex. One other important difference that can be seen in Figure 1.4b involves the ν_3 peak occurring at the highest wavenumber. This peak can weakly be seen in (c) at approximately 1160 cm^{-1}, in (b) at 1170 cm^{-1}, and in (a) at 1175 cm^{-1}. The observation that the position of this peak varies with pH would suggest that the peak is the result of an interaction of an electrostatic nature.

The results of fitting two spectra from the pH envelope of Figure 1.4 are shown in Figure 1.5. Figure 1.5a shows the peak fitting results from the pH 3.5 spectrum of Figure 1.4a, and Figure 1.5b shows the results of fitting the pH 5 minus pH 4 spectrum from Figure 1.4b. To accurately fit the spectrum in Figure 1.5a, Gaussian peaks were needed for all peaks. The dotted lines are peaks that are definitely associated with an inner-sphere complex, and the dashed peak centered at 1108 cm^{-1} is due to outer-sphere sulfate. The dashed peak at 976 cm^{-1} is less conclusively assigned, as both outer-sphere and inner-sphere sulfate have ν_1 absorbance bands in this region. It is interesting to fit the "pH 5 minus pH 4 difference" spectrum because there is no contribution from outer-sphere sulfate needed to describe its features. This means that this is a pure inner-sphere sulfate species. While the peaks at 1170, 1132, 1050, and 976 cm^{-1} remain in the same position, the quality of fit was improved by fitting peaks at 1132, 1050, and 976 cm^{-1} with Lorentzian peaks rather than with Gaussian peaks. The peak at 1170 cm^{-1} was still best described with a Gaussian peak. This suggests that in the case of the 1170 cm^{-1} feature that there is a high degree of disorder, such as

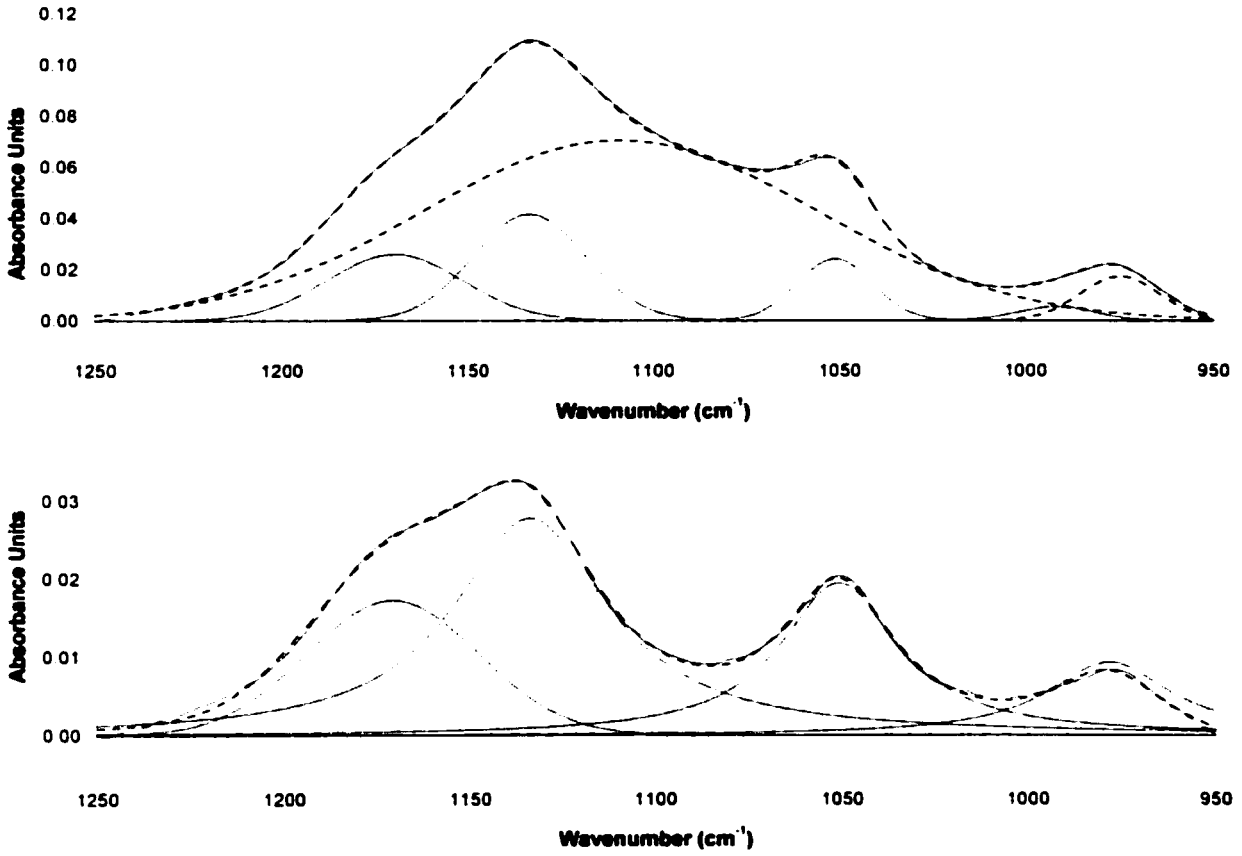

Figure 1.5 (1.5a) Fit of the pH 3.5 spectrum from the pH envelope shown in Figure 1.4a. The dotted lines denote the peaks arising from an inner-sphere complex, and the dashed lines are from the outer-sphere sulfate. (1.5b) Fit of the pH 4 minus pH 5 difference spectrum (b of Figure 1.4b).

an electrostatic bonding environment being responsible for the peak. In the spectrum of Figure 1.5a, the need to describe the inner-sphere complex with Gaussian peaks is likely the result of more than one inner-sphere complex of similar symmetry being present and contributing to the observed peaks. This is supported by the observation that a peak at 992 cm^{-1} in Figure 1.5a is consistent with a ν_1 band resulting from an inner-sphere complex, but it is not present in the difference spectrum of Figure 1.5b. This will be discussed later when the effect of surface loading at low pH is discussed.

To further refine the nature of the inner-sphere sulfate surface complex on goethite, sulfate adsorption on goethite at pH 3.5 was studied in D_2O. Using D_2O rather than H_2O can determine the importance of a proton to the surface complex. The results are shown in Figure 1.6. It can clearly be seen that conducting the experiment in D_2O causes the peaks occurring at 1133 and 1051 cm^{-1} in H_2O (splitting of the ν_3 band due to inner-sphere complexation) to be shifted approximately 8 cm^{-1} to 1125 and 1043 cm^{-1} in D_2O. This shift to lower wavenumbers is characteristic of substitution of a deuterium ion for a proton in a molecular complex. Since these peaks are the result of inner-sphere complexation, it is therefore reasonable to conclude that a proton is present in the inner-sphere surface complex. The only possible surface complexes that involve a proton are bisulfate sorbed as a monodentate complex or monodentate sulfate that is hydrogen bonded to an adjacent surface site. The fact that the shift is rather small suggests that the complex most likely involves an electrostatic interaction

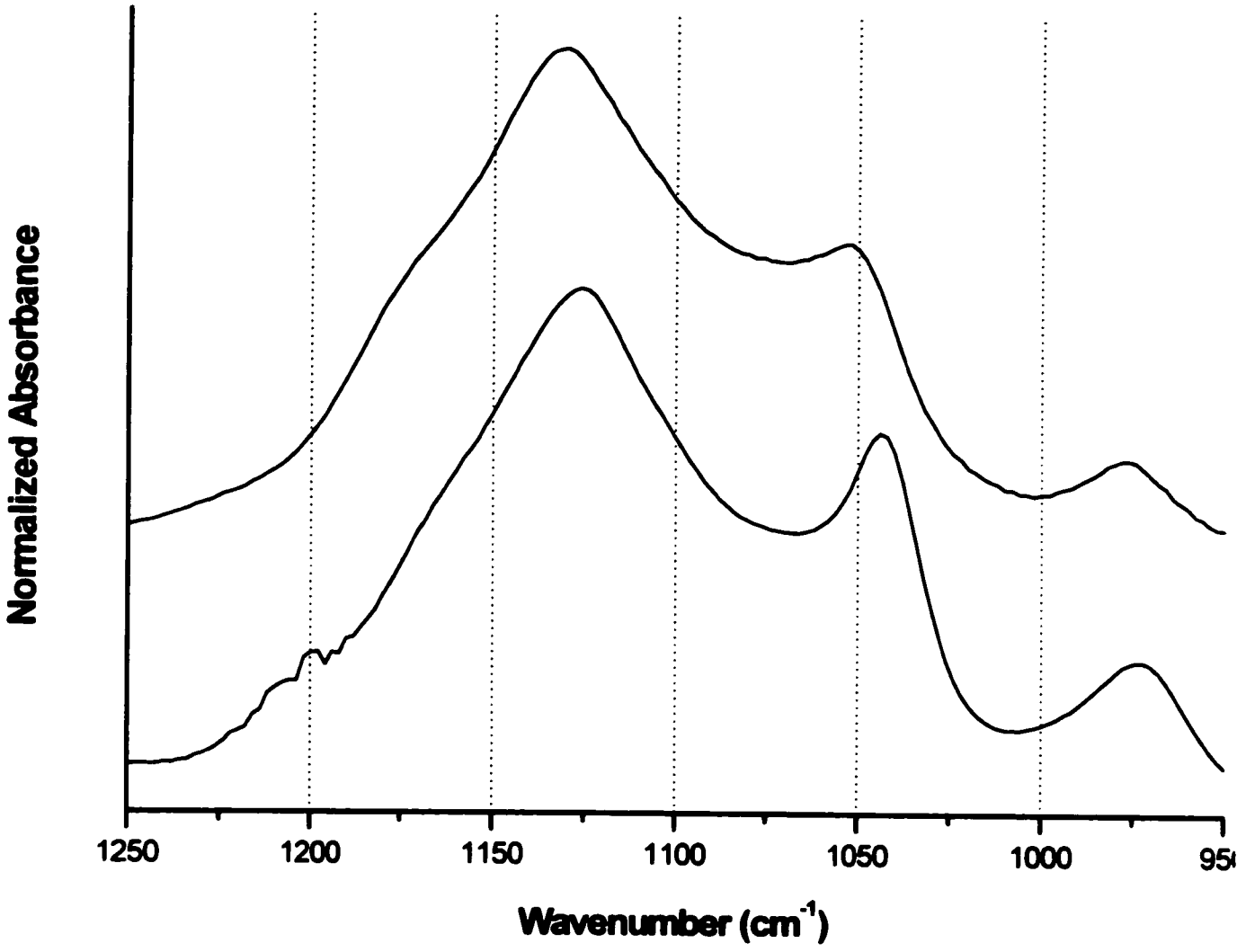

Figure 1.6 Comparison of spectra of adsorbed sulfate collected in **(a)** H_2O and **(b)** D_2O. In both cases the reaction conditions were pH 3.5, I= 0.05, and an initial sulfate concentration of 100 μM.

with a proton. This is because direct covalent bonding between a proton and sulfate (such as bisulfate) results in a large splitting in the spectra compared to complexation with Fe (III) in aqueous solution (Hug 1997). Additionally, the systematic shift of the peak at 1160-1175 cm^{-1} in Figure 1.4b to higher wavenumber as pH is lowered, along with the need to use a Gaussian peak to fit this feature both suggest an electrostatic interaction.

Influence of sorbent. On hematite, sulfate adsorption mechanisms are surprisingly quite different. Figure 1.7a shows spectra from a pH envelope of sulfate adsorption on hematite. Our results are in excellent agreement with those reported by Hug (1997). Strong splitting of the sulfate v_3 band into two peaks at 1126 cm^{-1} and 1060 cm^{-1}, and a clearly visible v_1 peak at 976 cm^{-1} can clearly be seen in all spectra. This C_{3v} symmetry suggests that sulfate forms primarily inner-sphere monodentate surface complexes on hematite over all studied pH values. When difference spectra are produced via the same method discussed for the sulfate/goethite envelope in Figure 1.4b, it can be seen that generally speaking, a monodentate surface complex indeed dominates the entire pH range studied. However, there appears to be some outer-sphere sulfate adsorption that causes the pH 7 minus pH 8 spectrum (e) to have less splitting of the two v_3 peaks than is seen in the lower pH difference spectra.

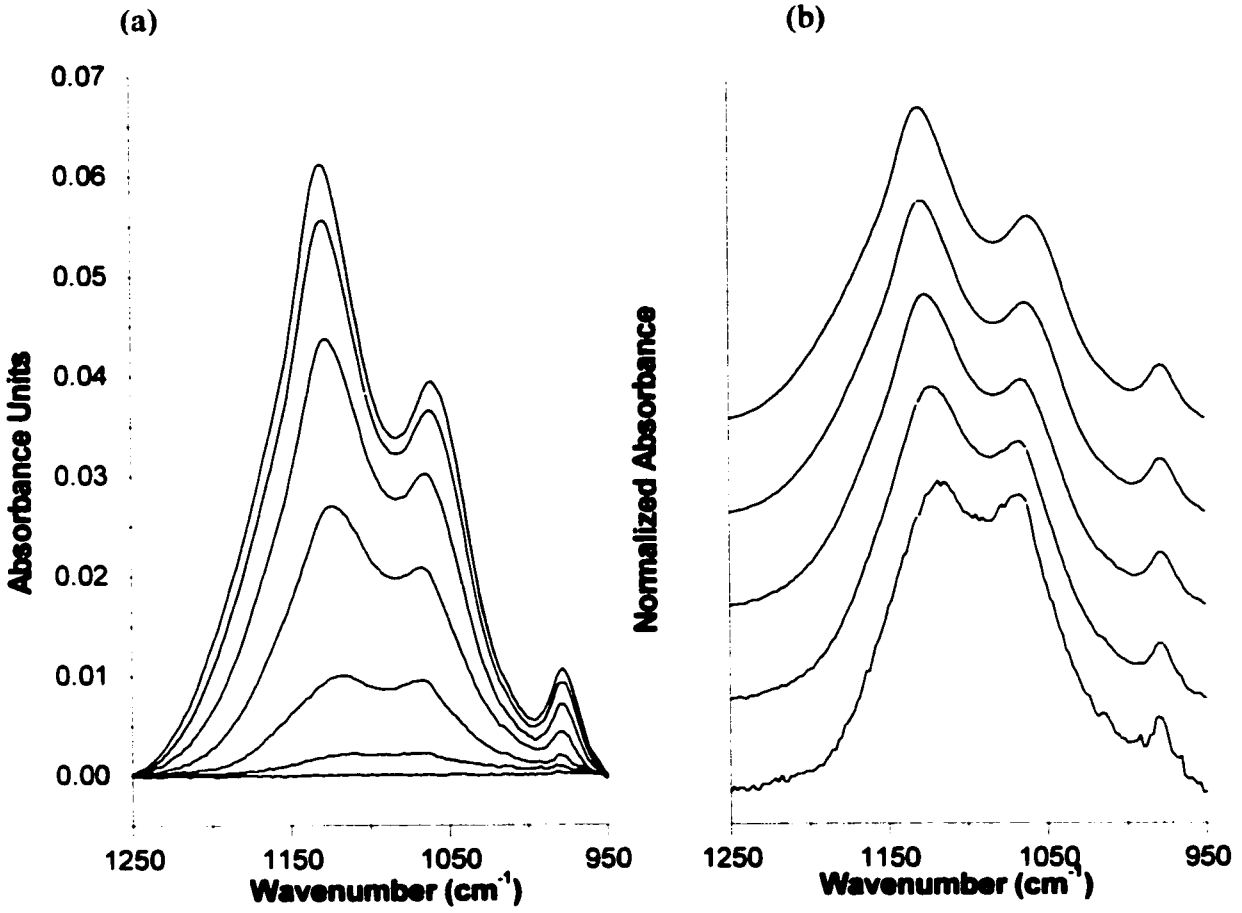

Figure 1.7 (a) Spectra from a pH envelope of sulfate adsorbed on hematite. Reaction conditions were 0.01 N NaCl as background electrolyte, 20 μM SO_4^{2-} added. The spectra were the result of 128 co-added scans at 4 cm^{-1} resolution. The spectra were collected at pH (from bottom): pH 8, 7, 6, 5, 4, and 3.5 (b) Difference spectra obtained by subtracting pH 8.0, 7.0, 6.0, 5.0, and 4.0 spectra from the pH 7, 6, 5, 4, and 3.5 spectra (respectively) of Figure 1.7a.

Both hematite and goethite are common crystalline iron (III) oxides, but in natural systems amorphous iron hydroxide can also be an extremely important sorbent. On hydrous ferric oxide, sulfate adsorption is substantially different from either goethite or hematite. Figure 1.8a shows a pH envelope of sulfate adsorption on ferrihydrite at an ionic strength of 0.01 M and C_{eq} of 20 μM sulfate. It is clear from the intensity of absorbance that far more sulfate adsorption occurs on ferrihydrite than on either of the crystalline iron oxides. This is to be expected, as the surface area of ferrihydrite is much greater than goethite or hematite. Also readily apparent is the fact that far more outer-sphere sulfate adsorption occurs on ferrihydrite. In fact, the spectra collected at pH 6, 7, and 8 perfectly match outer-sphere sulfate reference from Nakamoto (1986). As the pH decreases further more splitting of the ν_3 band can be seen. To determine whether this splitting is simply due to the increase of the positive surface charge of the sorbent as pH is lowered or due to the presence of a second inner-sphere complex, the difference spectra were also analyzed (Figure 1.8b). Looking at the pH 3.5 minus pH 4 spectrum and the pH 4 minus pH 5 spectrum (a and b, respectively) it can be seen that between pH 3.5 and 5, the spectra of the additional sulfate adsorption has peaks at 1115 and 1050 cm^{-1} and that a shoulder also appears around 1170 cm^{-1}. Such a large degree of splitting in the ν_3 band almost certainly results from an inner-sphere complex. The degree of splitting of the ν_3 band is less than when inner-sphere complexes form on goethite, but that could possibly be an artifact of the method of taking difference spectra. If additional outer-sphere sulfate also occurs (which appears

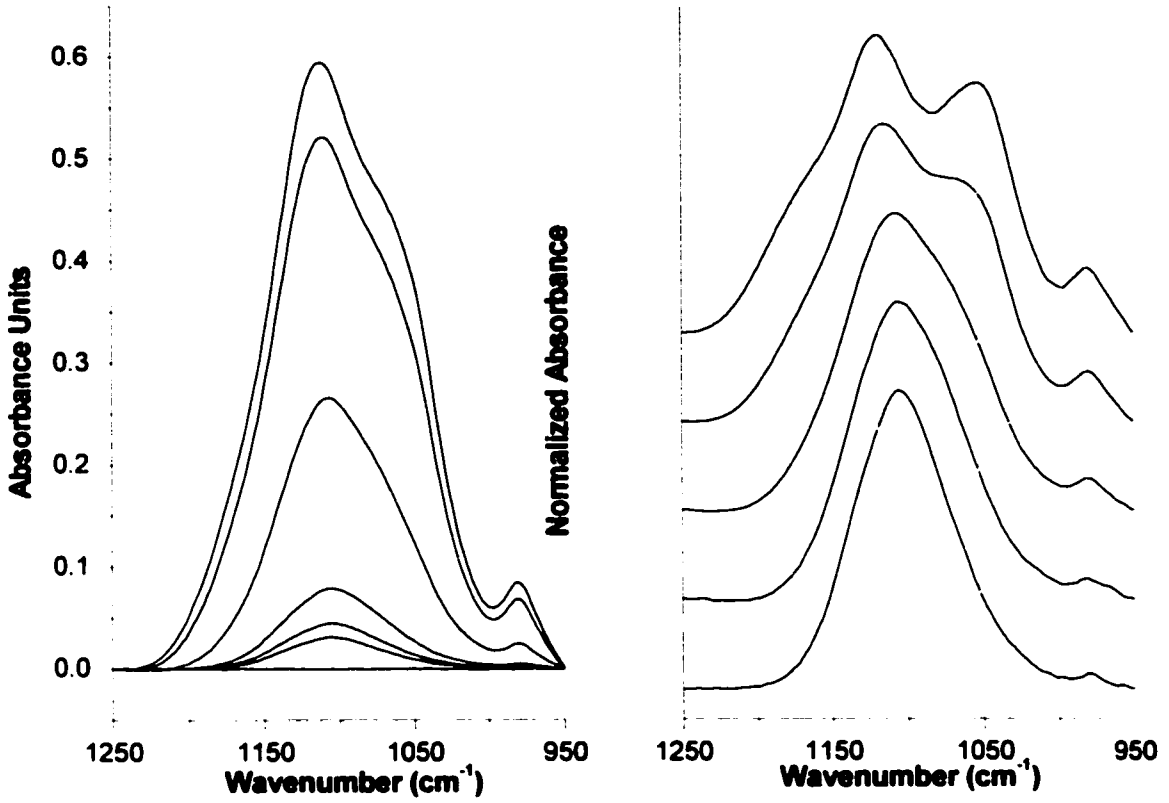

Figure 1.8 (a) Spectra from a pH envelope of sulfate adsorbed on ferrihydrite. Reaction conditions were 0.01 N NaCl as background electrolyte, 20 μM SO_4^{2-} added. The spectra were the result of 128 co-added scans at 4 cm^{-1} resolution. The spectra were collected at pH (from bottom): pH 8, 7, 6, 5, 4, and 3.5 (b) Difference spectra obtained by subtracting pH 8.0, 7.0, 6.0, 5.0, and 4.0 spectra from the pH 7, 6, 5, 4, and 3.5 spectra (respectively) of Figure 1.8a.

to be the case on ferrihydrite), then the peaks of the inner-sphere complex will not very well resolved in the resulting difference spectra.

Influence of sulfate concentration. In the case of sulfate adsorption on hematite, Hug (1997) reported that the same adsorption mechanism (an inner-sphere monodentate surface complex) occurs over a wide range of sulfate surface loading. On goethite, however, more than one adsorption mechanism is present. Therefore shifts from outer-sphere to inner-sphere surface complexes may potentially occur as loading increases. To investigate this, an adsorption isotherm was conducted at pH 5.0 and an ionic strength of 0.01 M (Figure 1.9). At this pH, there is a mixture of outer- and inner-sphere adsorption occurring. When one takes difference spectra from successively higher loading, (Figure 1.9b) then it becomes clear that as loading increases the additional adsorption occurs primarily due to an inner-sphere mechanism. At an equilibrium sulfate concentration less than 100 μM, both outer-sphere and inner-sphere complexation increase as loading increases, although the increase in inner-sphere surface complexation is greater than that of outer-sphere complexation. At equilibrium sulfate concentration above 100 μM, essentially all of the additional sulfate adsorption is inner-sphere. This mechanism seems to remain the same as the surface loading increases, because the ν_3 inner-sphere peaks at 1050 and 1133 cm^{-1} remain in the same position and the shoulder at 1170 cm^{-1} is very weakly visible in both (a) and (b).

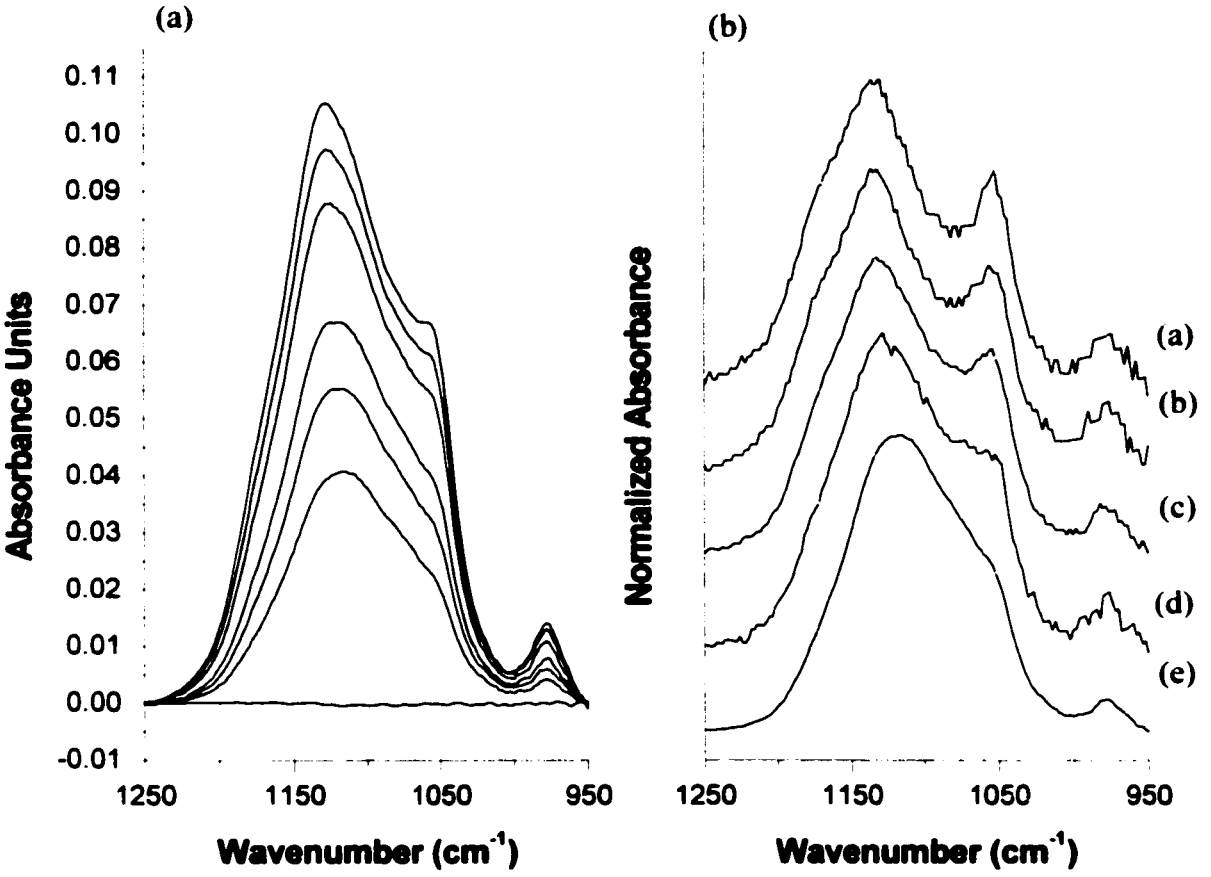

Figure 1.9 (1.9a) Spectra from a sulfate adsorption isotherm on goethite conducted at pH 5.0 and I = 0.01. The spectra are the result of (from bottom): (a) 0, (b) 5, (c) 10, (d) 25, (e) 100, (f) 250, and (g) 500 μM equilibrium sulfate concentration. (1.9b) Difference spectra obtained from 1.9a showing the mechanism of additional sulfate adsorption as loading increases.

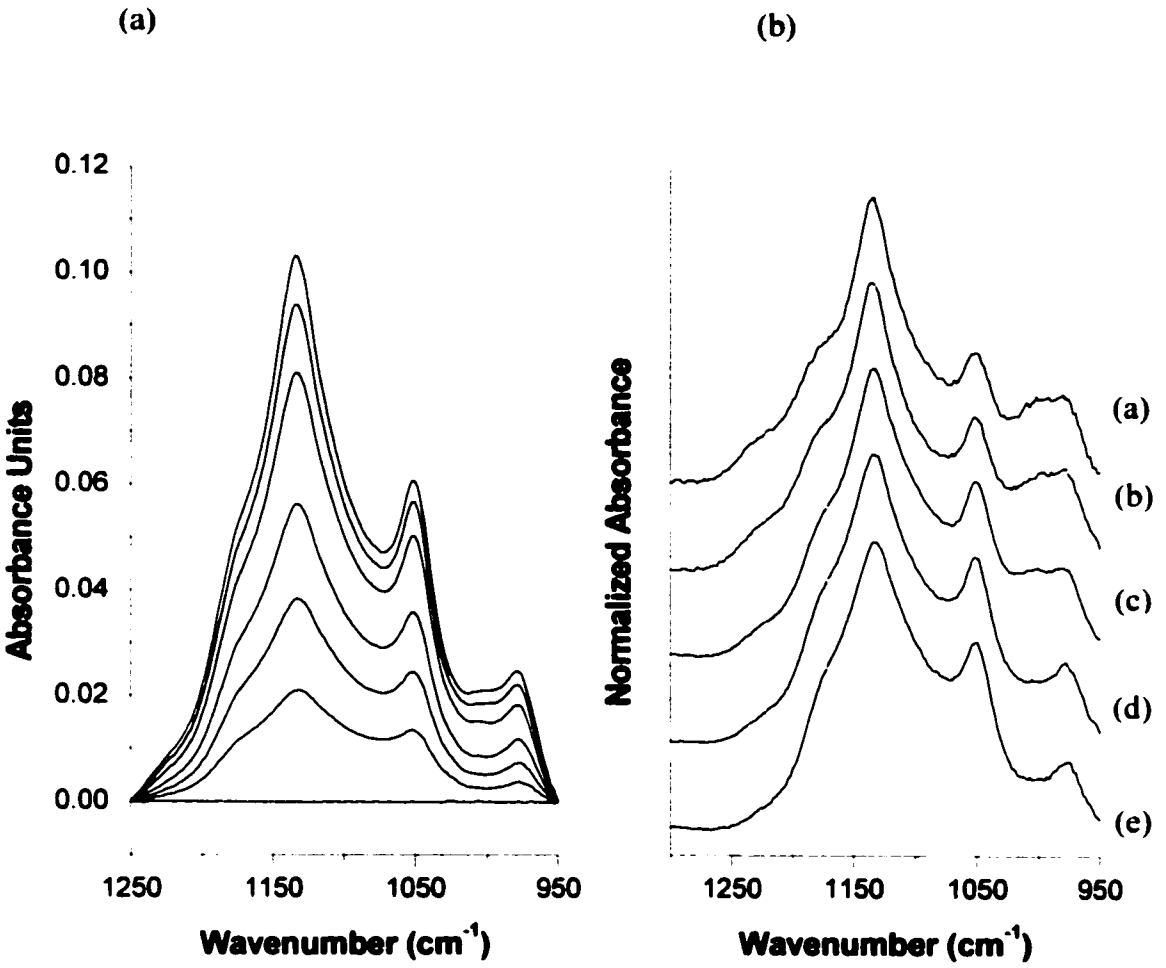

Figure 1.10 (a) Spectra from a sulfate adsorption isotherm on goethite conducted at pH 3.5 and I = 0.01. The spectra are the result of (from bottom): (a) 0, (b) 5, (c) 10, (d) 25, (e) 100, (f) 250, and (g) 500 μM equilibrium sulfate concentration. (b) Difference spectra obtained from 1.10a showing the mechanism of additional sulfate adsorption as loading increases.

On goethite at pH 3.5, both outer-sphere and inner-sphere surface complexes are seen, with much more inner-sphere adsorption occurring than at pH 5.0. To investigate the potential surface loading effects on inner-sphere sulfate complexation at pH 3.5, an ionic strength of 0.05 M was used to decrease the amount of outer-sphere complexation. The results of this isotherm can be seen in Figure 1.10. If one only looks at the raw spectra (Figure 1.10a) then it appears that no significant changes are occurring with increasing surface loading. But when difference spectra are examined (Figure 1.10b) then it becomes clear that increasing sulfate equilibrium concentrations does have an effect on surface complexation mechanisms. Two peaks at 1228 and 1000 cm^{-1} become visible as loading increases. These peaks suggest that another inner-sphere complex is present at higher loading. The fact that the ν_1 band is shifted to 1000 cm^{-1} would require the surface complex to have C_{2v} symmetry. There are two potential complexes that satisfy this; bidentate bridging (binuclear) and bidentate chelating sulfate. From references in Figure 2, if the complex were the result of a chelating sulfate, then all of the ν_3 bands would be expected to shift to higher wavenumber. While the feature at 1225 cm^{-1} does occur at a relatively high wavenumber for a sulfate ν_3 peak, the other ν_3 bands of this complex apparently overlap with those of the inner-sphere complex with C_1 symmetry (1050 and 1133 cm^{-1}) since no additional peaks are observed. This suggests that the bidentate binuclear inner-sphere surface complex is responsible for the observed features.

Influence of ionic strength.

Sulfate adsorption on goethite is influenced by ionic strength as well, with more adsorption occurring as ionic strength is decreased. It is important to separate ionic strength effects from surface loading effects that occur. Figure 1.11 compares sulfate adsorbed on goethite at pH 4.0 and different ionic strengths. Because different amounts of goethite were present in both experiments, the spectra were normalized to a maximum of 1. It is clearly shown that the peaks due to inner-sphere complexation become more pronounced as ionic strength increases. This occurs even though the total amount of adsorption is decreased. This is in contrast to the surface loading effect discussed above that caused increased inner-sphere complexation as loading increased. The earlier assignment of the peaks at 1110 cm^{-1} and 976 cm^{-1} to outer-sphere sulfate is also supported by these results, since the relative importance of these peaks is greater in lower ionic strength spectra (a) where there is more outer-sphere adsorption. The assignment of the peak at 976 cm^{-1} to the ν_1 band of outer-sphere sulfate is also supported by the observation that the ratio of the outer-sphere peak areas is 0.04:1.00 in both spectra. Since different amounts of goethite result in differences in total adsorption (and therefore absorbance) it was not possible to produce a difference spectrum to better illustrate the ionic strength dependence.

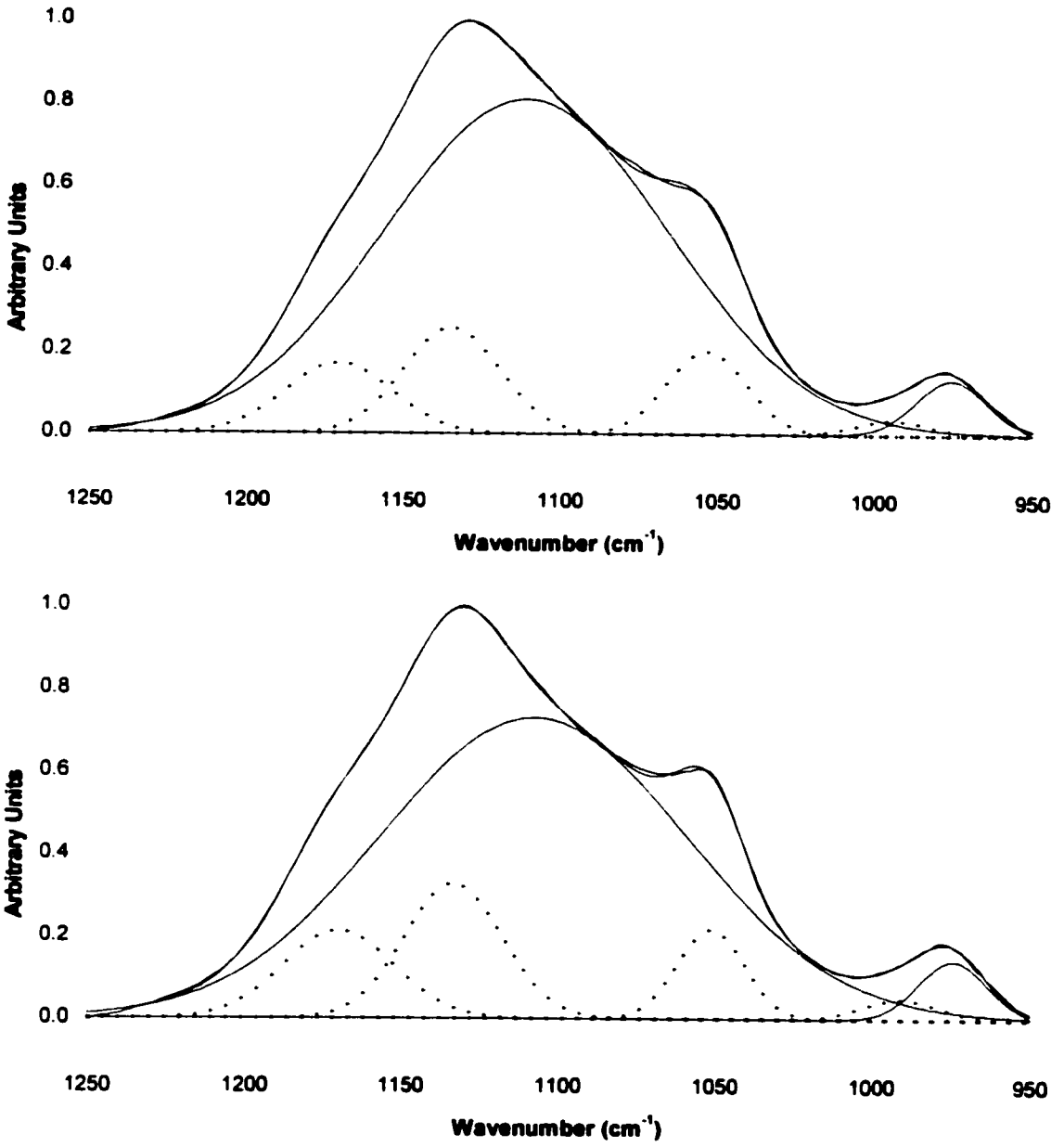

Figure 1.11 Spectra illustrating the variation of sulfate adsorption on goethite with ionic strength. In both cases the reaction conditions were pH 4.00 and 20 μM SO_4^{2-} added. Spectrum (a) was collected at ionic strength 0.005, while (b) was collected at I = 0.1.

DISCUSSION

In the broadest sense, sulfate adsorption on iron (III) oxides is similar for goethite, hematite, and ferrihydrite. Inner-sphere sulfate adsorption on iron oxides increases as pH is lowered, and outer-sphere adsorption increases as ionic strength is decreased. This adsorption behavior can be readily explained by the concept of ligand exchange. In basic conditions, the singly coordinated surface hydroxyls of metal oxides exist as either Me-O^- or as Me-OH functional groups. The bonds between the oxygen ligands and the metal center tend to be strong, and ligand exchange is less favorable since the hydroxide ligands are difficult to displace and are also present in higher concentrations in solution than is a trace adsorbate such as sulfate. As pH decreases, singly coordinated hydroxyls (Fe-OH) protonate to produce Fe-OH_2^+ functional groups. The water attached to the iron (III) is a weak ligand with high lability, and can more easily be displaced by a competing ligand such as sulfate, forming an inner-sphere surface complex. To fully understand the reactivity of sulfate with goethite, and to explain differences in sulfate adsorption on hematite and goethite, a detailed understanding of the surface-charging behavior of both iron oxides is required.

It is noteworthy that sulfate only forms inner-sphere monodentate surface complexes on hematite in aqueous solution (Hug 1997) while forming a mixture of outer-sphere and inner-sphere complexes on goethite (Peak 1999). Since both the goethite used in this experiment and the hematite used by Hug (1997) had a PZC between 8 and 8.5,

and in both cases the reactive site is probably $Fe\text{-}OH_2^+$, it is somewhat surprising that their reactivities are so markedly different. Differences apparently exist between the populations of functional groups at the metal oxide surface that can account for the different sulfate adsorption behavior observed in the two systems. Researchers (Venema et al. 1998) have successfully applied a Multi Site Complexation (MUSIC) approach to determine the relative site densities and log K values for all functional groups present on various crystal faces for both goethite and hematite. The results of this analysis can provide valuable insight into the observed adsorption behavior of sulfate, and are used as a point of reference for the discussion that follows.

On goethite, the 110 crystal face is dominant, and the sites that readily protonate are the singly coordinated (Fe-O) and about 67% of the triply coordinated (Fe_3O) surface groups. At the PZC (around 9.0) the singly coordinated surface groups exist as Fe-OH due to the extremely high log K, and the Fe_3O sites are ~70% Fe_3OH. As the pH is lowered from the point of zero charge, only the Fe_3O sites protonate until about pH 7. This explains the observed outer-sphere complexation, because this protonation increases the positive charge on goethite (Fe_3OH has $+^1/_2$ formal charge) and therefore increases sulfate adsorption. However, no $FeOH_2^+$ sites necessary for inner-sphere sulfate complexation appear until the pH is lowered further.

With hematite, the surface functional groups behave somewhat differently. The 110 and the 001 faces predominate. Since the 001 crystal face has a PZC close to that of the hematite used by Hug (1997), this crystal face likely contributed more to the results of Hug's (1997) experiments than the 110 face with its PZC of 11. It has also been determined that sulfate forms bidentate binuclear surface complexes on most crystal faces, and monodentate surface complexes only on the 001 planes (Sujimoto and Wang 1998). On the 001 face, surface functional groups occur due to imperfections in the crystal structure. Both Fe-O and Fe_2O functional groups exist. At the PZC, approximately 80% of the singly coordinated sites exist as $Fe\text{-}OH_2^+$, which are capable of ligand substitution reactions with oxyanions. As pH is decreased below the PZC, the remainder of the Fe-OH sites protonate and the Fe_2O^- sites protonate to form the neutral Fe_2OH. Since the reactive surface sites are formed at a much higher pH on hematite and protonation of the Fe_2O sites does not promote outer-sphere adsorption, inner-sphere surface complexes are more favorable. This can explain Hug's observation (1997) that sulfate forms primarily inner-sphere surface complexes over all pH values on hematite. The major points of this discussion are summarized in Figure 1.12 and 1.13.

Unfortunately, no CD-MUSIC proton affinity data exists for ferrihydrite due to its amorphous nature. However, recent research into the structure of ferrihydrite provides

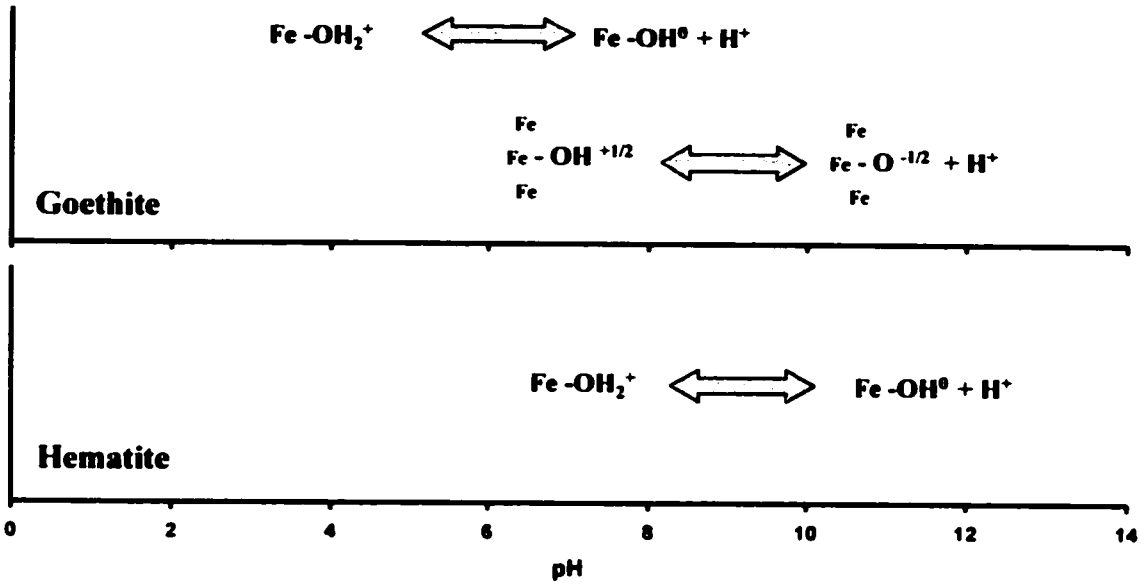

Figure 1.12 Illustration of the CD MUSIC model's description of surface hydroxyl protonation on goethite and hematite as a function of pH

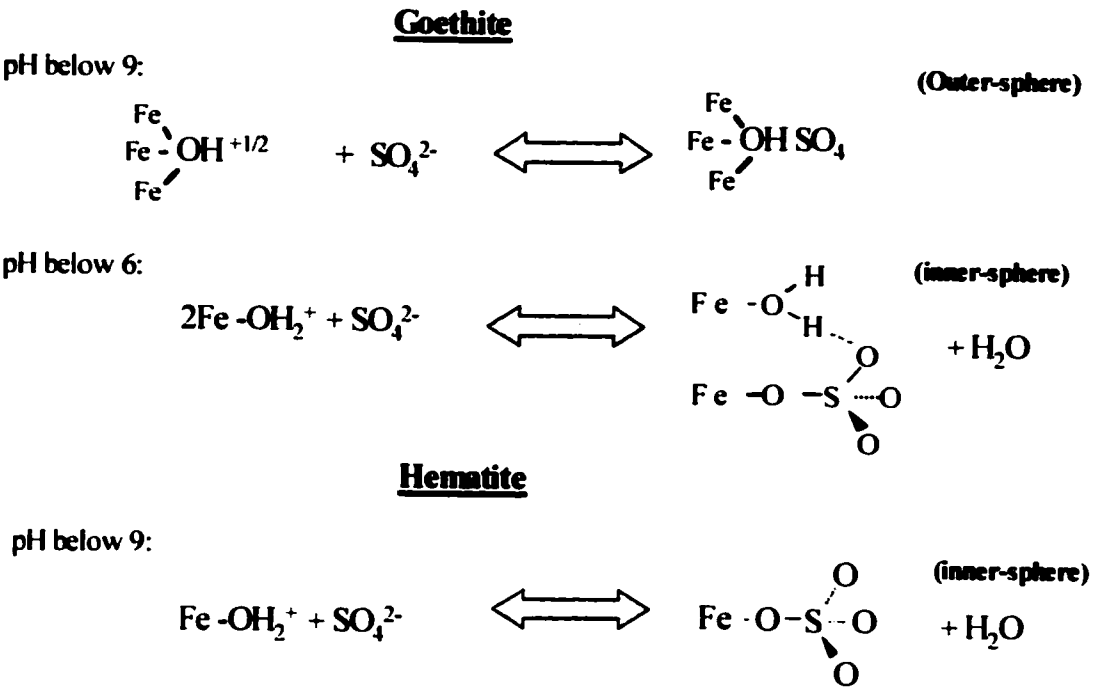

Figure 1.13 Illustration of sulfate surface complexation mechanisms on goethite and hematite as determined via ATR-FTIR spectroscopy

a potential explanation for sulfate adsorption on this sorbent phase. Ferrihydrite has an extremely small particle size (roughly 30 angstroms). This fact means that much more of the total mass of ferrihydrite is reactive surface area than crystalline iron oxides, in which much of the mass is present as a structural and unreactive mineral phase (Zhao et al. 1994). The lack of crystalline order also allows for greater surface site density. These differences between ferrihydrite and both goethite and hematite could be responsible for the observed tendency of sulfate to adsorb to ferrihydrite via an outer-sphere complexation mechanism relative to the crystalline sorbents. It has been discussed already that as surface loading increases on goethite, then sulfate adsorption mechanisms become increasingly inner-sphere. This can reasonably be expected to occur on ferrihydrite as well since a mixture of outer-and inner-sphere surface complexes are similarly seen. It is worth noting that the surface area of ferrihydrite is usually between 200 and 300 m^2g^{-1} (Schwertmann and Cornell 1991); roughly 5 times that of the goethite used in this experiment which had a surface area of 63 m^2g^{-1}. The maximum absorbance of sulfate in the pH envelopes at pH 3.5 is also about 5 times greater (0.6 absorbance units for ferrihydrite vs. 0.11 for goethite). However, this identical loading on a surface area basis could easily result in a much lower degree of surface site saturation if the density of the surface sites of ferrihydrite was significantly greater than goethite. Another possible reason for differences in complexation mechanisms between ferrihydrite and other iron oxides could be related to the structure of the mineral phase. While it is difficult to determine the exact

structure of ferrihydrite, several researchers have used EXAFS to probe the structure of ferrihydrite (Zhau et al. 1994). It has been determined that some surface irons are coordinatively unsaturated and therefore chemisorb water molecules. If the bonding between these Lewis acid sites and the adsorbed water is strong enough, it is possible that sulfate would simply adsorb as an outer-sphere complex to this positively charged site rather than displacing it via ligand exchange.

Dzombak and Morel (1990) extensively studied the adsorption of cations and anions to ferrihydrite and modeled the reactions using a generalized double layer model. They concluded that only one site was needed to model proton adsorption based on titration data, but that two sites (a high affinity site and a low affinity site) were necessary to describe metal adsorption. They concluded that one site was sufficient to describe anion complexation with ferrihydrite as well, with multiple surface complexes occurring on that single type of site. This theory that sites on the ferrihydrite surface can have different reactivity while having identical pK_a values is also a potential explanation for the observed mixture of outer-sphere and inner-sphere surface complexation of sulfate.

Another point for discussion is the difference in the identity of the inner-sphere surface complexes that form on goethite, hematite, and ferrihydrite. The most reasonable explanation is simply that on the goethite surface the density of surface sites makes it

possible for sulfate to form hydrogen bonds with adjacent sites when it adsorbs as an inner-sphere complex. Since this hydrogen bonding would lessen the effective negative charge that a monodentate sulfate surface complex adds to the surface, then it would be favored. It could be that on hematite the appropriate surface configuration simply does not exist in large enough amounts to influence monodentate bonding.

On goethite, the effects that ionic strength and solution sulfate concentration have on sulfate complexation also deserve discussion. These are two distinct effects, because increasing surface loading by increasing the equilibrium sulfate concentration results in an increase in inner-sphere sulfate complexation. However increasing the surface loading by lowering the ionic strength of the system results in additional outer-sphere complexation. This is because in the case of ionic strength effects, there is direct competition between sulfate and Cl^- ions that are used as background electrolyte for outer-sphere adsorption on goethite. Additionally, as ionic strength is increased, the electrical double layer is compressed and this also decreases the amount of sulfate that can form outer-sphere complexes. When ionic strength is held constant and loading is increased by raising the concentration of sulfate in solution, then additional adsorption occurs simply to maintain equilibrium between aqueous and adsorbed sulfate. Furthermore, because additional inner-sphere adsorption of the sulfate anion leads to decreased surface charge, inner-sphere complexation is favored. At pH 3.5, there is an additional effect of surface loading: the formation of an additional inner-sphere

surface complex of C_{2v} symmetry. This complex seems most likely to be a bidentate bridging complex, and probably forms as a result of surface crowding. A bidentate surface complex takes up less area on the surface than a monodentate complex even if the monodentate complex is hydrogen bonded to an adjacent surface site. Alternatively, this bidentate bridging surface complex could be the result of adsorption to less favorable surface sites that only occurs when a large solution sulfate concentration drives the reaction.

It is also noteworthy that on both goethite and ferrihydrite lowering solution pH generally results in additional inner-sphere surface complexation rather than a transformation from an outer-sphere surface complex to an inner-sphere surface species. The only exception that was seen in this research was when pH is lowered from 4 to 3.5 on goethite (Figure 1.4). Under this condition a negative absorbance in the region where outer-sphere sulfate occurs was noted. This possibly could be due to some transformation to an inner-sphere sulfate on the surface. Alternatively this could be explained by desorption of outer-sphere sulfate caused by decreased surface charge on the surface.

Conclusions

Sulfate adsorption on iron oxides and hydroxides is quite complex. It is important to consider not only the effects of pH, ionic strength, and reactant concentration on sulfate adsorption, but also the nature of the sorbent phase being studied.

Sulfate forms inner-sphere monodentate surface complexes on hematite from pH 8 to 3.5 and across a wide range of surface loadings. On goethite, however, sulfate forms only outer-sphere surface complexes at pH 6 and above, and forms a mixture of outer-sphere and inner-sphere complexes below pH 6. The inner-sphere sulfate surface complex is a monodentate complex that is hydrogen bonded to an adjacent surface site. Increasing the equilibrium sulfate concentration promotes additional inner-sphere sulfate adsorption at pH 4.5 - 6. At pH 3.5, raising the sulfate equilibrium concentration causes the formation of a second bidentate binuclear surface complex. Decreases in ionic strength lead to increased sulfate adsorption, with the additional sulfate being primarily outer-sphere. Finally, sulfate forms predominantly outer-sphere surface complexes on ferrihydrite. Some inner-sphere complexation occurs below pH 5.0, with the spectra suggesting a monodentate surface complex. The amount of adsorption on ferrihydrite is much greater than either of the crystalline iron oxides in this study. Much research in the scientific literature involves experiments conducted with goethite and hematite that was not treated to remove amorphous iron

oxides prior to adsorption studies. Since ferrihydrite was found to have far more outer-sphere adsorption of sulfate than either goethite or sulfate, this could potentially result in incorrect assessment of adsorption mechanisms on these sorbents

There are also some more important conclusions that can be drawn from this study. It is reasonable to assume that, similarly to sulfate, other oxyanions may also have very different adsorption mechanisms on hematite, goethite, and ferrihydrite. It is therefore of great importance to study how changes in surface functional group distributions and log Ks of iron oxides affect complexation mechanisms. Another important concept that seems to be becoming clearer to soil chemists is that in many systems multiple adsorption mechanisms are occurring simultaneously and that a continuum of adsorption processes exists. This is not only true for sulfate; it has been shown that organic ligands (Perrson et al. 1998) can adsorb as both outer-sphere or inner-sphere complexes as reaction conditions change. Metal ions also exhibit this trend, as competition between adsorption and precipitation has been seen in the case of mixed metal precipitate formation (Elzinga 2000) on some clay minerals. It therefore makes sense to use molecular-scale spectroscopy to study the effects that changing reaction conditions have on this continuum of reaction mechanisms.

Chapter 2

MECHANISMS OF SELENATE ADSORPTION ON IRON OXIDES AND HYDROXIDES

Selenate ($SeO_4^{2-}{}_{aq}$) is the fully oxidized form of selenium, and is often seen in aerated soils. Selenium is an essential micronutrient for animals, but when soil selenate levels are high it often accumulates in plants and can prove toxic to animals that ingest the vegetation. Alternatively, deficiency symptoms are commonly seen when selenium levels in plants are low (Zhang and Sparks 1990). Therefore understanding the chemistry of selenate in soils is important for minimizing potentially hazardous environmental effects. Selenate is a weakly basic Group VI oxyanion, and typically exists in natural aqueous systems as either the fully-deprotonated form or as the singly-protonated biselenate ($HSeO_4^-{}_{aq}$)(Shriver et al. 1994). Both of these ions have a hydrated radius of ~ 4 Å (Stumm and Morgan 1996). The pK_a for the protonation reaction is ~1.9, making the fully-deprotonated form the dominant ion under normal soil conditions.

Column studies that monitored selenate leaching through soils (Aldrichs and Hossner 1987) reported that selenate was very weakly bound, and could be completely leached from soils in a short period of time. The soils studied were sandy loam soils low in iron oxides and with smectites being the predominant clay minerals. Other researchers

(Bar-Yosef and Meek, 1987) reported only slight sorption of selenate to kaolinite and montmorillonite as a function of pH. Furthermore, selenate adsorption was found to be negligible on alluvial soils by Neal and Sposito (1989). None of the above studies utilized soils with a significant iron oxide component, however. Adsorption reactions of selenate with naturally occurring iron oxide minerals and amorphous iron hydroxide coatings may be substantial in soils that are slightly acidic due to their positive charge (PZC of 6-7 in the presence of carbonate) and high surface area.

Unfortunately, little macroscopic and modeling data is available in the literature for selenate adsorption on iron oxides. Davis and Leckie (1980) showed that pH envelopes for sulfate and selenate adsorption on ferrihydrite are identical. This suggests that both sorbates have the same affinity for the surface, and implies that the same mechanisms are present in both systems. Zhang and Sparks (1990) analyzed selenate adsorption on goethite using a triple layer model and pressure jump relaxation and found results consistent with outer-sphere complexation of selenate. Yamaguchi and colleagues (1999) compared volume changes due to sulfate and selenate adsorption on an amorphous iron oxide using dilatometry. The volume changes for sulfate and selenate were identical, again suggesting that similar reaction mechanisms were occurring with these ions. A large loss of waters of hydration was observed in both ions, which suggests that a ligand-exchange reaction occurred at the iron oxide's surface. Su and Suarez (2000) found that selenate adsorption on both goethite and

amorphous iron hydroxide shifted PZC to lower values using electrophoretic mobility. This would also suggest an inner-sphere adsorption mechanism. They also found a large ionic strength dependence on pH envelopes, with adsorption suppressed as ionic strength increased. This seemingly contradictory observation suggests an outer-sphere adsorption mechanism, but it was also noted that as selenate concentration in solution was increased that this ionic strength dependence became much smaller.

Early studies utilizing *ex situ* FTIR techniques observed inner-sphere bidentate binuclear complexes of selenate on iron oxides (Harrison and Berkheiser 1982). However, these studies involved extensive sample modification such as drying and subjection to vacuum. Such preparation may force inner-sphere surface complexes by removing waters of hydration from the mineral surface (Johnston and Sposito 1987), and has been shown to cause a conversion from monodentate to bidentate surface complexes (Hug 1997). Hayes and colleagues (1987) used EXAFS to study the adsorption mechanisms of selenate and selenite on goethite *in situ* and concluded that selenate adsorbs to goethite via an outer-sphere mechanism. In stark contrast, Manceau and Charlet (1994) conducted EXAFS experiments at the same pH and surface coverage as Hayes et al. (1987), and concluded that selenate forms inner-sphere complexes (bidentate binuclear and bidentate mononuclear) on both goethite and hydrous ferric oxide. Su and Suarez (2000) used both attenuated total reflectance (ATR-FTIR) and diffuse reflectance (DRIFT) spectroscopy to study selenate

adsorption mechanisms on amorphous iron oxides and concluded that selenate adsorbs via a mixture of monodentate and bidentate inner-sphere complexes under aqueous conditions, and forms bidentate inner-sphere complexes when dried. Wijnja and Schulthess (2000) utilized both ATR-FTIR and Raman spectroscopy to investigate selenate and sulfate adsorption mechanisms on goethite *in situ*. They found that selenate and sulfate adsorb to goethite via the same mechanisms, and that at pH 6.0 and above that the adsorption occurs via an outer-sphere surface complexation mechanism. At pH below 6.0, inner-sphere monodentate surface complexes were observed. This is consistent with results of Peak et al. (1999) who determined that between pH 6 and 9 sulfate forms only outer-sphere surface complexes on goethite, while at pH below 6.0 both outer-sphere and inner-sphere surface complexes are formed on the goethite surface.

It was the hypothesis of our research that differences in selenate adsorption mechanisms observed in spectroscopic studies from the literature could be explained by differences in reaction conditions in the studies. The objectives of this study were therefore to determine the effects that pH, surface loading, and ionic strength have on adsorption mechanisms of selenate on iron (III) oxides and hydroxides. Goethite, hematite, and amorphous iron hydroxide were the sorbents chosen due to their important differences in structure and their ubiquity in soils. EXAFS was the primary spectroscopic tool chosen due to its suitability to determine local bonding

environments of selenate on all three sorbent phases. Additional information about selenate adsorption mechanisms on hematite was obtained using ATR-FTIR spectroscopy.

Experimental Materials and Methods

Mineral Synthesis. The goethite used in this study was synthesized using the method of Schwertmann et al. (1985). Initially, ferrihydrite was precipitated by adding 50 mL of 1 M ferric nitrate solution to 450 mL of 1 M KOH. This suspension of amorphous hydrous ferric oxide was then aged for 14 days at 25° C. The suspension was washed with doubly deionized water via centrifugation, resuspended in 0.4 M HCl, and shaken for two hours using a mechanical shaker to remove any residual amorphous iron oxides from the surface of the goethite. The acidified goethite suspension was again washed with doubly deionized water to remove HCl and dissolved iron, dialyzed until the conductivity of the solution was equal to distilled water, frozen with liquid nitrogen, and freeze-dried. The solid was confirmed as goethite via infrared spectroscopy using both ATR and transmission mode KBr pellets. The external surface area determined from N_2 BET was 63.5 m^2g^{-1}. The hematite used in these experiments was synthesized from ferric perchlorate using the method of Schwertmann and Cornell (1991). It was acid-washed, dialyzed, and freeze-dried following the same procedure described above for goethite, and had an N_2-BET surface area of 14 m^2g^{-1}. Ferrihydrite (hydrous ferric oxide) was synthesized by

titrating 1 M ferric chloride to pH 7.5 with 1 M KOH. This precipitate was washed 3 times with 0.1 M NaCl to remove any residual iron, washed once with deionized water, and then dialyzed for 3 days in deionized water. Rather than freeze-drying, the ferrihydrite was kept as a 10 g/L suspension and placed into a refrigerator to slow conversion to crystalline forms.

Sorption Experiments.

All reactions of selenate with iron oxides were conducted in acid-washed 50 mL polypropylene centrifuge tubes. All chemicals used in sorption experiments were reagent grade or better. Reactants were added with electronic pipettes (Rainen) that were calibrated with an analytical balance using the mass of deionized water at current laboratory temperature prior to sample preparation. Goethite and hematite were added to reaction tubes from a concentrated (50 g/L) suspension prepared from distilled deionized water, sonified to thoroughly mix, and then stirred while aliquots were being transferred. A solid density of 10 g/L was used for the hematite and goethite experiments, and a solid density of 2.5 g/L was used in the ferrihydrite samples. The ferrihydrite stock suspension was allowed to return to room temperature prior to sample preparation and then added from the well-stirred stock suspension. Water and a portion of the required background electrolyte were next added. Background electrolyte (NaCl) was added from a 1 M stock solution; 50 µL less NaCl than the amount desired for the final ionic strength was initially added. This allowed for HCl to be used for pH adjustment without affecting ionic strength of the final sample.

Once the selenate was added to the reaction tubes and pH was adjusted to the desired value with 1M HCl, the necessary background electrolyte (50 μL - the amount of HCl used in μL) was finally added to the reaction vessels to adjust to the appropriate ionic strength. Samples were continuously mixed on a rotating shaker, and at 8 hours and 20 hours sample pH was measured and adjusted to the desired value with 0.1M HCl. After 24 hours the sample pH was recorded, and the samples were then centrifuged at 15,000 rpm for 10 minutes. The supernatant was filtered through a 0.2 μm filter and then analyzed for residual selenate via AAS (Perkin-Elmer model), while the solid was sealed in containers and refrigerated until EXAFS analysis.

EXAFS spectroscopy. EXAFS spectra were collected at the Se k edge (12.658 keV) at Beamline X11-A of the National Synchrotron Light Source at Brookhaven National Laboratory. The electron storage ring was operating at either 2.5 or 2.8 GeV, depending on the date of spectral collection. The monochromator used in all experiments was a Si(111) crystal, and a slit width of 0.5 mm was used before the monochromator. This allowed for a spectral resolution of approximately 0.5 eV. Calibration was done to a 10% wt elemental selenium standard, and detuning 30% at 900 eV past the Se edge minimized the effect of higher order harmonics. All samples were scanned in fluorescence mode using a Lytle detector with a Krypton-filled ionization chamber. The sample chamber was designed so that samples were placed at a 45° angle to the incident beam, and a wide-angle collector was 90° to the incident beam. An Arsenic filter was placed between the sample compartment and the

ionization chamber to eliminate elastically-scattered X-rays from entering the ionization chamber. Additionally, several thicknesses of aluminum foil were placed in front of the arsenic filter to reduce Fe K_α radiation (Bargar et al. 1997b). To ensure adequate signal to noise for data analysis, three scans per sample were collected.

EXAFS spectral analysis. WinXAS version 1.1 and 1.3 were used for all data analysis. Individual spectra were first averaged, and then backgrounds were subtracted by fitting a 1^{st} order polynomial to the pre-edge region and a 2^{nd} order polynomial to the post edge region. The resulting normalized spectra all have an edge jump of unity. Next, the normalized spectra were converted to a raw χ function. This was accomplished by setting E_0 equal to the inflection point of the second derivative of the normalized spectra to produce a mue function. Finally, a cubic spline was fitted to the mue function that was also weighted by k^3 to compensate for dampening of the EXAFS spectra at higher k ranges. This function was then Fourier Transformed with a Bessel window and choosing endpoints at nodes of the function to produce the radial structure functions (RSF) that are presented in this paper. The k^3-weighted χ functions were also fitted to theoretical scattering paths using FEFF7 code. For the fitting, an amplitude reduction factor was fixed to 0.93; a value that was obtained by fixing the Se-O coordination number to 4.0 when fitting diluted sodium selenate salt. When fitting EXAFS samples, coordination numbers, bond lengths and Debye-Waller factors were allowed to vary. E_0 shifts were constrained to be equal for both the Se-O and the Se-Fe scattering paths.

ATR-FTIR spectroscopy. A Perkin-Elmer 1720x spectrometer was used for all infrared analysis. The spectrometer was equipped with a Whatman purge gas generator to remove $CO_{2(g)}$ and $H_2O_{(g)}$ from the sample compartment, and a $N_{2(l)}$-cooled MCT detector was employed for data collection. A horizontal ATR sampling accessory and a trough-style sample holder with 45 ZnSe crystal (Spectra Tech) was utilized for sample analysis. For the aqueous SeO_4 standard, a 10mM SeO_4/D_2O solution and a pure D_2O were analyzed and then pure D_2O was subtracted from the standard to produce a spectrum of aqueous selenate. For the adsorption sample, hematite was deposited on the ZnSe crystal according to (24), and then 1.5 mL of a background solution of 0.01M NaCl in D_2O at a pD of 3.5 was placed in the trough over the deposit. The hematite was allowed to equilibrate with the solution for 1 hour, a background spectrum was collected, and then 1.5 mL of a D_2O solution containing 500 mM SeO_4 and 0.01M NaCl was added to the trough. This solution was allowed to mix and react for two hours, and then a spectrum was collected of the adsorbed selenate. For all spectra, 1000 scans were collected at a resolution of 4 cm^{-1}. A linear baseline was fit to all samples with Galactic Peaksolve.

RESULTS AND DISCUSSION

Macroscopic studies. Figure 2.1 shows the results from adsorption isotherms of selenate on HFO, goethite, and hematite at several different reaction conditions. In all isotherms, Langmuir type adsorption was observed. For goethite at pH 3.5 and an

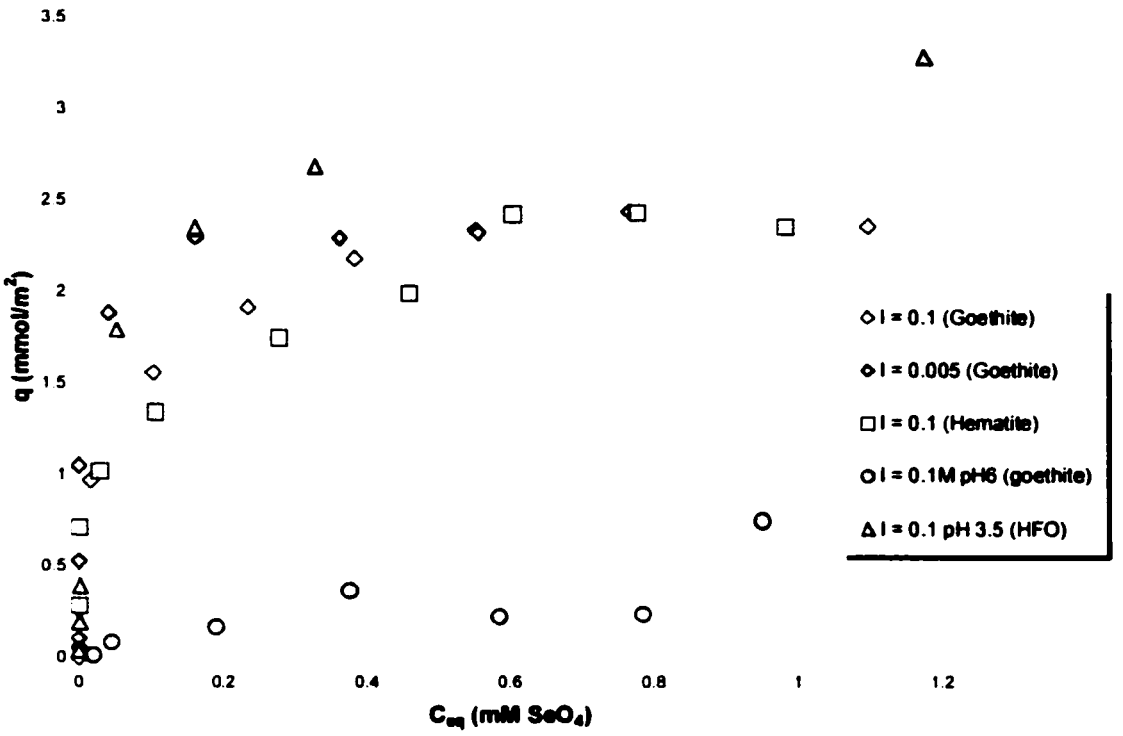

Figure 2.1 Adsorption isotherms for selenate sorbed on HFO, goethite, and hematite. The pH and ionic strength for the isotherms are identical to the samples chosen for EXAFS studies. It is possible to estimate q_{max} from the isotherms to be: ~ 2.5 μmoles/m^2 for SeO_4 on both hematite and goethite at pH 3.5; ~ 0.5 μmoles/m^2 for SeO_4 on goethite pH 6.0; and ~ 3.5 μmoles/m^2 for SeO_4 on HFO at pH 3.5.

ionic strength of 0.1M and 0.005M, and for hematite at pH 3.5 a sorption maximum (q_{max}) at approximately 2.5 μmol/m^2 was observed in the isotherms. This suggests that the density of sites reactive with selenate must be very similar for these two crystalline iron oxides. At pH 6.0, the q_{max} for selenate on goethite was much lower, occurring at approximately 0.5 μmol/m^2. This is reasonable since the number of fully-protonated surface sites on the goethite surface is much lower at pH 6 than it is at pH 3.5. In the case of HFO at pH 3.5, q_{max} was estimated at 3.5 μmol/m^2. For EXAFS spectroscopic studies, sample loadings will be expressed as a fraction of the sorption maximum, or q/q_{max}.

EXAFS Spectroscopy: Selenate adsorption on goethite. Based on results of *in situ* spectroscopic studies investigating sulfate (Peak et al. 1999; Wijnja and Schulthess 2000) and selenate (Wijnja and Schulthess 2000) adsorption on goethite, one would expect that pH, ionic strength, and surface loading all affect selenate adsorption mechanisms on goethite. Figure 2.2 shows the results of varying pH on selenate adsorption. In Figure 2.2a, the raw and fitted k^3-weighted chi data are shown, and in Figure 2.2b the Radial Structure functions are seen. As expected, the spectra of aqueous selenate (spectrum a) can be completely described with a single shell fit using 4 oxygen atoms at a distance of 1.64 Å. Similarly, the spectrum of selenate adsorbed at pH 6.0 can also be adequately fit using parameters identical to aqueous selenate. Therefore at pH 6.0, selenate adsorbs on the goethite surface via formation of an outer-

sphere surface complex. At pH 3.5 (spectrum c and d), however, the spectrum can no longer be fully described with a single oxygen shell. This is clearly shown in the spectrum labeled (c), as there are several features in the raw data that cannot be fit with

an oxygen backscatterer. If one analyzes the same spectrum with a 2-shell fit that includes an iron second shell with 1.5 Fe atoms at 3.31 Å (spectrum d), then the fit quality is improved and the spectrum can then be described. This demonstrates that at pH 3.5, inner-sphere complexation of selenate occurs on the goethite surface.

The effect that pH has on changing selenate adsorption mechanisms on goethite is quite dramatic, but other reaction conditions such as ionic strength and surface loading have a more subtle effect. Figure 2.3a shows the effect of changing ionic strength from 0.005 M to 1.0 M while maintaining a surface loading of 1.56 μmol/m^2 and a pH of 3.5. The spectra at both 1 M and 0.1 M ionic strength appear virtually identical, with 1.5 Fe atoms at a distance of 3.31 Å indicating inner-sphere complexation. At 0.005 M ionic strength, however, the second shell was too weak to fit consistently, although some contribution of Fe can be seen in the RSF. Figure 2.3b demonstrates that as surface loading is changed by a factor of 5 (from 0.78 to 2.5 μmol/m^2) while ionic strength and pH are kept constant (0.1 M and pH3.5, respectively) no change in bond distances of selenate can be observed with EXAFS. This suggests that the same complexation mechanism is occurring as loading changes.

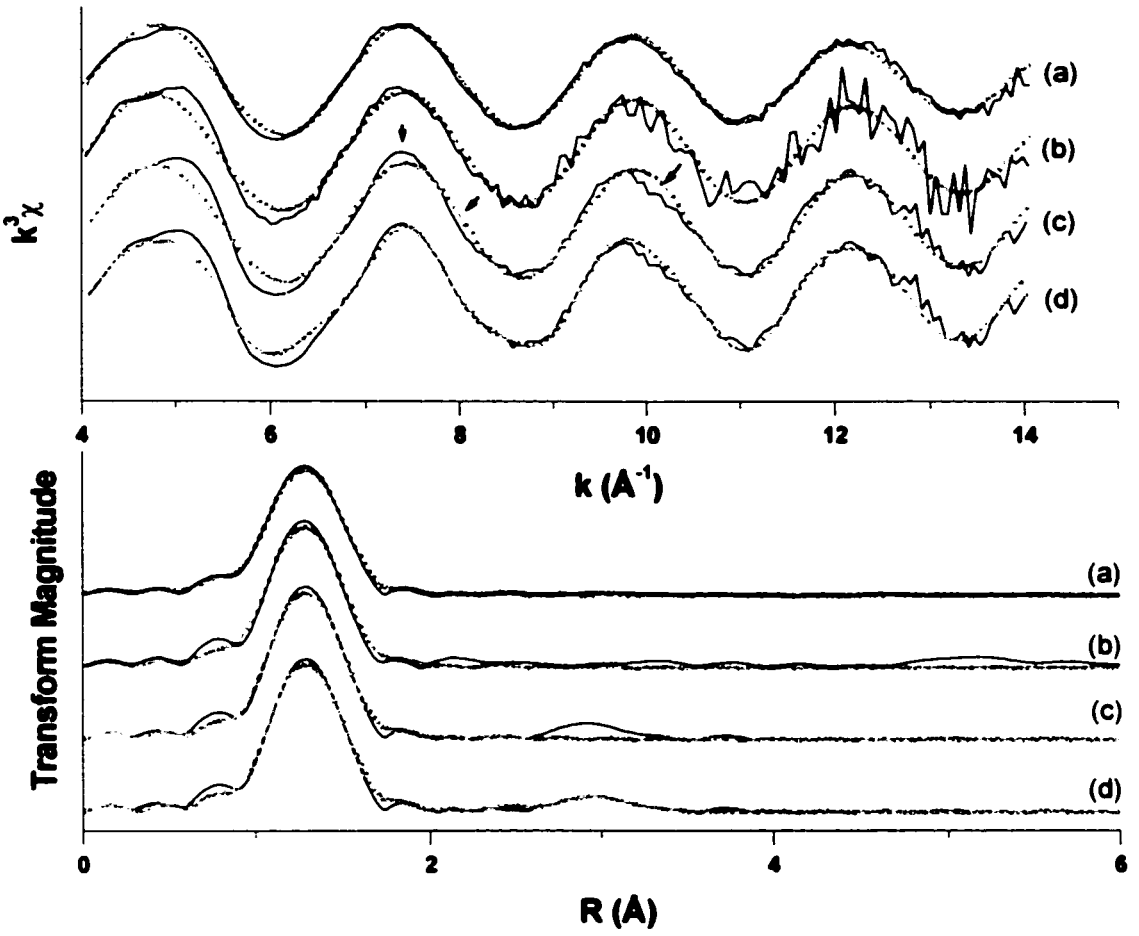

Figure 2.2 EXAFS spectra of selenate adsorbed on goethite at loading of 1.56 μmol/m^2 and ionic srength of 0.1 M. Solid lines representing the raw data, and the dotted lines are the fits to the data. The upper figure shows the raw k^3 weighted chi data, and the lower figure shows radial strucure functions. The spectra are as follows: (a) 10 mM SeO_4 and a single shell fit of 4 oxygens at 1.64 Å (b) 1 mM SeO4 adsorbed at pH 6.0 and a single shell fit of 4 oxygens at 1.64 Å (c) 1 mM SeO4 adsorbed at pH 3.5 and a single shell fit of 4 oxygens at 1.64 Å (d) 1 mM SeO4 adsorbed at pH 3.5 and a two shell fit of 4 oxygens at 1.64 Å and 1.5 Fe at 3.31Å. Note the features in the raw chi data of spectrum 1c pointed out with arrows where a single shell fit is unable to describe the pH 3.5 spectrum. When a second shell arising from Fe backscattering is added to the fitting procedure (1d) these features in the chi data are reproduced.

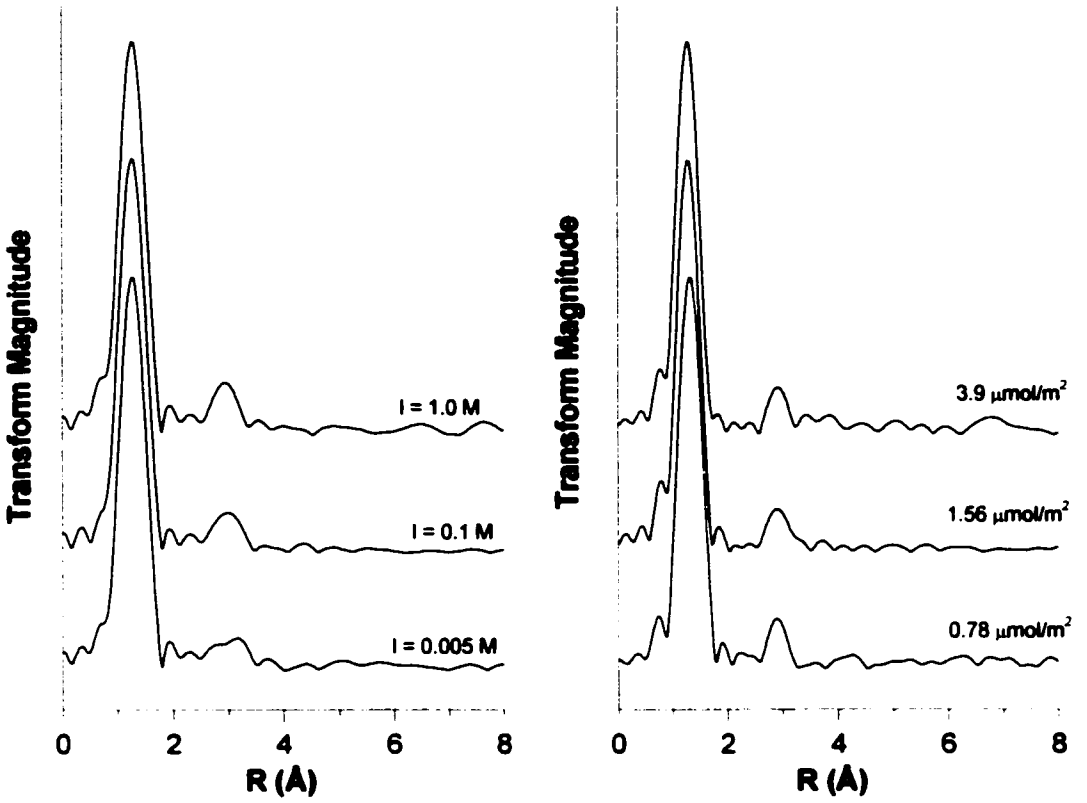

Figure 2.3 RSFs of selenate adsorbed on goethite at pH 3.5 as a function of (a) ionic strength and (b) surface loading. In Figure 2a, all samples have a surface loading of 1.56 μmol/m^2 Se. It can clearly be seen that as ionic strength is lowered from 1.0 M to 0.005 M, that the contribution of iron to the RSF becomes less important. This is evidence of increased outer-sphere complexation at low ionic strength. In Figure 2b, ionic strength was held at 0.1 M and surface coverage of selenate was varied. There is no change in the RSFs at these loadings, suggesting that the same inner-sphere surface complex forms over a range of surface loading.

Perhaps a large part of the discrepancies between the work of Hayes and coworkers (1987) and Manceau and Charlet (1994) can be described by differences in the ionic strength in the samples that they studied. Manceau and Charlet (1994) conducted all experiments at an ionic strength of 0.1 M $NaNO_3$ and a pH of 3.5, and Hayes and coworkers also studied adsorption at a pH of 3.5 but did not report ionic strength (Hayes et al. 1987). Another possibility is that EXAFS analysis of selenate adsorption on iron oxides requires good data quality out to high k range as mentioned by Manceau and Charlet (1994). EXAFS spectra of selenite adsorbed on iron oxides produces χ spectra that are completely out of phase from aqueous selenite, while adsorbed selenate χ spectra have dampening and destructive interferences that are much subtler.

EXAFS Spectroscopy: Selenate adsorption on other iron oxides. Figure 2.4 shows Fourier transformed spectra of several selenate reference spectra as well as selenate sorbed on goethite, hematite, and HFO at pH 3.5, an ionic strength of 0.1 M, and a surface loading of 3700 mg Se per kg sorbent. For aqueous selenate, one can readily see that the only structure is a single shell of 4 oxygen atoms at 1.64 Å. This is expected for the tetrahedral selenate molecule, and the observed Se-O bond distance is in good agreement with other EXAFS studies (Hayes et al. 1987, Manceau and Charlet 1994, Waychunas et al. 1995). For selenate-substituted schwertmannite, the central Se still has a tetrahedral coordination with a Se-O bond distance of 1.64 Å, but an additional contribution from Fe is also observed at 3.32 ?. This can be interpreted in

several ways. Schwertmannite is an iron(III) oxy-hydroxy-sulfate, with a tunnel structure that is similar to akageneite (Bigham et al. 1990). The actual bonding environment of sulfate in the tunnels is still the subject of debate. It is possible that the observed second shell is due to structural selenate, but the observed bond distance of 3.34 Å would place a large strain on the mineral's structure. An alternative explanation is that there are two bonding environments for selenate in the substituted schwertmannite: structural and sorbed. The structural selenate can then be present as the more favorable (from a crystallographic standpoint) outer-sphere counterion in the tunnels, while the sorbed selenate can form inner-sphere complexes on the surface that are seen with EXAFS spectroscopy. This is consistent with the *in situ* ATR-FTIR spectroscopic studies of sulfate bonding in schwertmannite (Peak et al. 1999), which showed both outer-sphere sulfate and inner-sphere sulfate present. The spectrum of Se-substituted schwertmannite in Figure 2.4 is quite consistent with the work of Waychunas et al. (1995), who reported a mean Se-Fe distance of 3.37 Å. They found an improved fit with two Se-Fe distances, one longer and attributed to structural (tunnel) selenate and a second shorter bond distance for inner-sphere sorbed selenate. However, they did not report the fitted distances.

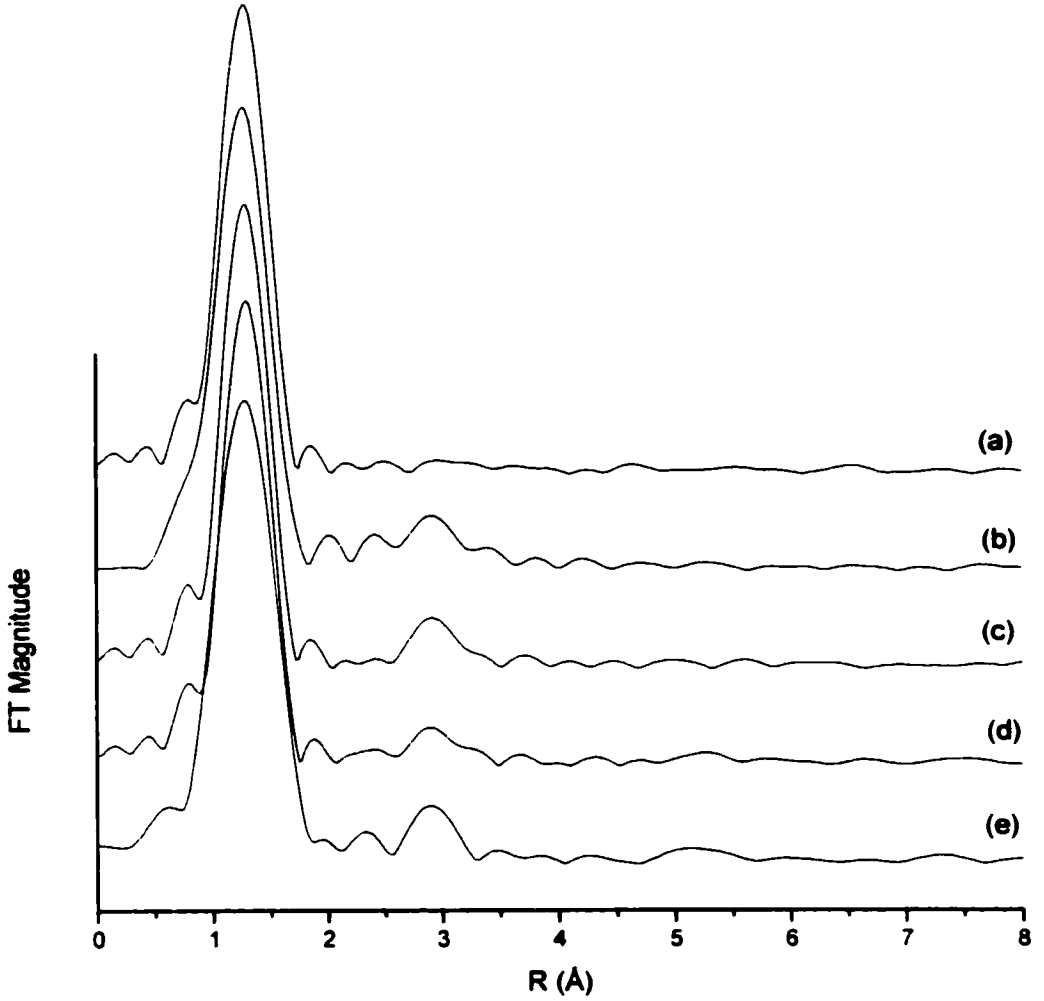

Figure 2.4 RSFs for (a) 10 mM $SeO_4^{2-}{}_{(aq)}$, (b) SeO_4 substituted schwertmannite, and SeO_4 adsorbed on (c)goethite (d)HFO, and (e) hematite. For all three adsorption samples, pH 3.5, 0.1 M I, and 1.56 μmol/m^2 SeO_4 were used.

The adsorption samples on hematite, goethite, and HFO all contain inner-sphere selenate surface complexes. This can be clearly seen from the second shell that is observed in all the Radial Structure Functions. The fit results from selenate adsorbed on different sorbents and on goethite under different reaction conditions are all compiled in Table 2.1. This second shell can be fitted with 1-1.5 Fe atoms at 3.31-3.33 Å depending on the sorbent. In the goethite and HFO samples, another weak shell can be seen in the RSF at a slightly longer bond distance, but was not significant enough to fit with precision. The position is similar to the distance observed in Se-substituted schwertmannite as well. The presence of inner-sphere selenate on goethite is consistent with the work of Manceau and Charlet (1994), and they reported a similar Se-Fe bond distance of 3.29 Å compared to 3.31 Å in this work. On hydrous ferric oxide (HFO), however, they found that their data were best described with 0.4 Fe at 2.80 Å and 1.8 Fe at 3.29 Å. They attributed the distance of 2.80 Å to an edge-sharing (bidentate mononuclear) surface complex, and the distance of 3.29 Å to that of a corner-sharing (bidentate binuclear) surface complex. This feature was not observed in our EXAFS samples, but there were differences in the reaction conditions between our study and Manceau and Charlet (1994). First of all, the sorption experiments of Manceau and Charlet were conducted on fresh (non freeze-dried) HFO that all had Se loadings of 1.3 %wt Se, whereas the selenate sorption samples on HFO in this study contained only 0.37 %wt Se. The tendency of selenate to form edge-sharing complexes on HFO may be dependent upon the surface loading, with less favorable

surface sites becoming more active in adsorption as surface loading increases. A second difference is the background electrolyte, NaCl in this study versus $NaNO_3$ in Manceau and Charlet (1994). Chloride is not an indifferent electrolyte (Bargar et al. 1998), and could possibly affect the tendency of SeO_4 to react with the edge sharing sites of HFO. We used a background of sodium chloride to be able to compare our results with ATR-FTIR spectroscopic studies, and also with previous ATR-FTIR (Hug 1997, Peak et al. 1999, Ostergren et al. 2000, Wijnja and Schulthess 2000) and Raman (Wijnja and Schulthess 2000) spectroscopic analysis of sulfate adsorption on iron oxides and hydroxides. Finally, our HFO sample was prepared from ferric chloride (to avoid nitrate contamination), and it is possible that the presence of chloride affects the structure of the amorphous HFO gel.

Table 2.1 Structural parameters of SeO_4 sorbed on iron oxides and for reference selenate compounds

				First Shell			Second Shell		
				Se-O			Se-Fe		
Sorbent	Loading (μmol/m^2)	q/qmax (%)	Reaction Conditions	R(Å)[a,d]	N[b,f]	$\Delta\sigma^2$ (Å^2)[c,e]	R(Å)[d]	N[e]	$\Delta\sigma^2$ (Å^2)[e]
goethite	1.56	62%	pH3.5, I=1	1.64	4	0.002	3.31	1.2	0.005
goethite	1.56	62%	pH3.5, I=0.1	1.64	4	0.0020	3.32	1.6	0.008
goethite	1.56	62%	pH3.5, I=0.005	1.64	4	0.0008	-	-	-
goethite	0.50	100%	pH6.0, I=0.1	1.64	4	0.0040	-	-	-
goethite	0.78	31%	pH3.5, I=0.1	1.64	4	0.0020	3.31	1.5	0.008
goethite	2.50	100%	pH3.5, I=0.1	1.64	4	0.0030	3.31	1.3	0.007
hematite	0.78	31%	pH3.5, I=0.1	1.65	4	0.004	3.3	1.7	0.01
HFO	0.78	31%	pH3.5, I=0.1	1.64	4	0.0020	3.30	1.87	0.0080
References									
Se-Schwertmannite				1.64	4	0.0080			
aqueous SeO_4^{2-}				1.64	4	0.0070			
Na_2SeO_4 salt				1.64	4	0.002			

[a] Interatomic distance; [b] Coordination number; [c] Debye-Waller factor
[d] Fit quality estimated accuracy: [e] ±0.02Å, [f] ±20%

Selenate ATR-FTIR spectroscopic studies. Vibrational spectroscopy is a useful complementary technique to EXAFS spectroscopy, because several structural configurations of oxyanions (for example monodentate versus bidentate) may result in similar Se-Fe bond lengths depending on the bond angles and geometry and the amount of distortion of the oxyanion tetrahedron. However, the different possible surface complexes will result in different molecular symmetries and therefore quite different vibrational spectra. Figure 2.4 shows the spectrum of aqueous selenate (in D_2O) compared to a spectrum of selenate adsorbed to hematite at pD 3.5, an ionic strength of 0.1 M, and an initial SeO_4 concentration of 250 μM. For aqueous SeO_4, there is only one broad peak occurring at 865 cm^{-1}. This peak corresponds to the infrared-active symmetric stretching ν_3 band of tetrahedral (T_d) SeO_4 molecule. When adsorbed on hematite at pD 3.5, selenate has a symmetry of C_{3v}, with the ν_3 splitting to two peaks at 880 and 850 cm^{-1}, and the ν_1 peak at 820 cm^{-1} becoming infrared active. The observed C_{3v} symmetry is the result of a monodentate selenate surface complex, which has previously been observed for sulfate adsorption on hematite (Hug 1997). Unfortunately, ATR-FTIR experiments using goethite and HFO as the sorbent phase were unsuccessful due to overlap of infrared peaks of the iron oxides with the Se-O vibrational modes. Even without direct ATR-FTIR spectroscopic studies, it is reasonable to conclude that since selenate and sulfate both form monodentate complexes on hematite, that selenate can be expected to form the same types of surface complexes on goethite and HFO as does sulfate. A sulfate monodentate inner-

sphere surface complex has previously been observed at low pH on goethite by several researchers (Peak et al. 1999, Wijnja and Schulthess 2000, Ostergren et al. 2000). An additional component of hydrogen bonding to an adjacent surface site is sometimes proposed rather than a simple monodentate surface complex (Peak et al. 2000, Ostergren et al. 2000). Hydrogen bonding can easily be seen with vibrational spectroscopy due to the effects that the proton has on the vibration of the adjacent Se-O bond, but it is unlikely to affect the EXAFS spectra enough to be observable since a proton is not likely to change bond distances between Se and Fe. Hydrogen bonding to an adjacent site would also tend to bring the selenate tetrahedron closer to the surface and therefore produce Se-Fe bond distances intermediate between monodentate and bidentate. This lends credence to our assignment of a monodentate inner-sphere surface complex for SeO_4 adsorbed to iron oxides at pH 3.5. Wijnja and Schulthess (12) used Raman spectroscopy to study SeO_4 adsorption on goethite and found outer-sphere complexation at pH 6.0 and above and an inner-sphere monodentate surface complex at pH below 6.0. This is in good agreement with our EXAFS results in this study as well as consistent with previous *in situ* spectroscopic studies of sulfate adsorption on goethite.

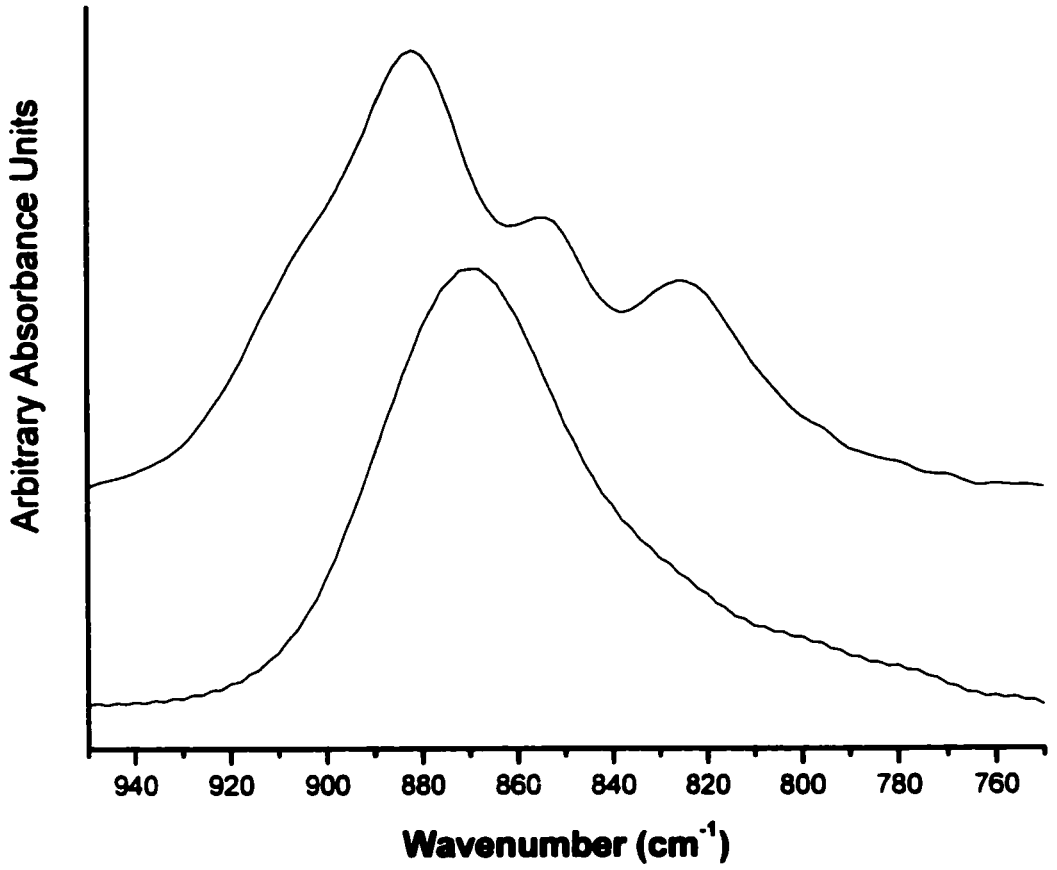

Figure 2.5. ATR-FTIR spectra of (a) selenate adsorbed on hematite at pD 3.5, I = 0.1M, and Ceq = 250 μM SeO_4 and (b) 10 mM $SeO_4^{2-}{}_{(aq)}$. Spectra are the result of 1000 co-added scans at 4 cm^{-1} resolution

Importance of outer-sphere adsorption. One of the primary goals of this research was to investigate the continuum between outer-sphere and inner-sphere complexation of selenate on different iron oxides. This continuum of adsorption mechanisms is difficult to demonstrate with EXAFS spectroscopy, as the only effect that increasing the ratio of outer-sphere to inner-sphere surface complexes has on Se EXAFS spectra is a decrease in the intensity of iron contribution in the Fourier transforms. As outer-sphere selenate concentrations increase, the Se-Fe contribution to the overall spectra is being diluted by adding only more Se-O signal since no iron backscattering can be seen from the outer-sphere selenate. All comparisons of second shell intensities should made with caution, as there is a large error in the intensity associated with RSFs. However, there is no other way to judge the contribution of outer-sphere selenate to the overall adsorption mechanism. If one looks at the RSFs in Figures 2.2 and 2.3 then it becomes clear that as pH increases from 3.5 to 6.0, that the importance of inner-sphere selenate to the EXAFS spectrum decreases. Similarly, as ionic strength is decreased from 1M to 0.005M, one can see that there is less inner-sphere selenate on goethite. This is consistent with the continuum of adsorption mechanisms proposed for sulfate adsorption on goethite (Peak et al. 1999). Figure 2.4 also displays a similar trend when compared to sulfate FTIR data. In the case of hematite, only inner-sphere monodentate surface complexes are seen, and the EXAFS spectrum of selenate on hematite has a single strong well-defined second shell. In the case of HFO, the second shell is much less prominent; suggesting that while there is inner-sphere

selenate, there is also a substantial outer-sphere component. This is consistent with ATR-FTIR spectroscopic studies of sulfate adsorption on HFO (Peak et al. 2001), where it was observed that complexation mechanisms are similar between goethite and HFO, but that HFO had a much larger amount of outer-sphere sulfate complexation. So while the exact amount of outer-sphere selenate is impossible to determine with EXAFS, the relative size and order of the second shell observed in all our spectra seem consistent with a mixture of outer-sphere and inner-sphere selenate on goethite and HFO that is affected by pH and ionic strength. No noticeable change occurs with surface loading (Figure 2.3b) at low pH, suggesting that at least for selenate, that this reaction variable is less important in determining adsorption mechanisms than pH or ionic strength.

It is becoming increasingly clear that adsorption mechanisms of oxyanions on metal oxides need not be either outer-sphere or inner-sphere but instead can be a mixture of both. It was theorized by Sposito (1984) that some oxyanions such as sulfate adsorb with intermediate strength, sometimes forming inner-sphere complexes and sometimes forming outer-sphere complexes. This continuum of adsorption mechanisms has been demonstrated with direct spectroscopic evidence in the case of sulfate adsorption on goethite (Peak et al. 1999) and HFO (Peak et al. 2001), selenate adsorption on goethite (Wijnja and Schulthess 2000), arsenite adsorption on aluminum oxides (Arai et al. 2001) and iron oxides (Goldberg and Johnston 2001). It is therefore of vital

importance to widely vary reaction variables such as pH, ionic strength, and surface loading in sorption experiments to accurately describe the effects that reaction conditions have on the distribution of adsorption mechanisms. Environmental scientists who are developing surface complexation and larger-scale transport models can then use this complete understanding of how oxyanions adsorb over all reaction conditions.

CHAPTER 3

ATR-FTIR SPECTROSCOPIC STUDIES OF BORON ADSORPTION ON HYDROUS FERRIC OXIDE

Boric acid $B(OH)_3$ and its anion borate $B(OH)_4^-$ have solution chemistry that is quite different from most other oxyanions. Borate forms by the addition of a hydroxyl group to the trigonal planar boric acid molecule, forming a tetrahedral anion. The pK of this reaction is approximately 9.3.

$$B(OH)_3 + OH^- \leftrightarrow B(OH)_4^- \qquad pK = 9.3$$

Boric acid and borate both typically exist as monomers in solution at concentrations below 25 mM, but at higher concentrations many poly-borate polymers are known to form (Cotton and Wilkinson 1980). Boron is an essential micronutrient for plant growth. Like many micronutrients, boron is required in low concentrations for the growth of plants but can be quite toxic to plants at higher levels. The range between these extremes is quite narrow. Borate toxicity is a major concern for agriculture in both arid regions of the United States and in poorly drained soils of high salinity. High levels of borate are also commonly found in irrigation water. Borate deficiency has also been reported in over forty U.S. states (Keren and Bingham 1985).

Most of the research of boron chemistry by soil chemists has provided information about the sorption of boron on soils and soil components. In all cases, researchers have noted that boron adsorption results in a bell-shaped pH envelope, with an adsorption maximum occurring near the pKa of boric acid (pH 9.3). Researchers have shown that the mineralogy of the sorbent has a large role on both the extent and mechanism of borate adsorption. Goldberg and colleagues (Goldberg et al. 1993) found that ionic strength effects could be used to separate boron adsorption mechanisms on soil components and on soils. They used batch adsorption experiments and electrophoretic mobility experiments to study these ionic strength effects. On variably charged sorbents such as metal oxides and kaolinite, an inner-sphere complexation mechanism is suggested by the small influence of ionic strength on adsorption as well as by a shift of the point of zero charge to lower pH. In contrast, on montmorillonite and whole soils a large ionic strength dependence suggested an outer-sphere adsorption mechanism for boron. Electrophoretic mobility experiments on these permanently charged sorbents were not feasible, as they have a negative charge over all pH. Interestingly (and somewhat counter to intuition), boron adsorption at high ionic strength is always greater than at low ionic strength. Research by Keren and coworkers examined this phenomenon in more detail. By comparing the adsorption of boron on illite and montmorillonite (common 2:1 clay minerals) in CaCl and NaCl solutions of constant ionic strength (Keren and O'Connor 1982), it was shown that Ca stimulated boron adsorption on montmorillonite far more than Na. This

was explained by the fact that in alkaline conditions borate adsorption is limited by the negative permanent charge of the planar sites of both montmorillonite and illite. At higher ionic strength (and in the presence of divalent cations) this surface charge is minimized by non-specific adsorption of cations, the electrical double layer is compressed, and borate reaction with aluminol groups on the edge sites of the clay become more favorable. In the case of illite, much of the interlayer sites are filled with fixed potassium. This potassium satisfies much of the permanent charge of this clay mineral and as a result there is less effect of ionic strength on borate adsorption. The importance of sorbent mineralogy was also investigated by studying the adsorption of boron on pyrophyllite (Keren and Sparks 1994). Since pyrophyllite is an ideal 2:1 clay mineral, it has no permanent charge due to isomorphic substitution and no interlayer space. This results in far less charge repulsion and therefore a greater boron adsorption capacity.

Very little spectroscopic studies of boron interactions with soil components have been attempted. Beyrouty et al. (1984) used transmission mode FTIR spectroscopy to investigate the effect that boric acid adsorption had on the crystallization of an aluminum hydroxide gel. It was determined that boric acid adsorption retarded the transformation of amorphous aluminum hydroxide to gibbsite. The researchers concluded that due to this inhibition of gibbsite formation the boron must form direct bonds to the aluminum hydroxide. Potentiometric titrations also showed that the PZC

of the gel was lowered in the presence of boric acid, also suggesting specific adsorption. However the researchers could not determine the exact nature of boron adsorption with FTIR and concluded that precipitation, adsorption, and surface polymerization were all possible. In a similar experiment, Su and Suarez (1997) used diffuse reflectance FTIR (DRIFT) to study boron sorption and release from allophane, an amorphous aluminosilicate. They compared the sorption of boric acid on allophane after allophane precipitation to the precipitation of allophane in the presence of boric acid. They determined that both trigonal and tetrahedral boron was present, with trigonal boric acid being the dominant sorbed species. More boron was sorbed when the allophane was co-precipitated with boric acid, and the resulting product had more tetrahedral boron (borate) than the samples where boron was sorbed to allophane after precipitation. It was assumed that borate could substitute for silicate in the allophane structure. It must be stressed that it is possible that sample preparation (dilution in KBr after sample drying or dilution of moist samples) could have affected the results of both these experiments.

Su and Suarez (1995) also used ATR-FTIR spectroscopy to study the adsorption of boric acid on soil components *in situ*. They examined boron adsorption on amorphous aluminum and iron oxides, allophane, kaolinite, quartz, and calcite over a range of pH and boron surface loadings. Unfortunately, interference of Si-O and Al-O infrared bands with tetrahedral boron peaks made a clear interpretation of the aluminum oxide,

allophane, and quartz adsorption spectra impossible. In the iron hydroxide samples, they saw clear evidence of trigonal boron at pH 7, a mixture of both trigonal and tetrahedral boron at pH 9, and the spectra were dominated by tetrahedral boron at pH 11. The possibility of polymeric boron and boron precipitation was mentioned, but could not be distinguished from boron adsorption in their studies.

The objectives of this study were to examine complexation of boric acid and borate with hydrous ferric oxide (HFO) *in situ* over a range of pH (6.5-11.5) and at concentrations well below bulk polymerization of boron (50 μM-1 mM). Previous studies of HFO/boron interactions (Su and Suarez 1995) found that adsorption of both boric acid and borate occurs on HFO, but some of their their spectra were collected at concentrations close to bulk polymerization (up to 23mM B). If one is to utilize FTIR spectroscopy to accomplish these objectives, it is important to fully understand how infrared spectra of different boron compounds are affected by their molecular structure.

Infrared theory. The majority of boron infrared studies concentrate on distinguishing boric acid from borate at the mineral surface. This is reasonably straightforward, as there is ample infrared spectral data for minerals containing trigonal B (BO_3^{3-} and $B(OH)_3$), tetrahedral B (BO_4^{5-} and $B(OH)_4^-$) groups (Ross 1974). From the variation

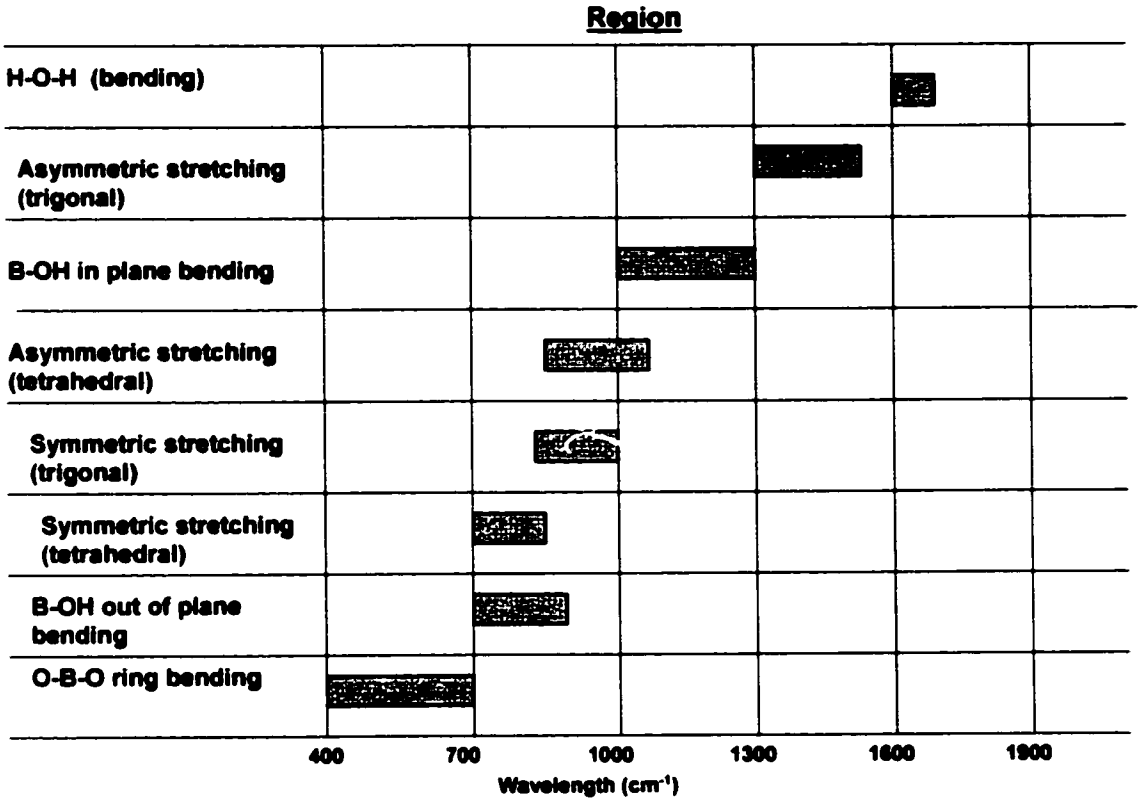

Figure 3.1. Summary of infrared peaks of boric acid and borate that are accessible to *in situ* infrared studies.

of mineral spectra with structure, it is possible to get a good grasp of what vibrational bands are accessible in the mid-infrared region and how to interpret them. As one can see from Figure 3.1, some of these regions of infrared absorbance overlap. This fact makes conclusive peak assignment in samples with mixtures of trigonal and tetrahedral boron quite problematic. This is especially difficult when attempting to assign peaks for tetrahedral boron, as peaks from B-O-H bending, trigonal B-O stretching, and tetrahedral B-O stretching all occur in the 700-1000 cm^{-1} region.

None of the previous boron/mineral adsorption studies thoroughly discuss the relationship between infrared spectra and the structure of boric acid on the surface of minerals. This is likely due to the fact that the relationship between molecular symmetry and infrared spectra of boron containing compounds has not been specifically discussed in the infrared literature, as is the case for phosphate (Nakamoto 1987) and sulfate (Nakamoto 1987). This means that the symmetry rules must be worked out for the bands that are accessible for mid-infrared spectroscopic studies in aqueous suspensions. Experimental constraints mean that the region from 800 to 1600 cm^{-1} is available for study. It is convenient to consider the O-H ligand as a single entity for purpose of determining symmetry rules. This is reasonable since the center of mass for B-O-H is not greatly shifted from the position of B-O molecules and also because in aqueous solution the movement of H around the O atom is essentially unconstrained. One complication occurs with boric acid, since the hydroxyls are not

symmetrical and instead the protons are at an angle resulting in a horizontal axis of rotation.

For boric acid, the trigonal planar molecule has C_{3h} symmetry, and should have one IR active peak (1500-1300 cm^{-1}) for the asymmetric B-O stretching (ν_3) as well as an inactive or weakly IR active (depending upon the molecules distortion) symmetric B-O stretching (ν_1) band (1100-950 cm^{-1}). In pressed disks of solid boric acid, this ν_1 peak is clearly visible, but in aqueous solution it is not usually observed. If one proton of the boric acid molecule is substituted with metals (in our study Fe) then the symmetry of the molecule is lowered to C_{2v}. This reduction in symmetry causes the asymmetric ν_3 band to become doubly degenerate, and two peaks should be seen in the infrared spectrum between 1250 and 1500 cm^{-1}. The symmetric stretch also becomes fully infrared active so there are a total of three B-O vibrations visible in a monodentate metal-boric acid complex. For bidentate metal boric acid complexation, the symmetry remains C_{2v}, and so the number of peaks remains unchanged. The splitting of the two ν_3 bands is expected to increase and/or shift when the number of iron atoms increases, but that is not sufficient to distinguish monodentate from bidentate boric acid. Nonetheless, infrared spectroscopy is capable of separating aqueous, weakly bound, and inner-sphere boric acid from one another. The predicted changes in the infrared spectra of boric acid complexes with different symmetry are summarized in Figure 3.2a.

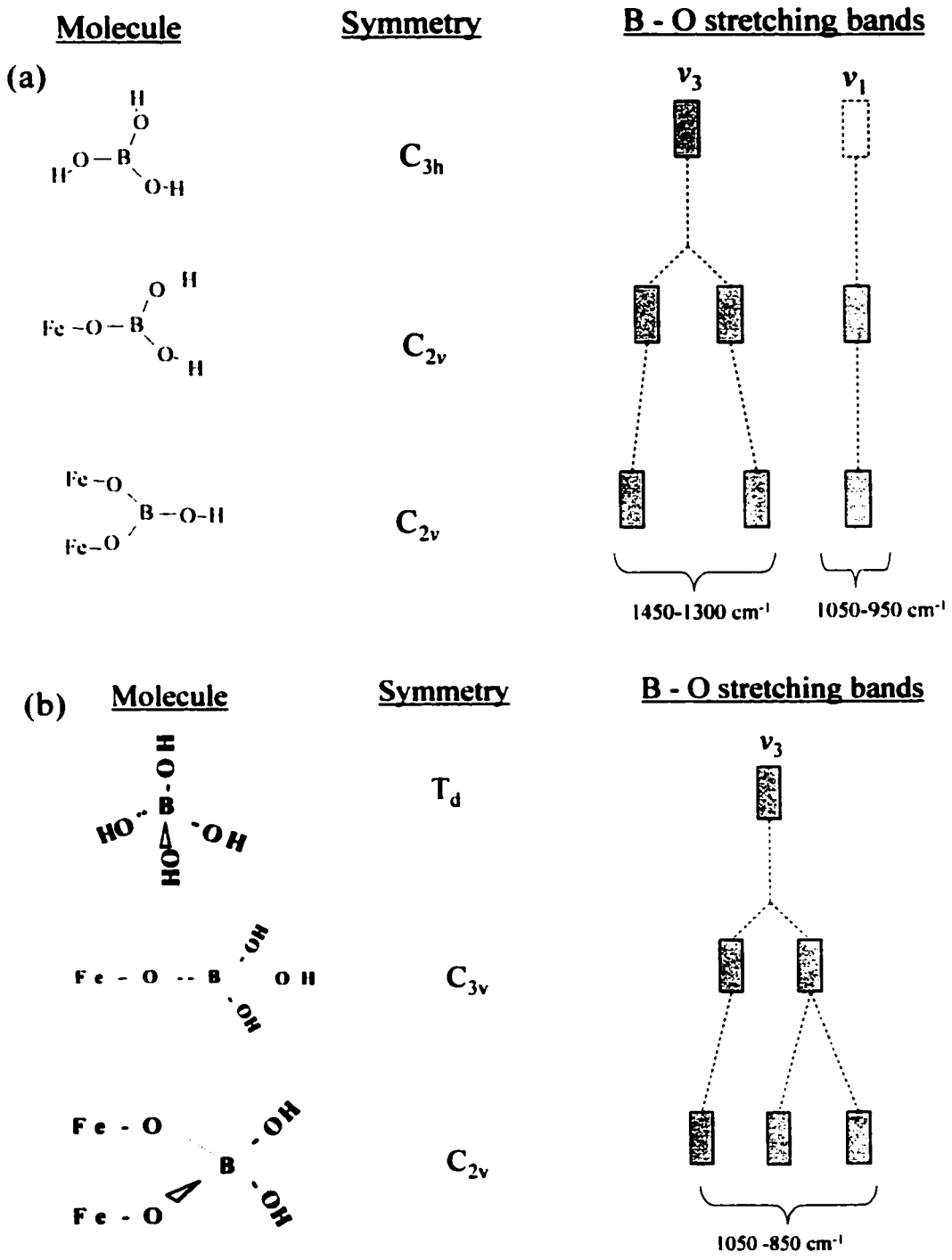

Figure 3.2. Relationship between molecular symmetry and B-O vibrations in the mid-infrared region.

The symmetry of the tetrahedral borate molecule is much more straightforward, as it is identical to sulfate and phosphate, which have been extensively studied with infrared spectroscopy (references). As the free borate anion, the molecule has T_d symmetry and one broad ν_3 asymmetric stretching band at approximately 950 cm^{-1}. The symmetric stretching (ν_1) band will be either weakly active or completely inactive, but it typically is obscured by water in any case. The symmetry of borate is lowered to C_{3v} by forming a monodentate complex with a single Fe atom and the ν_3 band splits into two peaks. If a bidentate complex is formed with two of the protons on borate being substituted by Fe, then the resulting complex has C_{2v} symmetry, the ν_3 band becomes fully degenerate, and three peaks will appear in the infrared spectrum. The predicted changes in the infrared spectra of borate complexes with different symmetry are summarized in Figure 3.2b.

The above discussion has separated the contributions of B-O-H bending modes to the overall spectra of boron compounds. However, in the actual spectra there are additional broad peaks that arise from in plane B-O-H bending (1300-1000 cm^{-1}) and out of plane bending (850-700 cm^{-1}). These vibrations overlap with some of the other B-O stretching vibrations and can make data analysis more difficult.

Materials and Methods

All chemicals used in these experiments were reagent grade or better, and deionized distilled water (18MΩ) was used for all studies.

Mineral Synthesis. The hydrous ferric oxide (HFO) used in all experiments was synthesized by the following method. A 500 mL solution of 1M $Fe(NO_3)_3$ was prepared and placed into a 2L container. A lid was placed on the container with ports for a N_2 purge line, a mechanical overhead stirrer, a pH meter, a dispensing tip for a pH stat, and a sampling port with lid. The solution was stirred at ~300 rpm with the overhead stirrer and purged with nitrogen for approximately an hour, then a funnel was placed into the sampling port. Enough 1M KOH was slowly poured into the container to raise the pH to a value of 5, and then the pH stat (Metrohm model 716) was engaged to dispense 1M KOH to an endpoint of pH 7.5. The endpoint of pH 7.5 was maintained for one hour, and then the iron hydroxide precipitate was separated into several 250mL high speed centrifuge bottles and washed via centrifugation (10,000 rpm for 5 minutes) with 0.1M NaCl. This washing procedure was repeated twice to remove any potassium and non-precipitated iron. Then, the solid was washed three more times using the same procedure with d-dei H_2O and then placed into dialysis tubing and dialyzed in distilled water for 48 hours. After dialysis, the solid was placed into a 1L container; the pH was lowered to 5.5 with 0.1M HCl to minimize the amount of carbonate contamination, and stored at 5C until use in experiments. The solid

density of this stock suspension was determined to be 18 g/L, and the surface area (N_2-BET) of the freeze-dried solid was 255 m^2/g. The PZC was determined to be 8.5 via potentiometric titrations in $NaClO_4$.

Sorption experiments. All sorption experiments were done inside a glove box under N_2 atmosphere to eliminate CO_2 from the system. Initially, suspensions of HFO, background electrolyte (NaCl), and distilled-deionized H_2O (18MΩ) were prepared with a final solid density of 1 g/L. The calculation for amount of background electrolyte added to obtain a final ionic strength of 0.01 M was based upon the concentration of borate anion in the final sample as well as an estimation of the amount of acid or base needed to adjust the pH of the final sample. This suspension was adjusted to the desired pH and placed on a rotating shaker for ~ 8 hours and then pH was measured and adjusted again. After 24 hours, the suspensions were again adjusted to the proper pH, and boric acid was added from a 10 mM stock solution to the unreacted solids, and pH was again adjusted. At this time, a calculation was made to account for the contribution of NaOH or HCl to the suspensions ionic strength and then to determine how much additional NaCl should be added to the suspension to obtain an ionic strength of 0.01 M. The samples were then shaken for ~8 hours and the pH was adjusted with either 0.01M NaOH or 0.01M HCl. The samples were adjusted for pH again at 24 hours and 32 hours while the reaction proceeded, and then

after 48 hours the pH was measured and the samples were filtered and the supernatent was acidified and analyzed via ICP spectrometry.

ATR-FTIR spectroscopy. A Perkin Elmer 1720X FTIR spectrometer was used for all spectroscopic studies. The instrument was equipped with a Whatman purge gas generator to remove water vapor and CO_2, a $N_{2(l)}$-cooled MCT detector, and a horizontal ATR-FTIR accessory from Spectra-Tech. Aqueous samples were placed in a trough sampler with a 45 ° ZnSe crystal, and adsorption studies were conducted using a Spectra Tech ATR-flow cell with a 45 ° ZnSe crystal. A more detailed explanation of the deposition method can be found in previous papers (Hug et al. 1994, Hug 1997, Peak et al. 1999, Elzinga et al. 2001, Peak et al. 2001, Wijnja and Schulthess 2001). The primary advantage of the deposition technique is that it results in an extremely high solid concentration at the ZnSe crystal surface. Since adsorbate also accumulates at the mineral/water interface, the concentration of surface species in the path of the infrared beam is much higher than when applying pastes or slurries of mineral sorption samples. As a result, bulk solution concentrations of reactant can remain well below infrared detection limits while adsorption reactions proceed. The spectra collected are therefore only surface complexes of reactant, and typically have sharper and more easily resolved peaks than other ATR-FTIR approached. All infrared spectra were analyzed using Peaksolve (Galactic Industries) by fitting a linear

baseline through the data and then normalizing the spectra so that absorbance was equal to zero at 800 and 1800 cm^{-1}.

For the flow cell experiments, a small quantity (~3mg) of HFO was deposited on the surface of the ZnSe crystal and allowed to air dry. Then, the deposit was carefully washed several times with background electrolyte to remove any non-adhering HFO, allowed to dry again, and placed into the flow cell. The flow cell was then placed into the FTIR, and tygon tubing was used to connect the flow cell to a peristaltic pump and reaction vessel. The reaction vessel was nitrogen purged, well mixed with a stir bar, and pH was monitored with a Corning pH electrode. Additions of 0.01M acid or base were made with Rainen electronic pipette to adjust pH to the desired value. Initially, a background electrolyte of 0.01M NaCl was pumped through the flow cell at a rate of 1.0 mL min^{-1}. An infrared spectrum of the entire flow cell assembly (background electrolyte solution, HFO, and ZnSe crystal) was collected and then ratio to itself at later times to monitor changes in the infrared spectra. Initially, the spectra will change as a function of time due to carbonate desorption, protonation or deprotonation of the HFO surface hydroxyls, rehydration of the HFO, changes in ionic strength, and removal of a small amount of HFO from the system via the flow of background electrolyte. After approximately two hours, no further change in the spectra was observed, and so a new background was collected to be used for all successive scans. At this time boric acid was added at a known amount, allowed to react with the HFO

surface, and adsorption spectra were collected. An operational equilibrium was applied when no change in the infrared absorbance was found for samples 15 minutes apart in reaction time. Each addition required from 30 minutes to 2 hours to come to equilibrium with the surface, and required reaction time was found to be inversely related to boric acid concentration in solution. After collecting a spectrum of boric acid at a given solution concentration, more boric acid was then added to the reaction vessel and the process was repeated to generate adsorption isotherms inside the flow cell.

Results and Discussion

Results from adsorption isotherms conducted at pH 6.5, 9.4, and 10.4 are shown in Figure 3.3. In all cases, samples were prepared volumetrically and an ionic strength of 0.01M NaCl and a 0.5 gL^{-1} solid density were used. No attempts were made to convert the surface loading from μmoles per gram to μmoles per m^2, as the surface area for a freeze-dried HFO is undoubtedly quite different from that of a freshly prepared HFO gel. From the isotherm there are several aspects of boron adsorption of interest. First of all, boron sorption is close to a maximum at pH 9.4, which is the pK of boric acid. Boron adsorption decreases rapidly above the pK of boric acid, suggesting that perhaps boric acid is the preferred sorptive species. Additionally, the isotherms do not display a particularly high affinity of boric acid for the HFO surface: to achieve a high surface loading, a high solution concentration must also be present.

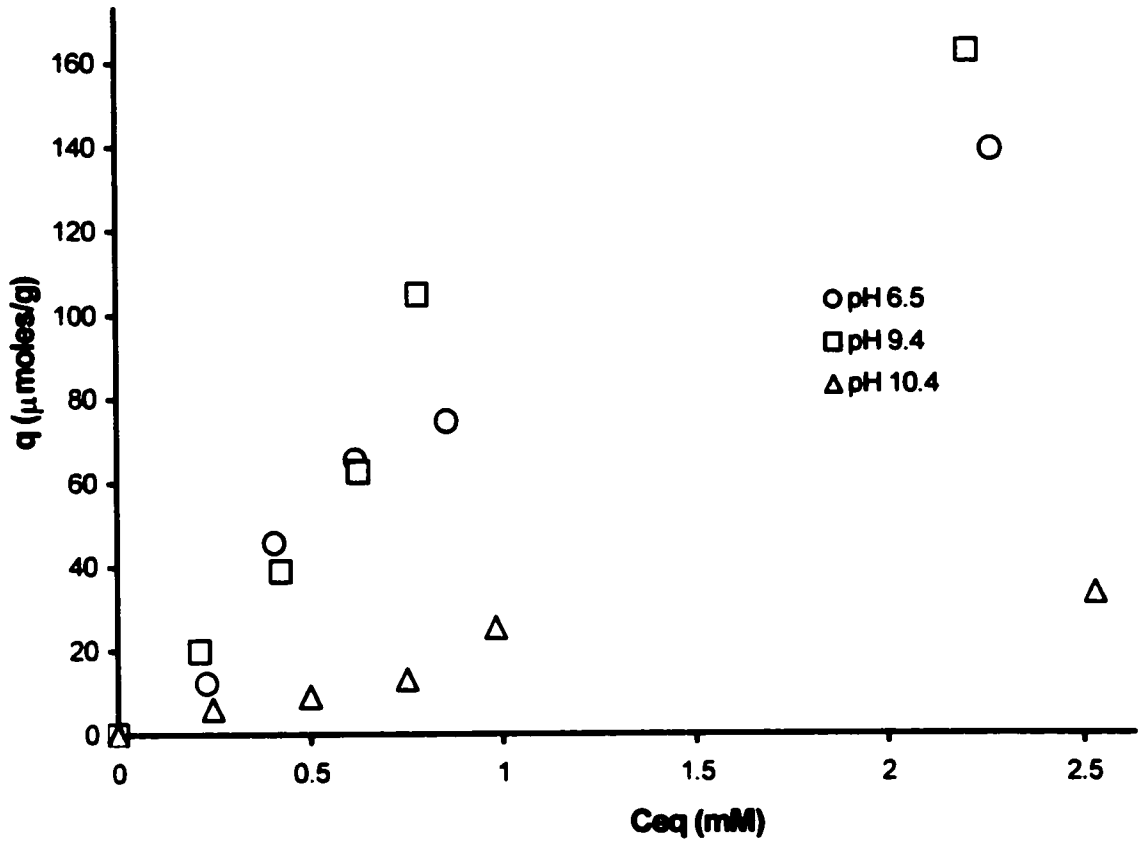

Figure 3.3. Boron on HFO adsorption isotherms at three different pH values. For all experiments, an ionic strength of 0.01M (NaCl) and a suspension density of 0.5 g/L was used. Note the S-shaped isotherms.

In fact, all isotherms exhibit an "S shaped" curve, which suggests that at low concentrations boron has a low affinity for the surface, with an increasing affinity for adsorption as equilibrium solution concentrations increase. There is no clear sorption maximum for any of the isotherms.

Figure 3.4 shows ATR-FTIR spectra of boric acid at pH 6.5 (Figure 3.4a) and at pH 11.5 as its conjugate base borate (Figure 3.4b). For the trigonal planar boric acid, one can clearly see one peak at 1400 cm^{-1} caused by asymmetric B-O stretching (ν_3) as well as the in-plane B-O-H bending at 1150 cm^{-1}. For borate, the asymmetric stretching band occurs at 950 cm^{-1}, while the B-O-H in plane bending appears in a similar location to the trigonal species (~ 1150 cm^{-1}). The in-plane bending peak of borate is much broader than boric acid, suggesting that there may possibly be more than one peak in the region. This is especially pronounced at concentrations above 20mM, which is consistent with the observation (Cotton 1985) that boric acid polymerizes above 25 mM and that polymerization is enhanced at high pH. The presence of some tetrahedral boron polymers would result in multiple OH vibrations, but there is no splitting of the ν_3 band at 950 cm^{-1} that would accompany borate polymerization. This is partly due to the overwhelming concentration of aqueous borate, and so when spectra are normalized to the same maximum absorbance (Figure 3.5) there are slight differences that can be observed. At 100 mM, there is some broadening of the B-O peak that could represent the presence of some polymeric

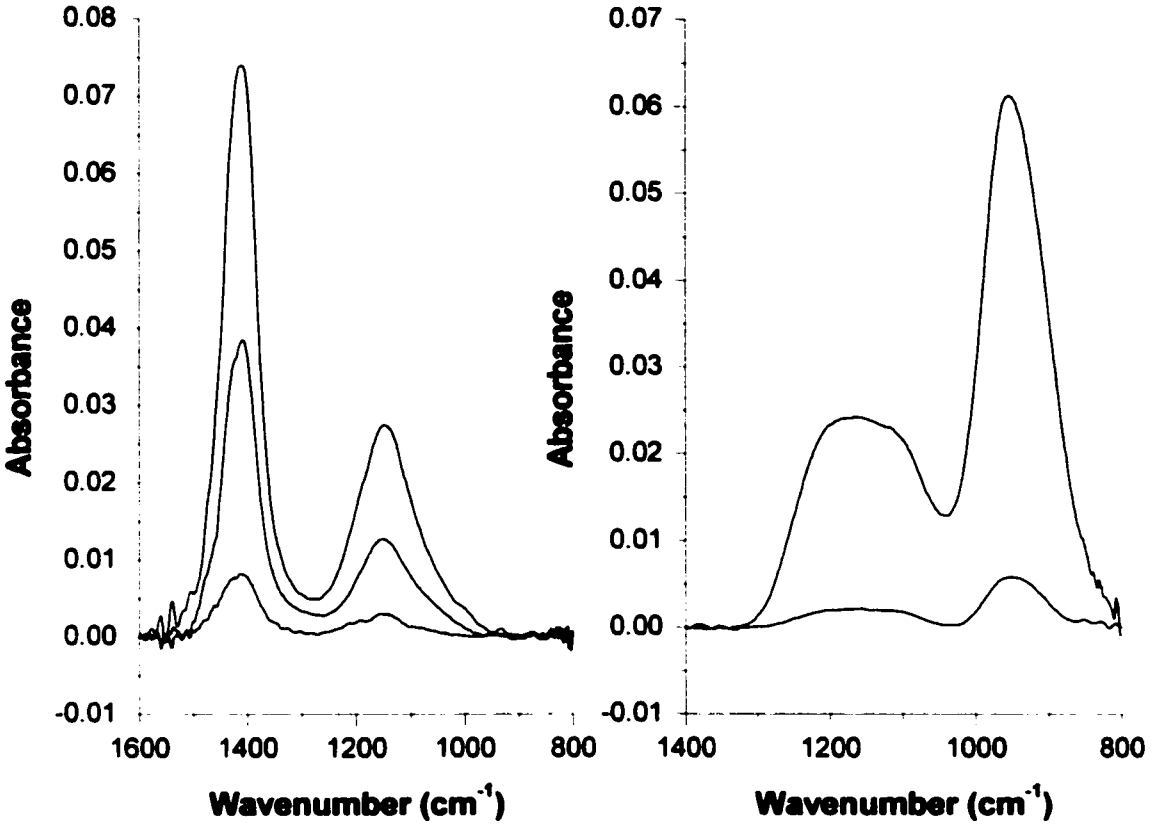

Figure 3.4. ATR-FTIR spectra of (a) boric acid and (b) borate collected at different concentrations. Total boron concentrations are (from bottom) 10, and 100 mM.

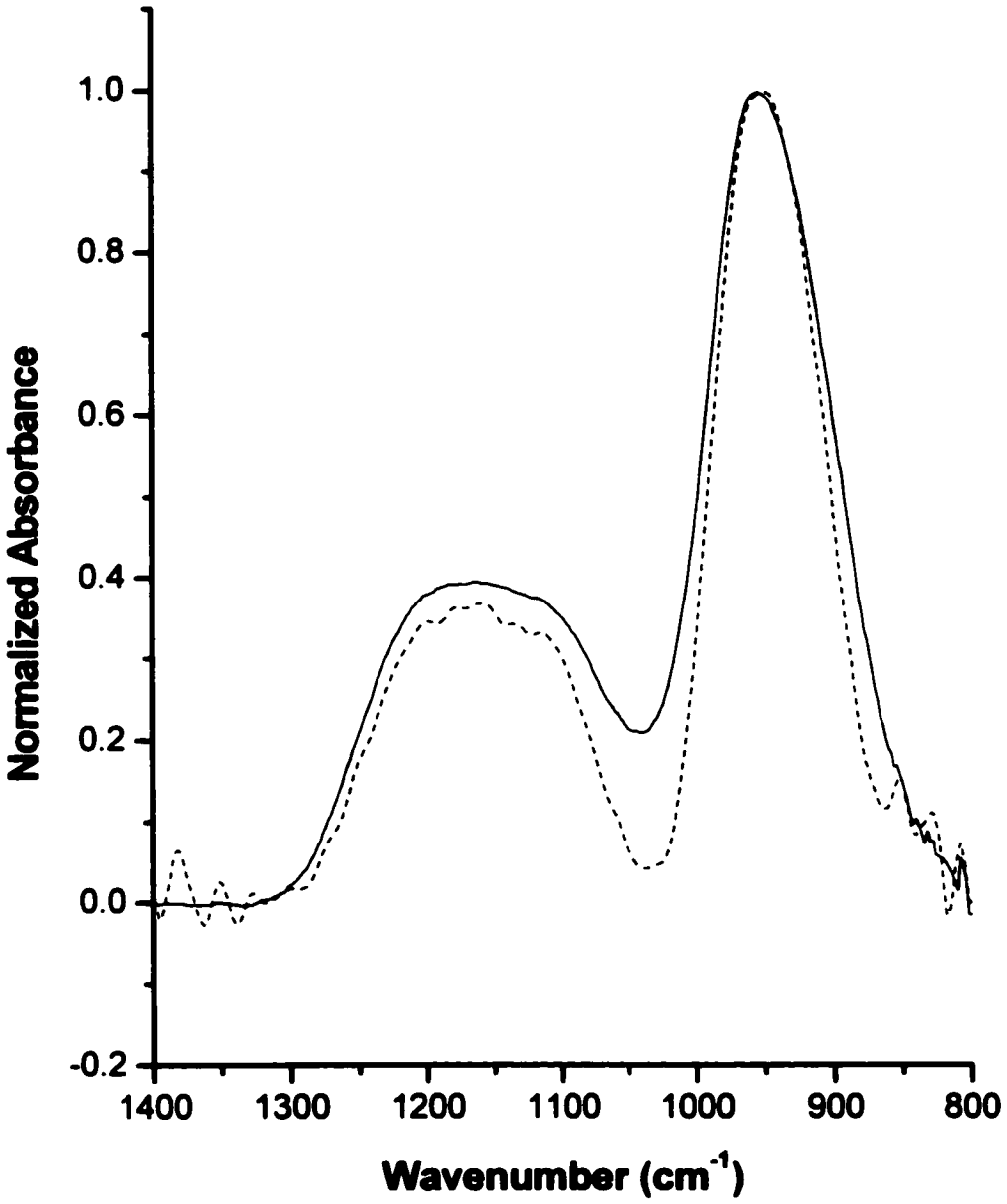

Figure 3.5. Borate spectra from Figure 3.4b that were analyzed by normalizing to a maximum absorbance of 1.0. The solid line is 100 mM borate, and the dashed line is 10 mM borate. Note the broadening of the B-O peak at 950 cm^{-1} in the 100 mM spectrum; peak width at half height is 72.4 ± 0.8 for 10mM borate and 89.6 ± 0.7 for 100 mM borate.

borate. Peak fitting of the normalized and background subtracted spectra (with Gaussian peaks) resulted in a peak width at half height of 72.4 ± 0.8 at 10mM borate and 89.6 ± 0.7 at 100 mM borate. However, there is no clear splitting or separation into multiple peaks, so it can be concluded that it will be very difficult to distinguish spectra of adsorbed borate from aqueous borate. Furthermore, since the splitting is not well-resolved for inner-sphere borate (polymeric forms) vs. aqueous borate, conclusive identification of monodentate versus bidentate boron at the HFO surface may also be extremely difficult.

Infrared spectra from an adsorption isotherm of boric acid on HFO at pH 6.5 and I = 0.01M are shown in Figure 3.6. Figure 3.6a shows the full spectra from 1800-800 cm^{-1}, while Figure 3.6b shows only the 1100 to 800 cm^{-1} region in more detail. There are several features that are common to all of the adsorption spectra that were collected, so they should be discussed first. All of the spectra feature negative absorbance peaks at 1625 cm^{-1} and at 1490 cm^{-1}. These peaks are from the loss of water and carbonate (respectively) from the path of the infrared beam. In the case of carbonate, it is quite likely that there is some strongly bound carbonate present at the HFO surface (from being exposed to air while drying) that is not being desorbed as the system equilibrates. This carbonate could possibly be desorbed as the adsorption of boric acid occurs.

The remaining peaks in the spectra are the result of adsorbed boric acid on the HFO surface. There are three peaks in the region of trigonal B-O v_3 bands, at 1395, 1330, and 1250 cm^{-1}. Since the v_3 band of trigonal boron complexes is only doubly

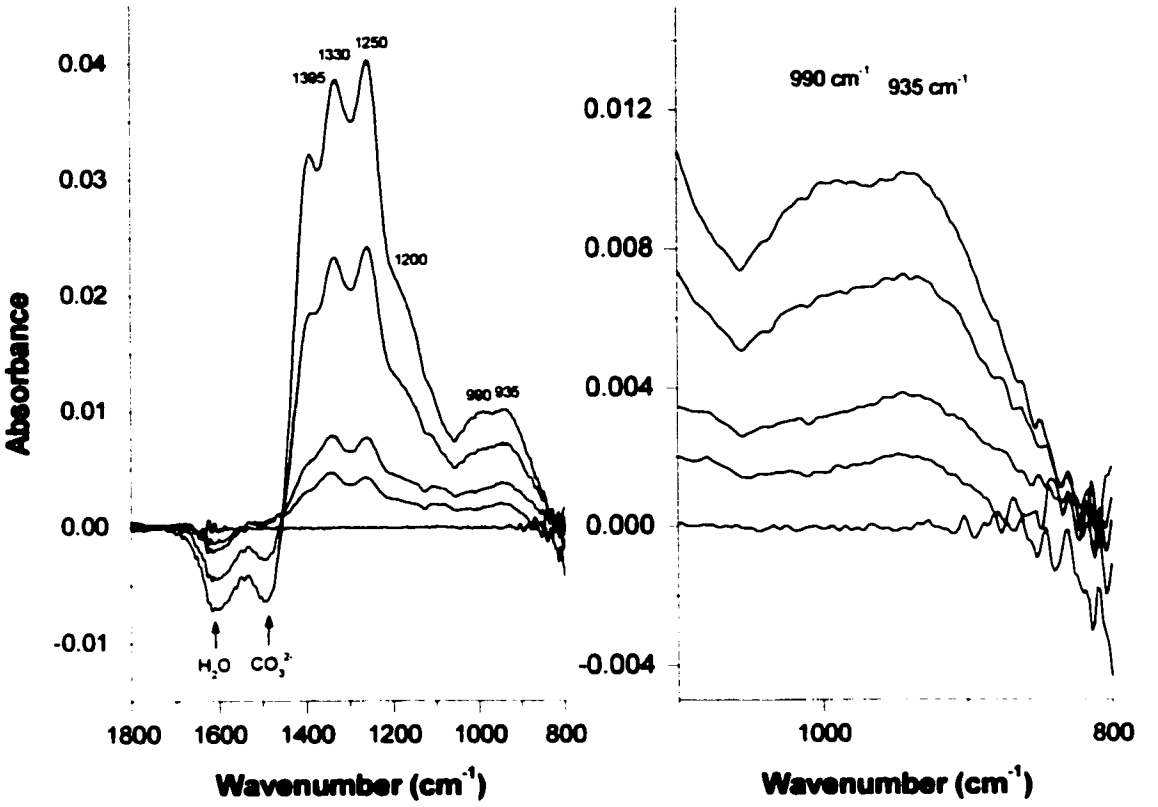

Figure 3.6. ATR-FTIR spectra of boron adsorbed on the HFO surface at pH 6.5 and I = 0.01M as a function of concentration. Aqueous equilibrium boron .concentrations are (from bottom) 0, 50. 100, 500, and 1000 μM. (b) Same samples as in (a) with the 1100-800 cm^{-1} region expanded for clarity.

degenerate, there must be more than one surface species present to account for three distinct peaks in this region. There are two possibilities that could result in multiple surface complexes. It is possible that the peak at 1250 cm^{-1} (which is larger in intensity than the other peaks) is present in the same position for both monodentate and bidentate trigonal boron while the other two peaks represent a monodentate and a bidentate bonding environment. This seems rather unlikely, as bands typically split in opposite directions as symmetry is reduced, and one peak remaining in precisely the same position while the second peak shifted upfield or downfield is not at all typical. Another possibility is that the peak at 1395 cm^{-1} is a separate trigonal species with symmetry similar to aqueous boric acid, while the second complex with peaks at 1330 and 1250 cm^{-1} is the result of an inner-sphere trigonal surface complex. Several common compounds that possibly are present can be eliminated as the source of the 1395 cm^{-1} peak: aqueous boric acid, polymeric trigonal boron, and outer-sphere boric acid. The solution concentrations are below detection limit for aqueous boric acid, and at pH 6.5, boron does not polymerize. Therefore, this C_{3h} symmetry surface complex is best explained by outer-sphere complexation of boric acid to the HFO surface. The observation that a neutral molecule (boric acid) can adsorb as an outer-sphere surface complex on the iron oxide surface at first seems counter-intuitive, as discussion of outer-sphere complexation typically occurs due to electrostatic attraction of an ion for an oppositely charged surface. However, if one considers that boric acid is a Lewis acid (electron acceptor), then attraction to the surface becomes more reasonable. The

Lewis acid boron metal center will have an affinity for the Lewis base oxygen of a surface functional group, and will attract electron density, such as is present in the O atoms of the many surface hydroxyls and bound waters at the HFO/aqueous interface. This Lewis acid/base pairing may be further stabilized by hydrogen bonding. Outer-sphere surface complexes of the neutral $As(OH)_3$ molecule have been observed to form on iron and aluminum oxides using Raman spectroscopy (Johnston and Goldberg 2001) and on aluminum hydroxides using EXAFS spectroscopy (Arai et al. 2001) at pH below the PZC of the metal oxide. Therefore it will be useful to monitor changes in the intensity and position of this peak as pH changes. The B-O-H in-plane bending is present in the adsorption spectra as predicted from theory, but shifted to somewhat higher wavenumber (1200 cm^{-1} vs. 1150 cm^{-1} for aqueous boric acid). The overlapping peaks due to the trigonal B-O vibrations make it impossible to draw much information from the OH bending as the peaks are mostly obscured.

Figure 3.6b expands the spectra from Figure 3.6a so that bands in the 1100 to 800 cm^{-1} region can be more clearly discerned. There are at least two overlapping peaks in this region observed at 990 and 935 cm^{-1}. The first instinct would be to assume that these arise from the ν_3 asymmetric stretch of tetrahedral borate, and that the borate adsorbs on the surface as a monodentate complex with C_{3v} symmetry. Accordingly, the peak at 985 cm^{-1} was previously (Su and Suarez 1995) attributed to tetrahedral borate adsorption in the literature. However, when boric acid forms inner sphere complexes

(as observed by the strong splitting of the trigonal ν_3 peaks) then the symmetric stretching band (ν_1) should also become infrared active in the 1100-950 cm^{-1} range. Based upon the spectra at pH 9.4 and 10.4 (to be discussed later), the peak at 1005 cm^{-1} can be assigned to the ν_1 from inner-sphere boric acid surface complexation. The remaining peak at 940 cm^{-1} is either a result of borate on the surface or is due to vibrations from out of plane B-O-H bending. The broadness of the peak (peak width at half height of 146cm^{-1}) indicates that multiple peaks may be present and overlap to generate a single broad peak. It would be convenient to assign the single broad peak to outer-sphere borate adsorption, but at pH 6.5 solution borate concentrations are extremely small (~0.1%) and it is unlikely that outer-sphere borate accumulation at the surface would occur.

Figure 3.7 shows the spectra of boric acid adsorbed on the HFO surface at 9.4, which is close to the pK of boric acid as well as slightly above the PZC of HFO. The most obvious differences between the spectra at pH 6.5 and pH 9.4 are the disappearance of the peak at 1395 cm^{-1} and the increase in the absorbance in the 800-1000 cm^{-1} region when pH is raised to 9.4. The disappearance of the 1395 cm^{-1} peak (attributed to physically adsorbed boric acid) is consistent with how arsenite's outer-sphere complexation vanishes above the PZC of the sorbent. The remaining trigonal ν_3 peaks at 1250 and 1330 cm^{-1} are again consistent with inner-sphere boric acid adsorption. In Figure 3.7b, the region where tetrahedral boron bands are expected is shown in greater

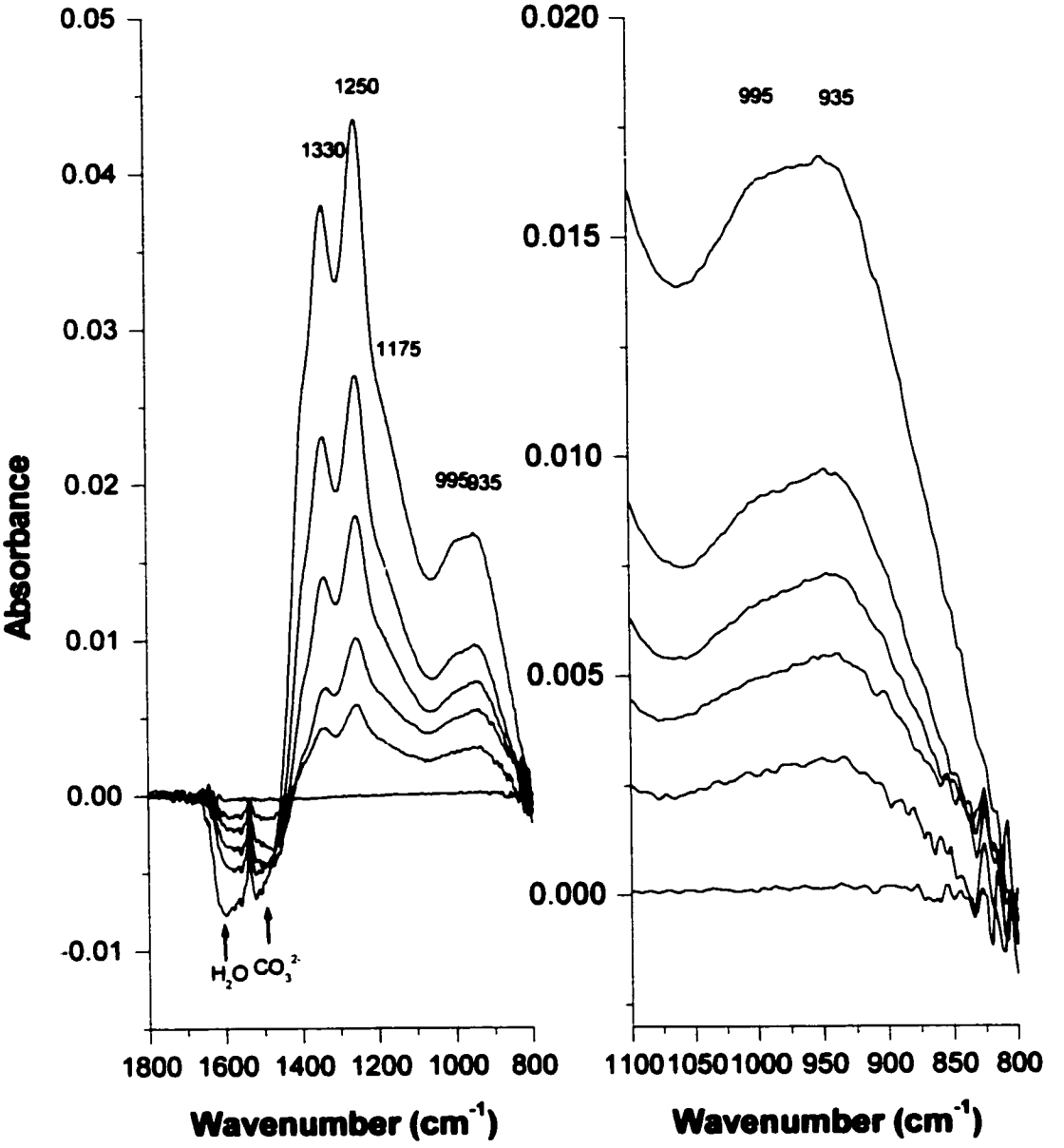

Figure 3.7. ATR-FTIR spectra of boron adsorbed on the HFO surface at pH 9.4 and I = 0.01M as a function of concentration. Aqueous equilibrium boron .concentrations are (from bottom) 0, 50. 100, 250, 500, and 1000 μM. (b) Same samples as in (a) with the 1100-800 cm^{-1} region expanded for clarity.

detail. As with Figure 3.6b, there are two infrared active peaks at 995 and 935 cm^{-1}. The peak at 935 cm^{-1} has a greater intensity at pH 9.4 than it does at pH 6.5, which is consistent with the assignment of the 935 cm^{-1} peak to tetrahedral B-O ν_3. At pH 9.5 the borate concentrations in solution are approximately 50% of the total boron concentration at pH 9.4 and so more borate is expected at the surface than at pH 6.5 when only ~0.1% is tetrahedral in solution. When the results of peak fitting are compared, the area under the peaks at ~1000 vs. ~940 cm^{-1} changes from 0.73:1 at pH 6.5 to 0.68:1 at pH 9.4. Background subtraction becomes difficult due to water interferences in this region, so there is some difficulty in determining the absolute importance of the peak at 935 cm^{-1} to the absorbance in the 800-1100 cm^{-1} range.

Finally, the spectra of boric acid adsorbed on HFO at pH 10.4 are shown in Figure 3.8. The spectra all appear very similar to the pH 9.4 data in Figure 3.7 with the exceptions that the absorbance is less than at pH 9.4 (indicating that less boric acid is adsorbed on the HFO surface) and that far more absorbance occurs in the 1000-800 cm^{-1} region. One can still see two clear asymmetric stretching peaks between 1250 and 1350 as well as the shoulder at 1010 cm^{-1} that is diagnostic for inner-sphere boric acid adsorption. It is noteworthy that the ν_1 band shifted almost 10 cm^{-1} when pH is adjusted from 9.4 to 10.4. Studies of boric acid-containing minerals and polymers typically report values of around 1075-950 cm^{-1} (Ross 1974) for the ν_1 band, so this peak still falls within the predicted range. A shift in position could be caused by a

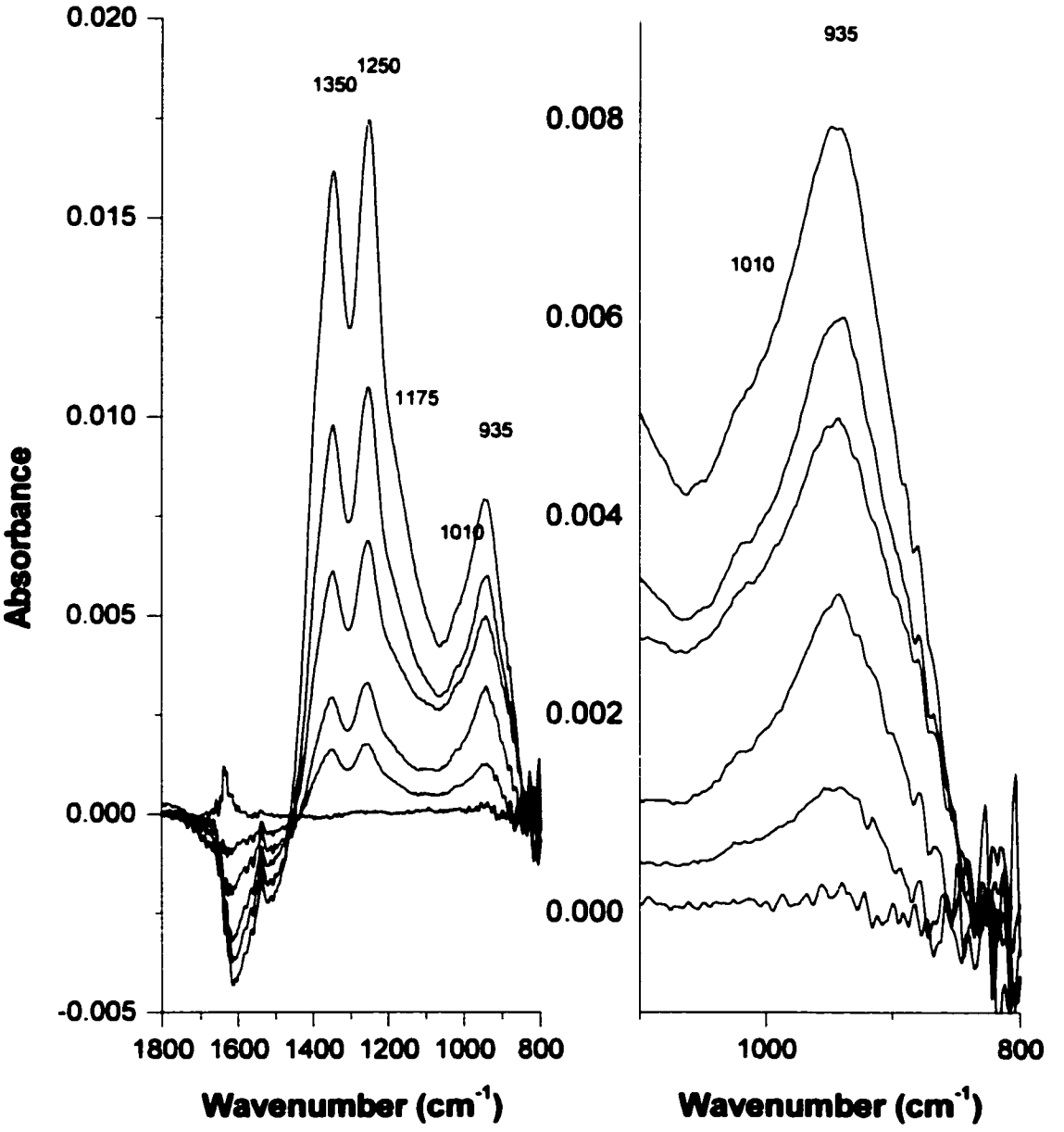

Figure 3.8. ATR-FTIR spectra of boron adsorbed on the HFO surface at pH 10.4 and I = 0.01M as a function of concentration. Aqueous equilibrium boron .concentrations are (from bottom) 0, 50. 100, 250, 500, and 1000 μM. (b) Same samples as in (a) with the 1100-800 cm^{-1} region expanded for clarity.

conformational change of boric acid from monodentate to bidentate at the HFO surface, or it alternatively could be caused by a new trigonal species (such as multinuclear boron clusters with some boric acid moieties). The relatively strong shoulder at 1000 cm^{-1} in the pH 6.5 data is now much weaker than the peak at 925 cm^{-1}. The ratio of peak areas for the fitted peaks produces a ratio of 0.73:1 at pH 6.5, but at pH 10.5 the ratio of areas has been reduced to 0.49:1. No clear splitting of the v_3 band can be observed in the spectra, although the peak is very broad. There are two reasonable explanations for the inability to see distinctive splitting of tetrahedral v_3 vibrational bands in the results. Potentially, there could be a multitude of different borate inner-sphere surface complexes that overlap and produce a single broad band. Alternatively, it was observed in the pH 11.5 solution spectra of Figure 3.5 that even in the presence of borate polymers that little splitting of the v_3 bands occurs. It is possible that polymeric boron of a tetrahedral (or mixed tetrahedral and trigonal) geometry could result in the single peak at 935 cm^{-1}. However, the solution concentrations were well below the established aqueous polymerization level of 25 mM (5-500 μM aqueous boric acid was used in the present studies). Previous researchers (Alvarez and Sparks 1985) have shown with *in situ* spectroscopic techniques that silicate polymerization occurs in concentrations quite a bit lower than originally predicted. The same could be true for boron and so this possibility cannot completely be discounted.

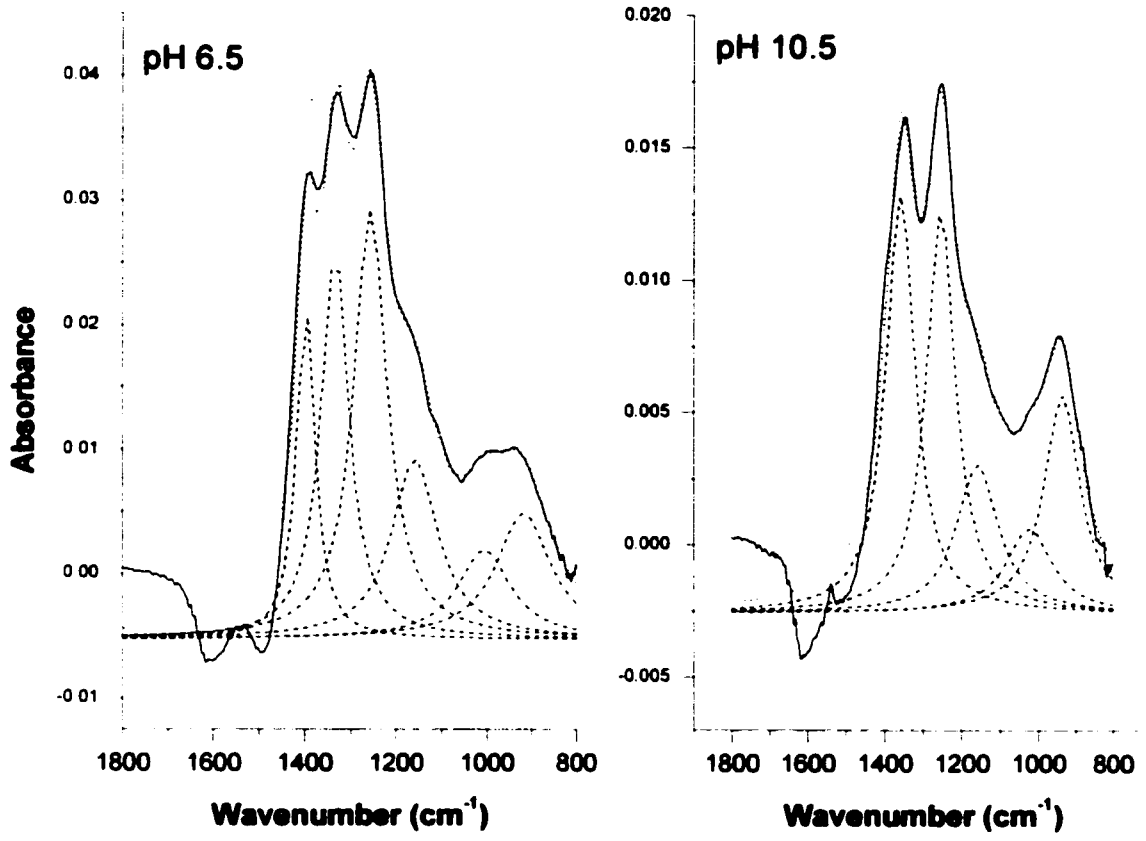

Figure 3.9. Results of fitting Lorentzian peaks to boric acid adsorption data at pH 6.5 and pH 10.5. Note the disappearance of the peak at 1395 cm^{-1} and the increasing importance of the peak at 930 cm^{-1} to the overall absorbance between 1100 and 800 cm^{-1}at pH 10.5.

Peak fitting is quite difficult for the obtained spectra due to the many peaks that are present as well as the difficulty of baseline subtraction at low wavenumber. Figure 3.9 shows the results of spectral peak fitting of the 500 mM boric acid spectra at pH 6.5 (Figure 3.9a) and pH 10.5 (Figure 3.9b). Lorentzian peaks were used to fit the data, and there were several items of note in the fits. The most interesting item for discussion is the 1100-800 cm^{-1} region of the data. There are two distinct peaks in this region: a peak attributed to the asymmetric stretch of adsorbed borate centered at 925 cm^{-1} at pH 6.5 and at 935 cm^{-1} at pH 10.5 and a second peak attributed to the symmetric stretch of adsorbed boric acid centered at 1005 cm^{-1} at pH 5.6 and at 1023 cm^{-1} at pH 10.5. The large shift in these peaks with changing pH along with the broadness of the fitted peaks (the peak width at half heights are larger for these two peaks than from the trigonal peaks that are over twice as large) suggest that there are more peaks present that cannot be resolved by traditional peak fitting routines. This strengthens the theory that there is inner-sphere borate present at the surface, and that the bands simply overlap too much to make exact identification possible with ATR-FTIR.

Possible mechanisms consistent with the observed spectra for adsorbed boron are illustrated in Figure 3.10. For both the trigonal and tetrahedral complexes it is not possible to distinguish monodentate from bidentate with our FTIR spectra, and so

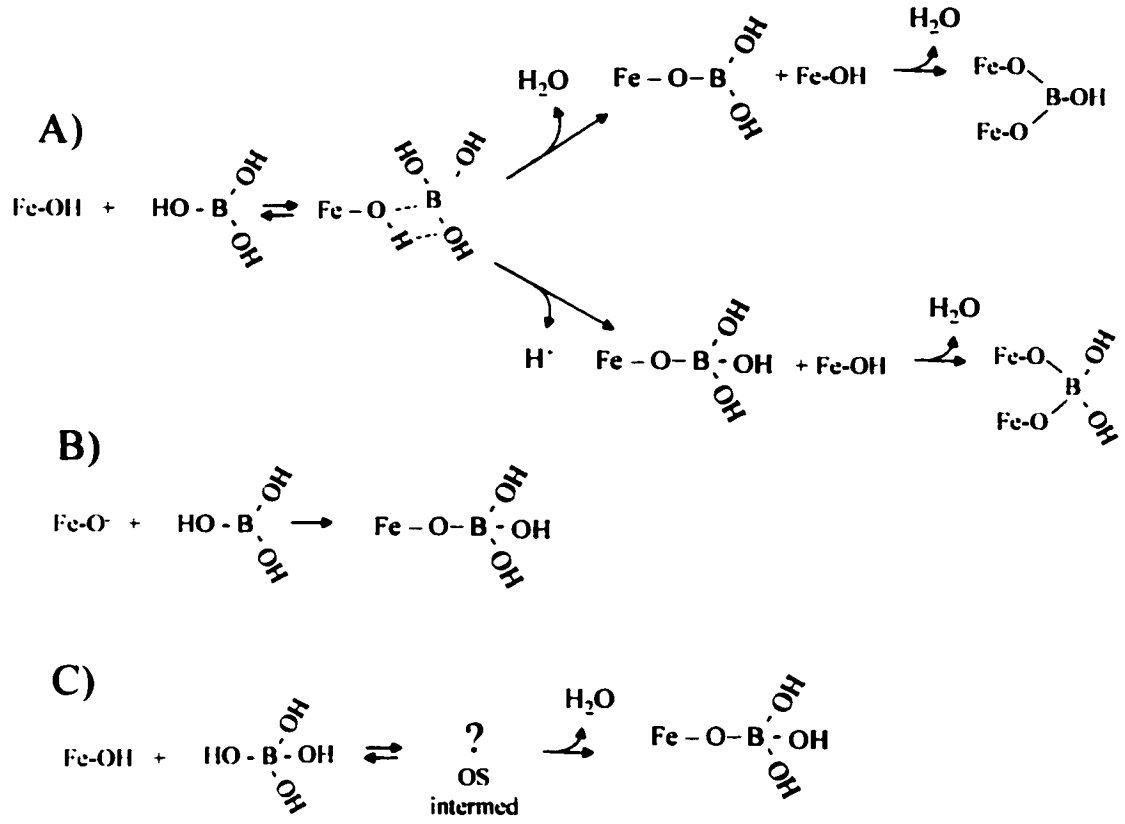

Figure 3.10. Proposed reaction mechanisms of boric acid at the HFO surface. The most likely mechanisms based upon FTIR spectroscopy are the ones described by 4.10a.

reaction mechanisms that explain conversion from monodentate to bidentate are proposed as possible. Mechanisms in Figure 3.10a discuss reactions of trigonal boric acid with FeOH groups on the HFO surface to produce both trigonal and tetrahedral surface complexes. Initially, an outer-sphere surface complex is formed as a result of the Lewis acidity of the boron metal center. This surface complex is actually observed in the pH 6.5 and 9.4 FTIR spectra, and appears to be a stable surface species rather than a transient intermediate. Once outer-sphere surface complexation occurs, ligand exchange can proceed in two separate pathways that produce either trigonal or tetrahedral inner-sphere surface complexes of boron. For the trigonal complexes, a water ligand would be displaced. This can occur due to strengthening of the boron Lewis acid/base bonding with the oxygen of the surface hydroxyl accompanied by the weakening of the surface functional group's proton bond. This results in an increase in the stability of the hydrogen bonding between a boric acid hydroxyl and the proton from the surface hydroxyl, producing a water ligand that is released. The resulting complex would be monodentate, but could also react with another surface hydroxyl in a second ligand exchange reaction that would release another H_2O molecule and form a bidentate surface complex. Since all of the molecules and surface groups involved in this reaction are formally neutral, there is no change in the surface charge (or overall pH) that would accompany these reactions. This reaction would be expected to occur more favorably at neutral to slightly alkaline pH values, since the FeOH surface group is a stable species and boric acid is the dominant B species.

Also in Figure 3.10a is a second pathway following outer-sphere boric acid adsorption. Instead of a ligand-exchange reaction accompanied with release of water, a proton from the surface hydroxyl is the leaving ligand. This covalent bond formation between the oxygen of the surface group and the boron of boric acid causes a shift to tetrahedral boron adsorbed on the HFO surface. Initially, a monodentate surface complex would form, but it is possible that the reaction would further progress via a second ligand exchange reaction with water as a leaving group to form a bidentate binuclear tetrahedral borate surface complex. Formation of tetrahedral boron on the surface from a trigonal outer-sphere intermediate is consistent with the observation of tetrahedral boron at the surface at pH 6.5 since borate in solution is not necessary for this reaction pathway to occur. The observation that borate adsorption becomes more pronounced at higher pH is also consistent with this mechanism since H^+ released into solution via ligand exchange will rapidly be neutralized (thus driving the reaction). The release of a proton from the surface in the ligand exchange reaction would also result in surface charge becoming more negative, which is consistent with the electrophoretic mobility measurements of Su and Suarez (1994). This mechanism is also consistent with the observation from macroscopic experiments that boron adsorption decreases markedly above the pK of boric acid since concentrations of boric acid would greatly affect reactivity in 4.10a.

Figure 3.10b demonstrates a second potential reaction mechanism: direct formation of an inner-sphere surface complex via a Lewis acid-base mechanism. This mechanism is not likely to be particularly important, because for FeO^- to be present the solution pH must be very high (typically several units above the PZC). If solution pH is high enough to produce FeO^- groups, then conversion of boric acid to borate in solution will also occur so the concentrations of the reactants for 4.10b are not expected to ever simultaneously be present in large quantities.

Finally, Figure 3.10c discusses potential mechanisms of borate adsorption. For an inner-sphere complex to form between a surface hydroxyl and borate, an outer-sphere intermediate would typically be needed to bring the borate to the surface. There was no evidence of a particular intermediate, though the extremely broad borate ν_3 bands might contain a peak arising from outer-sphere borate. This outer-sphere complex would have to be dominated by hydrogen-bonding since the surface is either neutral or negatively-charged at pH where borate forms in solution. Alternatively, a 5-coordinate boron intermediate would be needed. This is possible for boron hydrides but is not probable for boron oxides or hydroxides. This complex would then undergo ligand exchange via losing a water molecule and forming an inner-sphere borate surface complex. Because there is no clear driving force for the initial outer-sphere intermediate, this set of reaction mechanisms also seems less reasonable than 4.10a.

Conclusions

The chemistry of boron adsorption is both varied and complex, with multiple surface inner-sphere surface complexes occurring (trigonal and tetrahedral) and with the additional formation of outer-sphere surface complexes of boric acid. The geometry of inner-sphere boron surface complexes (trigonal versus tetrahedral) is always quite different than the speciation of boron in the bulk solution. By approaching the adsorption reaction from a mechanistic standpoint, this anomaly can largely be explained by the reaction of boric acid to form an outer-sphere intermediate complex that reacts with the HFO functional groups to form trigonal or tetrahedral complexes. Borate is not required in solution for tetrahedral boron to be present at the surface, since ligand exchange reactions could result in a conversion of boric acid to tetrahedral geometry at the surface. As pH is increased, the amount of tetrahedral boron on the surface also increases due not primarily to changes in surface speciation of boron but instead due to an increased tendency for proton release (and formation of tetrahedral boron complexes) rather than water release (and maintaining trigonal geometry) in the ligand exchange reaction. Other reaction mechanisms seem less favorable, and so the dominant reactant is predicted to be boric acid.

Outer-sphere boric acid complexation is also substantial on HFO at pH 6.5. The presence of outer-sphere boron adsorption has some important implications for plant

toxicity and availability. Since physically-bound boric acid can be readily leached, it can be expected to move with water flow in soils. This is consistent with high boron content in irrigation water in arid regions as well as consistent with low boron concentrations in humid regions where boron leaches from the surface soils. Outer-sphere boron would also be expected to be more available for plant uptake than more strongly bound boron complexes because it should more readily return to the soil solution when concentrations in the bulk decrease.

Chapter 4

EFFECTS OF SULFATE ON LEAD ADSORPTION AND DESORPTION ON GOETHITE

Lead (Pb) contamination of soils and sediments is one of the most common environmental problems in the United States, and Pb is accordingly considered a priority pollutant by the USEPA. Understanding reactions of lead in soils is therefore vital to accessing the threat to the environment from lead contamination and to predicting the ultimate fate of lead in contaminated areas. Since natural systems are seldom (if ever) at true equilibrium (Sparks 1995), it is important to not only conduct equilibrium studies such as pH edges and adsorption isotherms, but also to evaluate the importance of adsorption and desorption kinetics of lead. Several researchers have studied the sorption and desorption rates of lead with soils and soil components (Bunzl et al. 1976; Benjamin et al. 1981; Hayes et al. 1986; Ainsworth et al. 1994; Strawn et al. 1998; Eick et al. 1999) and noticed the biphasic reaction typical of many metals. A pressure jump chemical relaxation technique has been successfully used to determine the actual rate of reaction of lead on aluminum hydroxide, and it was found that there was a two step process defined as an outer-sphere intermediate followed by an inner-sphere surface complex (Yasunaga and Ikeda 1986).

Several researchers have also investigated the reversibility of lead adsorption by conducting desorption studies. Many metals have shown pronounced residence time effects, where adsorbed metals are increasingly resistant to desorption as their contact

time with soils increases. It was shown by Eick et al. (1999) that the residence time effect on lead desorption using a miscible displacement method was relatively minor. Similarly, Strawn and Sparks (2000) used a stirred flow reactor to investigate lead adsorption and desorption on a Matapeake silt loam soil. It was found that if organic matter was extracted prior to lead adsorption that the lead adsorption was fully reversible. However, in the presence of organic matter lead was strongly retained by the Matapeake soil. Similarly, Strawn and coworkers (1998) found that a resin method to desorb Pb from γ-Al_2O_3 resulted in complete removal of adsorbed lead.

While the above macroscopic studies all provided insight into equilibrium and kinetic behavior of lead, one cannot assign mechanisms for metal surface reactions from macroscopic data alone; complementary molecular scale investigation is also needed (Sparks 1995). Several researchers have studied lead adsorption mechanisms on whole soils, clay minerals, and organic matter using molecular scale techniques such as X-ray Absorption Near Edge Structure (XANES) spectroscopy and Extended X-ray Absorption Fine Structure (EXAFS) spectroscopy. Strawn and Sparks (2000) studied Pb adsorption on Matapeake silt loam soil, and found that complexation with organic functional groups (not specified) was dominant in samples with organic matter present, but that surface complexes of Pb dimers on silanol surface functional groups of clays was found in samples with organic matter removed. Strawn and Sparks (1999) also found that, on montmorillonite, Pb formed a mixture of outer-sphere and

inner-sphere complexes depending upon pH and ionic strength, with the inner-sphere complexes sometimes polymerizing to forms similar to $Pb_4(OH)_4^{4+}{}_{(aq)}$. Manceau and coworkers (1996) studied Pb retention mechanisms in natural soils compared to a variety of Pb-organic complexes and determined that Pb was held primarily by chelation with a mixture of salicylate and catecholate functional groups.

Since metal oxides are common in soils and have been found to be important geosorbents of metals, particular emphasis in the EXAFS literature has been placed upon Pb/metal oxide adsorption mechanisms. In particular, research has been conducted in depth as to Pb adsorption mechanisms on iron (Bargar et al 1997b) and aluminum (Bargar et al. 1996; Bargar et al 1997a; Strawn et al. 1998) oxides and hydroxides. It was learned that for aluminum hydroxides, Pb tends to form primarily inner-sphere bidentate edge-sharing complex, with Grazing incidence/X-ray Standing Wave studies (Bargar et al. 1996) observing that some crystal faces of corundum bind Pb as an outer-sphere complex. On goethite, it was shown by Bargar that at low pH (4.5-5.5) a mixture of inner-sphere bidentate edge-sharing and bidentate corner-sharing complexes form, and that at higher pH (6.5 and above) only the bidentate edge-sharing is formed on the surface. This observation has also been reported by other researchers (Ostergren et al. 2000a,b; Elzinga et al. 2001).

The above studies when taken as a whole present a wealth of information about Pb adsorption and desorption reactions with soils and soil components. However, all of the above studies were conducted with indifferent or weakly reactive background electrolytes to access fundamental Pb adsorption reactions. In natural systems, there are many other ions present in the soil solution such as other metals and alkaline earth cations, inorganic anions such as halogens and oxyanions, and organic ligands of widely varying molecular weight and reactivity. The potential for co-occurring ions to affect Pb retention mechanisms is therefore very high, but is still rather poorly understood. In fact, there are few studies that investigate the influence of anions on reactivity of metals. So that there is no confusion in the remainder of this study, single solute reactions with the sorbent phase (such as reactions of Pb and goethite in an indifferent electrolyte) will be referred to as a binary system, and reactions of two ions with the sorbent (such as Pb and SO_4 reactions with goethite) will be referred to as ternary systems. For conditions when a direct interaction between Pb and SO_4 occurs at the surface, the term ternary complex will be used.

There are several possibilities for interaction between co-occurring ions and lead in natural systems: competition for adsorption sites leading to a decrease in lead adsorption, synergistic effects where anion adsorption lowers the PZC of the surface and thus enhances lead adsorption, direct interactions of lead and anions to form ternary complexes that may or may not enhance lead adsorption, and precipitation of

lead-anion neophases that increase the removal of Pb from solution. For ternary complex formation, there are several different potential types of ternary complexes that were first classified by Benjamin and Leckie (1981). Ternary complexes may either have the metal bound directly to the surface with the ligand bound to the metal and away from the surface (Type A), the ligand bound to the surface and the metal bound to the ligand away from the surface (Type B), or both the metal and the ligand bound to the surface (Type C).

While not specifically discussing Pb chemistry, several studies have made significant progress in ourcurrent understanding of ternary cation-anion-surface reactions. Benjamin and Leckie (1981, 1982) studied the effects of different anions upon metal adsorption, and modeled the interactions with the triple layer model. Ali and Dzombak (1996b) modeled macroscopic data (primarily adsorption edges and envelopes) of interactions between copper and sulfate on goethite using the general two layer model. Both models suggested that ternary complexes might be important to consider when modeling metal reactions in the presence of sulfate. Cresenti and Sverjinsky (1999) have modeled the adsorption behavior of several different divalent transition metals and found that to adequately describe pH dependence of adsorption over a wide pH range that ternary complexes of metals with Cl^-, NO_3^-, and even ClO_4^- are needed at the mineral surface. Furthermore, they describe a speciation at the surface that is somewhat independent of solution speciation, and furthermore found

that the ternary complex formation was pH independent. Van Riemsdijk and coworkers (2001) found that Ca/PO_4/goethite reactions could be described using the CD MUSIC model by considering the interaction to be primarily electrostatic with adsorption of Ca and PO_4 occurring in different planes. Boyle-Wight (2002a,b) studied Co/Se (IV) and Co/Se(VI) reactions on γ-Al_2O_3 and determined that SeO_4 had no noticeable effect upon Co sorption, but that SeO_3 substantially changed the extent and mechanism of Co uptake on the alumina surface. The insensitivity of Co^{2+} adsorption to selenate is consistent with the *in situ* Raman spectroscopic findings of Wijnja and Schulthess (2001) that sulfate and selenate form only outer-sphere surface complexes on aluminum oxides.

Several researchers have investigated ternary complex formation between Pb and anions at the surface of goethite with spectroscopic tools and found interactions of ligands with Pb at the goethite surface to be important. Bargar and coworkers (1997c) observed a stabilization of corner-sharing Pb on the goethite surface in the presence of chloride and attributed this to the formation of a Type A ternary complex with metal bound to the goethite surface and Cl^- bound to the Pb. Carbonate interactions with Pb were studied by Ostergren et al (2000a) using both EXAFS and ATR-FTIR, and it was found that, similarly to Cl^-, at low pH (4.5-6.5) that Pb adsorption was enhanced and that edge sharing Pb complexes were stabilized. By combining their ATR-FTIR results, EXAFS, and bond valence theory, Ostergren and

coworkers suggested that the most likely mechanism for their data was a Type A ternary complex with Pb bound to the surface and carbonate bound to the Pb ion. At pH 6.7 and above, Ostergren and coworkers found that Pb adsorption was decreased in the presence of carbonate, which was attributed to competition between the goethite surface and aqueous $PbCO_3$ complexes.

Interestingly, three different studies of Pb/SO_4/goethite ternary reactions have been conducted with *in situ* spectroscopy. The Pb/SO_4/goethite system is particularly amenable to study because the single sorbate adsorption mechanisms of Pb and SO_4 on goethite over a wide range of reaction conditions have been previously determined by various methods. Peak and coworkers (Peak et al. 1999, Peak et al. 2001) utilized a flow through ATR-FTIR technique to investigate sulfate adsorption on goethite and observed that at pH 6.0 and higher sulfate formed only outer-sphere surface complexes. At pH below 6.0, a mixture of outer-sphere and inner-sphere sulfate was observed, with the sulfate having a monodentate configuration and some additional hydrogen bonding to adjacent surface sites. Later ATR-FTIR (Wijnja and Schulthess 2001; Ostergren et al. 2000) and Raman (Wijnja and Schulthess 2001) studies also reported a shift from outer-sphere to a mixture of outer and inner-sphere sulfate as pH decreased below 6.

Weesner and Bleam utilized EXAFS spectroscopy to monitor Pb adsorption mechanisms, and Ostergren et al. (2000) and Elzinga et al. (2001) both utilized a combination of Pb L_{III} EXAFS spectroscopy and sulfate ATR-FTIR spectroscopy to try and characterize the interaction of sulfate with both Pb and the iron oxide surface. All of the above researchers found direct interactions between Pb and SO4 occurred, but each study had different interpretations as to the nature of the ternary complex. Weesner and Bleam (1999) suggested that $PbSO_4$ precipitate phases occurred that were anglesite precursors. However, their initial concentrations of Pb were relatively high, and homogeneous precipitation of $PbSO_4$ could not be ruled out in their results.

Ostergren et al. (2000b) conducted experiments with much lower Pb concentrations, and determined that, based upon valence bond theory, ATR-FTIR, and EXAFS, ternary complex formation was occurring. Similarly to their work with carbonate (Ostergren et al. 2000a), it was found that stabilization of a corner-sharing Pb complex occurs in the presence of sulfate. Their sulfate ATR-FTIR studies determined that new surface complexes of sulfate formed in the presence of Pb, suggesting that the enhancement of corner sharing Pb was due to a type A ternary complex with Pb bound in a bidentate binuclear complex on the goethite surface and with sulfate bound as a monodentate complex with the adsorbed Pb.

Elzinga and coworkers (2001) were in reasonable agreement with the ternary complex proposed by Ostergren, but proposed an additional weak ternary complex that resulted from Pb and SO_4 both being adsorbed on the iron oxide surface and interacting electrostatically with each other. This is similar to a Type C ternary complex, with the interaction between the adjacent adsorbate being weaker in nature. It can also be considered to be analogous to ion pair formation on the goethite surface. They also proposed that, in addition to ternary complex formation, that sulfate affects Pb adsorption via electrostatic means as well. Elzinga (2001) further suggested that ternary complex formation was more important at low pH and higher Pb concentrations, whereas electrostatic effects are more important at higher pH and lower Pb concentrations. At high Pb concentrations, some conversion of inner-sphere sulfate/goethite complexes to goethite/Pb-SO_4 ternary complexes was observed. Additionally, higher Pb concentrations resulted in a more positive surface that enhanced outer-sphere sulfate adsorption. Proposed mechanisms of Pb and SO_4 (single ion and co-adsorbed) from the different researchers discussed above are depicted in Figure 4.1.

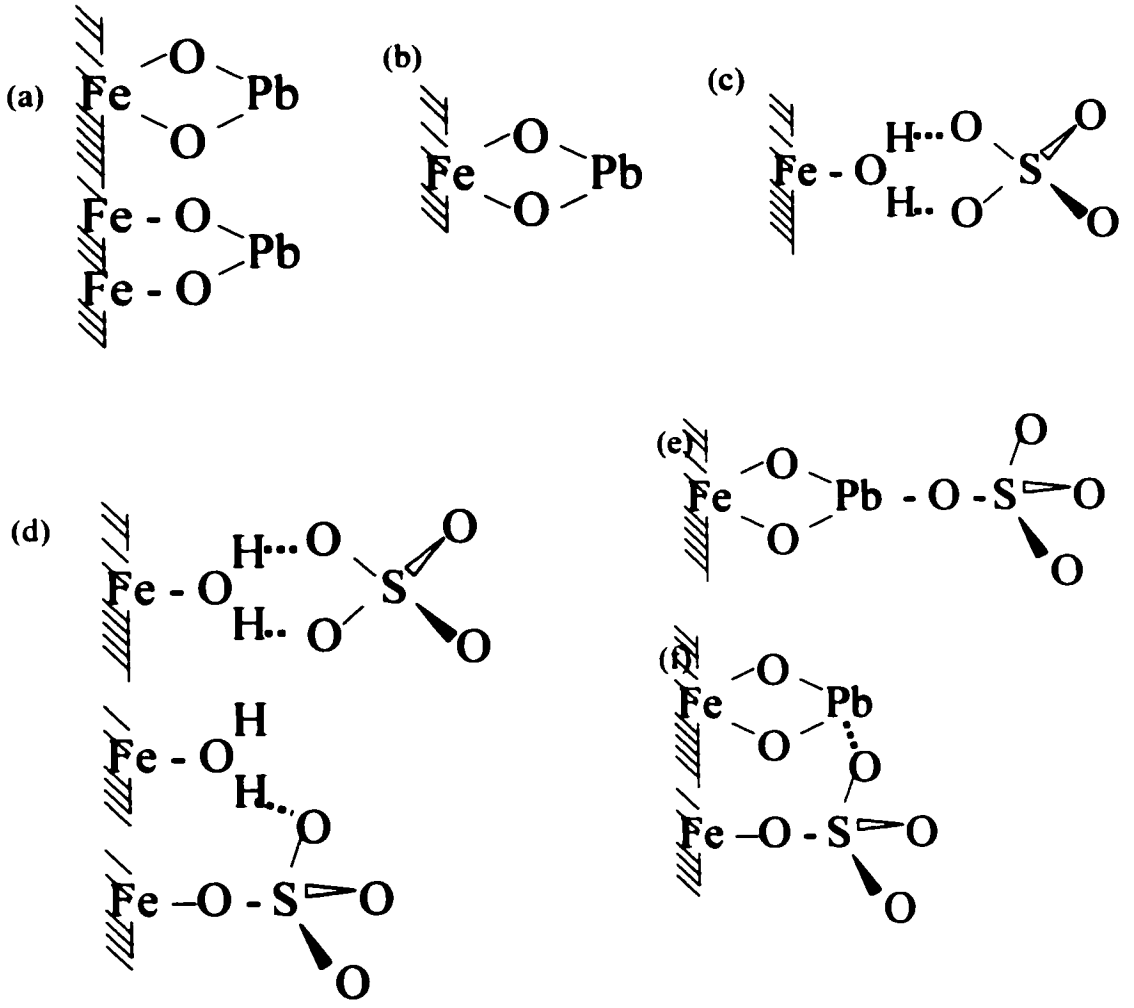

Figure 4.1 Drawings of Pb, SO_4, and Pb-SO_4 surface complexes confirmed to form at the goethite surface. (a) Edge and corner sharing bidentate Pb. These complexes are seen at pH 4.5 on goethite in the absence of sulfate (Bargar et al. 1997b). (b) Edge sharing bidentate Pb. This is the only complex observed at pH 6 and above on goethite in the absence of sulfate (Bargar et al. 1997b). (c) Electrostatically bound (outer-sphere or H-bonded) sulfate. This is the only species observed at pH 6 and above in the absence of Pb (Peak et al. 1999). (d) Inner-sphere and outer-sphere sulfate. These complexes both occur at pH 4.5 in the absence of Pb (Peak et al. 1999). (e) Type A ternary complex with strong bonding between Pb and sulfate (Ostergren et al. 2000b). (f) Type C ternary complex with weak bonding between Pb and sulfate. May also be considered surface ion-pair formation (Elzinga et al. 2001).

It seems clear from the above spectroscopic studies that the presence of sulfate substantially changes lead adsorption mechanisms between pH 3 and 6. Several spectroscopic studies all suggest that ternary complexes at the goethite surface are important in describing the system under these conditions. However, no research to date has focused upon how the presence of sulfate may change the kinetics of Pb adsorption, and no one has studied whether the additionally adsorbed Pb is retained differently when desorption takes place. Therefore the objectives of this study were to compare the kinetics of Pb adsorption in the presence and absence of sulfate, and to also compare the kinetics of Pb release in the absence and presence of sulfate to determine if the additionally adsorbed Pb is more or less stable than the Pb surface complex with goethite.

Materials and Methods

All chemicals used in experiments were reagent grade or better, distilled deionized (18MΩ) water was used in preparation of all solutions and suspensions, and all experiments were conducted in cleaned and acid-washed (1.0M HCl) containers. All samples were filtered through 200 nm filter paper, acidified, and analyzed for Pb via ICP-AES spectrometry.

Mineral synthesis. The high surface area, low cystallinity goethite used in these studies was synthesized via the method of Cambier and coworkers (1985). Amorphous ferric

hydroxide is first precipitated at pH 11 by mixing 1M $Fe(NO_3)_3$ with 1M NaOH, then the suspension is aged at 25C for 14 days with constant shaking on a reciprocal shaker. After 14 days, the product was centrifuged, resuspended in distilled deionized H_2O, shaken for two hours, centrifuged again, and then resuspended in an HCl solution such that the final pH is 0.4. This acid washing is sufficient to rapidly remove residual amorphous $Fe(OH)_3$ without substantial dissolution of the goethite. This goethite suspension was shaken for two hours and then centrifuged, resuspended with distilled water, and placed into freshly washed dialysis tubing. The goethite was then dialyzed until its conductivity matched freshly distilled water, flash-frozen with liquid nitrogen, and freeze dried. X-ray diffraction and FTIR spectroscopy confirmed that the product was goethite, and N_2 BET surface area analysis reported a specific surface area of 64 ± 7 m^2g^{-1}. The final product had a PZC of 8.4 determined via potentiometric titration in 0.1, 0.01, and 0.005M $NaClO_4$ electrolyte.

Adsorption Edges and Isotherms. All equilibrium studies were conducted in a glove box under N_2 atmosphere to remove the possibility of CO_2 contamination. A suspension density of 0.5 g/L and a final ionic strength of 0.01M were chosen for all studies. For the Pb only studies, the background was 0.01M NaCl, and for the studies with both Pb and SO_4, the background electrolyte used was 0.007M NaCl and 1mM Na_2SO_4 (final I = 0.01). A batch technique was utilized for the isotherms and envelopes, with a final sample volume of 40mL being reacted in an acid-washed 50mL

disposable centrifuge tube. Initially, goethite was added to the centrifuge tube from a 5.0 g/L stock suspension and then H_2O and 1M NaCl were added. Next, the pH was adjusted with 0.1M HCl to the desired pH (constant for the isotherms and between 3.5 and 5.5 for the pH envelopes) and the suspension was placed on a rotating shaker. The suspension's pH was again adjusted at 2, 8, and 24 hours, and then Pb was added to the samples. For the pH envelopes, Pb (as $Pb(NO_3)_2$ was added from a 1 mM stock solution for a final concentration of 10 μM Pb and pH was allowed to vary through the reaction. For the adsorption isotherms, different amounts of Pb were added and pH was held constant by adjustment with 0.01M HCl or NaOH immediately after Pb addition, and again after 4 hours, 8 hours, 24 hours and 30 hours. Both pH envelopes and adsorption isotherms were equilibrated for 48 hours total, but after 24 hours there was no change in pH of the suspensions.

Adsorption kinetics. Adsorption kinetics experiments were conducted in a polypropylene reaction vessel that was placed inside a glass water jacket connected to a circulating water bath to control reaction temperature at 25.0C. A Metrohm 718 pH stat Titrino was used to control pH to ±0.02 units, and an overhead stirrer was employed to mix the suspension at a rate of 400 rpm. This mixing speed was sufficient for eliminating mass-transfer limitations to the overall reaction rate. To reduce the effects of carbonate in the system, nitrogen was sparged through the solution, and the reaction vessel was covered with an acrylic lid with ports for stirring,

burette, nitrogen gas, pH electrode, and sampling. Parafilm was used to seal the interface between the vessel and the lid, and a rubber cork stoppered the sampling port when not in use.

For kinetics experiments, the goethite suspension density was equal to 0.5 g/L in the reaction vessel, and was added 24 hours before the reaction to equilibrate in the case of the experiments where only Pb was present and in experiments where Pb was added to goethite suspensions with sulfate already adsorbed. For the simultaneous reaction experiments, Pb and sulfate were added to a background electrolyte solution and pH adjusted and nitrogen purged. A 9 g/L goethite stock suspension was also pH adjusted and purged in a separate reaction vessel that was also water jacketed to control temperature, but stirred via a magnetic stirrer as the volume was only 100 mL. At time zero, enough of the goethite stock was added to the reaction vessel to bring the overall suspension density to 0.5 g/L, and then sampling began. Samples were collected by extracting ~7 mL of suspension using a syringe with a piece of Teflon tubing on the end. This suspension was then filtered through a 0.2 μm filter paper, acidified, and analyzed via ICP-AES.

Desorption studies. For desorption studies, a simple replenishment method was used with a contact time of 1 hour between replenishments. Initially, adsorption samples were produced at pH 4.5 with a reaction time of 24 hours, and then 50 mL of the 0.5

g/L adsorption sample was placed into high speed centrifuge tubes, centrifuged for 10 minutes at 15,000 rpms, and then resuspended in 10 mL of desorbing agent. There were several different desorbing solutions chosen to represent the effects of changing solution conditions: either pH 4.5 or pH 3.5 to study the effects that lowering reaction pH has upon desorption and by changing the desorbing agent from 0.01M NaCl (desorbs both Pb and SO_4) or 0.007 M NaCl and 1 mM SO_4 (desorbs Pb without as much SO_4 desorption). The replenishments were all conducted in duplicate, and were limited by the fact that after several replenishments the suspensions became difficult to decant without losing some goethite in the supernatant.

Results and Discussion

Adsorption edges and isotherms.

An adsorption isotherm at I = 0.01 conducted at pH 4.5 is shown in Figure 4.2. To obtain an ionic strength of 0.01M, 0.01M NaCl background or 0.007M NaCl + 1 mM SO_4 background was used. It can clearly be seen that addition of sulfate greatly increases the capacity of goethite to adsorb Pb at pH 4.5. For the sulfate-free experiment, the isotherm follows a general Langmuir type trend, but in the presence of sulfate no maximum is observed. Samples were not prepared at higher Pb concentrations because the solubility of $PbSO_4$ is reached at around 50 μM Pb.

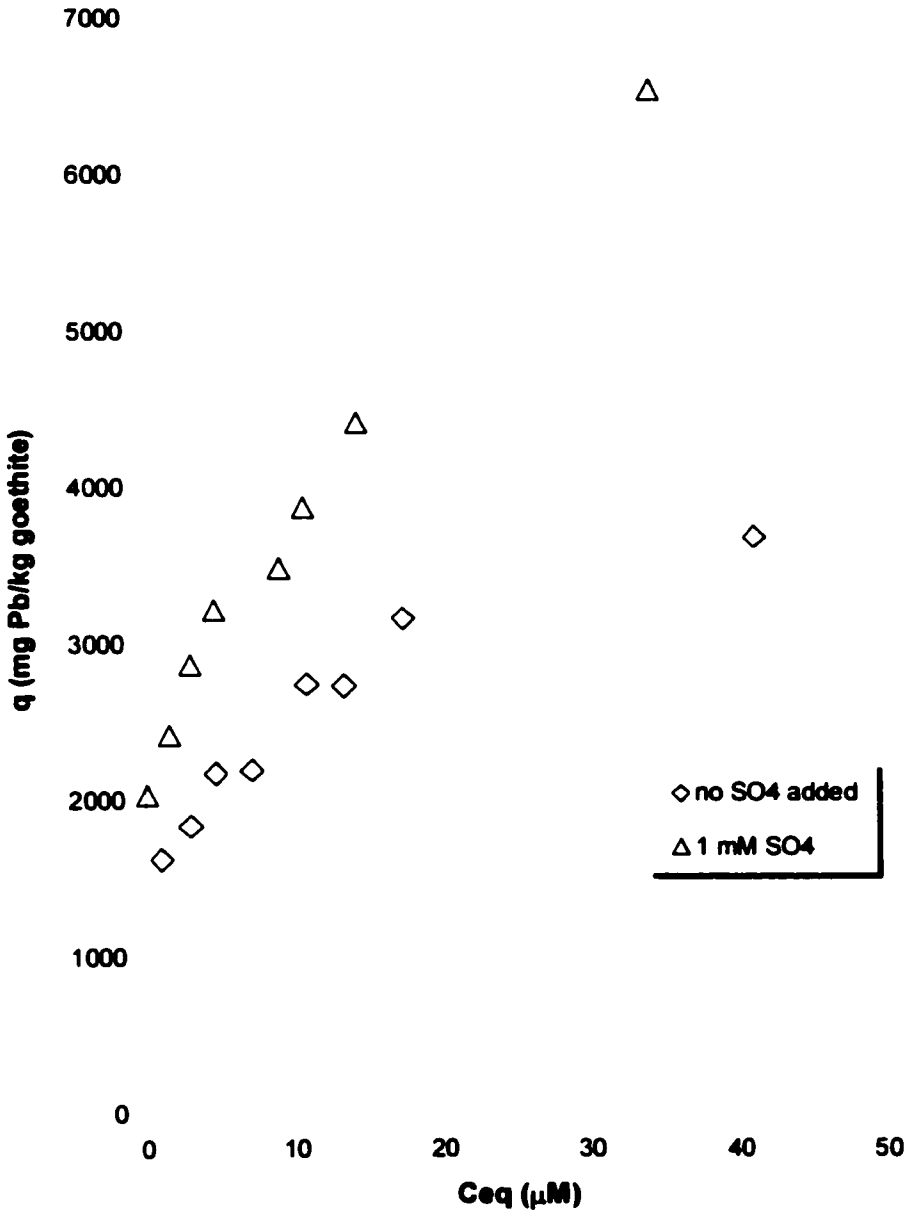

Figure 4.2 Pb adsorption isotherms conducted at I = 0.01, pH = 4.5, 0.5 g/L goethite, and either in the absence or presence of 1 mM sulfate.

In Figure 4.3, a pH envelope of Pb adsorbed on goethite in a 0.01M NaCl background is compared to Pb adsorbed in a 0.01M ionic strength background containing 1 mM SO_4. It can clearly be seen that the addition of 1mM SO_4 enhances Pb adsorption for any given pH value, and also shifts Pb adsorption to lower pH values if the curves are taken as a whole. It should be noted that at all pH values, ~20% of the total Pb in solution is of the form $PbSO_{4(aq)}$, and that the increase in Pb adsorption on goethite in the presence of SO_4 is approximately the same. However, other mechanisms besides adsorption of $PbSO_4$ could explain the adsorption increase equally well. For example, the fraction of inner-sphere sulfate may also be around 20-30% at pH 4.5 and adsorption of inner-sphere SO_4 might decrease surface charge enough to adsorb additional Pb. One point to make about the effects of inner-sphere sulfate on surface charge is that as reaction pH changes from 4 to 6, inner-sphere sulfate becomes vanishingly small (Peak et al. 1999) whereas the increased adsorption of Pb in the presence of sulfate continues to be observed.

Adsorption kinetics. Figures 4.4 and 4.5 show results from adsorption kinetics conducted at pH 4.5 (Figure 4.4) and pH 5.5 (Figure 4.5). In all experiments, a final ionic strength of 0.01M and an initial Pb concentration of 10 μM Pb were used. In addition to simply comparing Pb adsorption in the absence and presence of sulfate, the effects of sulfate addition order were also studied by either adding sulfate simultaneously with Pb or by adding the sulfate 24 hours prior to Pb addition.

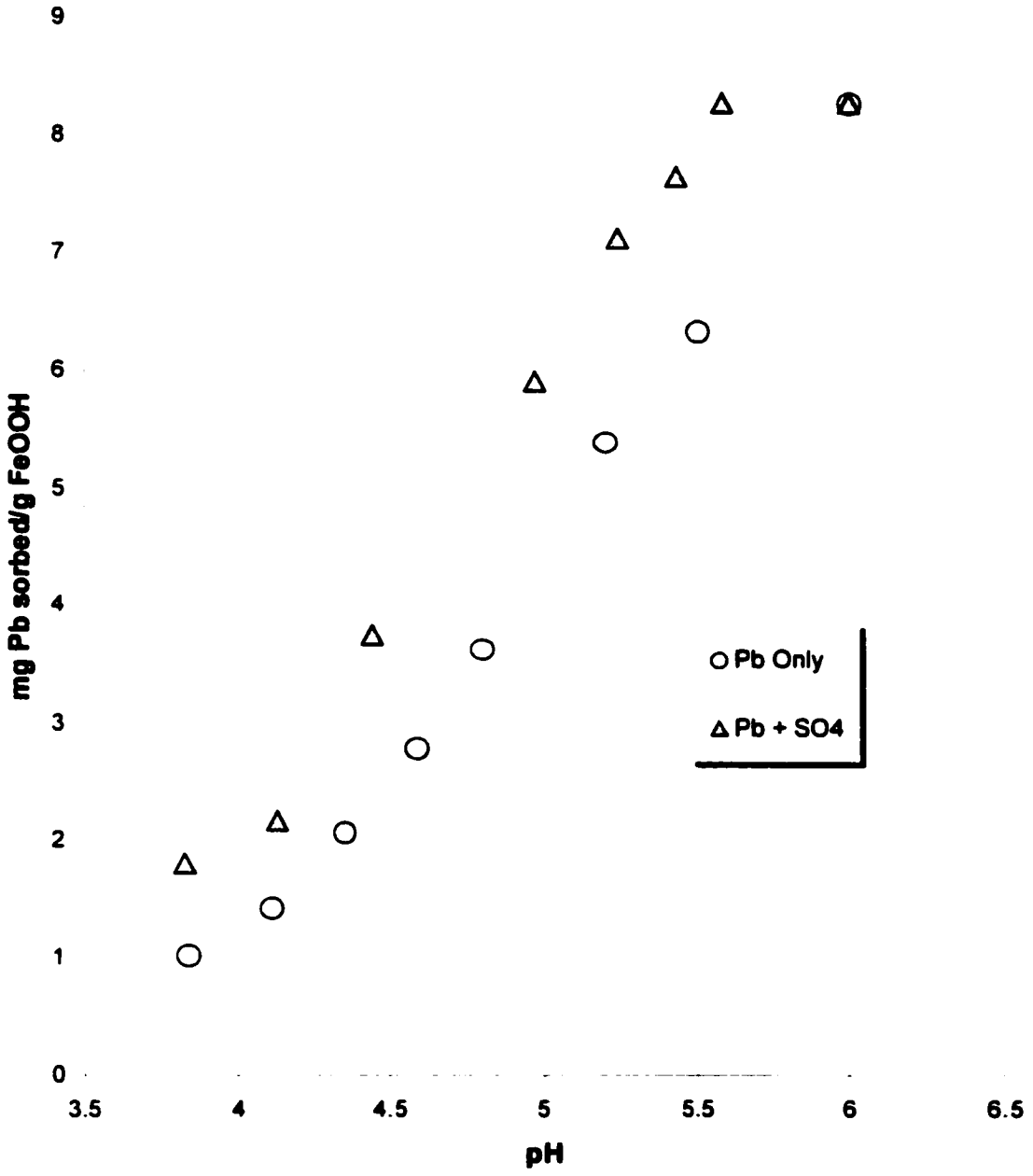

Figure 4.3 Pb adsorption edges conducted at I = 0.01M, 0.5 g/L goethite, initial Pb concentrations of 20 μM, and either in the absence or presence of 1 mM sulfate.

For the pH 4.5 data in Figure 4.4, there are several interesting observations that can be made. First of all, Pb adsorption is increased in the presence of sulfate regardless of addition order. However, both the extent of the increase and the kinetics of adsorption are substantially different depending upon order of sulfate addition. When sulfate is equilibrated with goethite prior to Pb addition (Pb added last), then the rate of reaction was too rapid to measure with a batch technique and had already reached equilibrium at 1 minute. The Pb reaction kinetics are quite similar to those of sulfate adsorption on goethite (Peak et al. 1999), which is also too rapid to measure with a batch reactor. However, when Pb and sulfate are added simultaneously, the reaction kinetics mirror those of the Pb only experiments, except that there is a larger amount of Pb adsorbed. When comparing the amount of Pb adsorbed at equilibrium, it can be seen that at pH 4.5 much more (90% vs. 70%) is adsorbed when Pb and sulfate are added simultaneously than when Pb is added to a sulfate saturated goethite.

These effects of sulfate upon Pb adsorption kinetics become far less pronounced when the reaction pH is raised. Results from kinetics experiments conducted at pH 5.5 are shown in Figure 4.5. The adsorption kinetics of simultaneous addition of Pb and sulfate are very similar in shape to those of Pb only, while the experiment where Pb is added to a surface with sulfate present has more rapid kinetics. This behavior is similar to the pH 4.5 data in Figure 4.4.

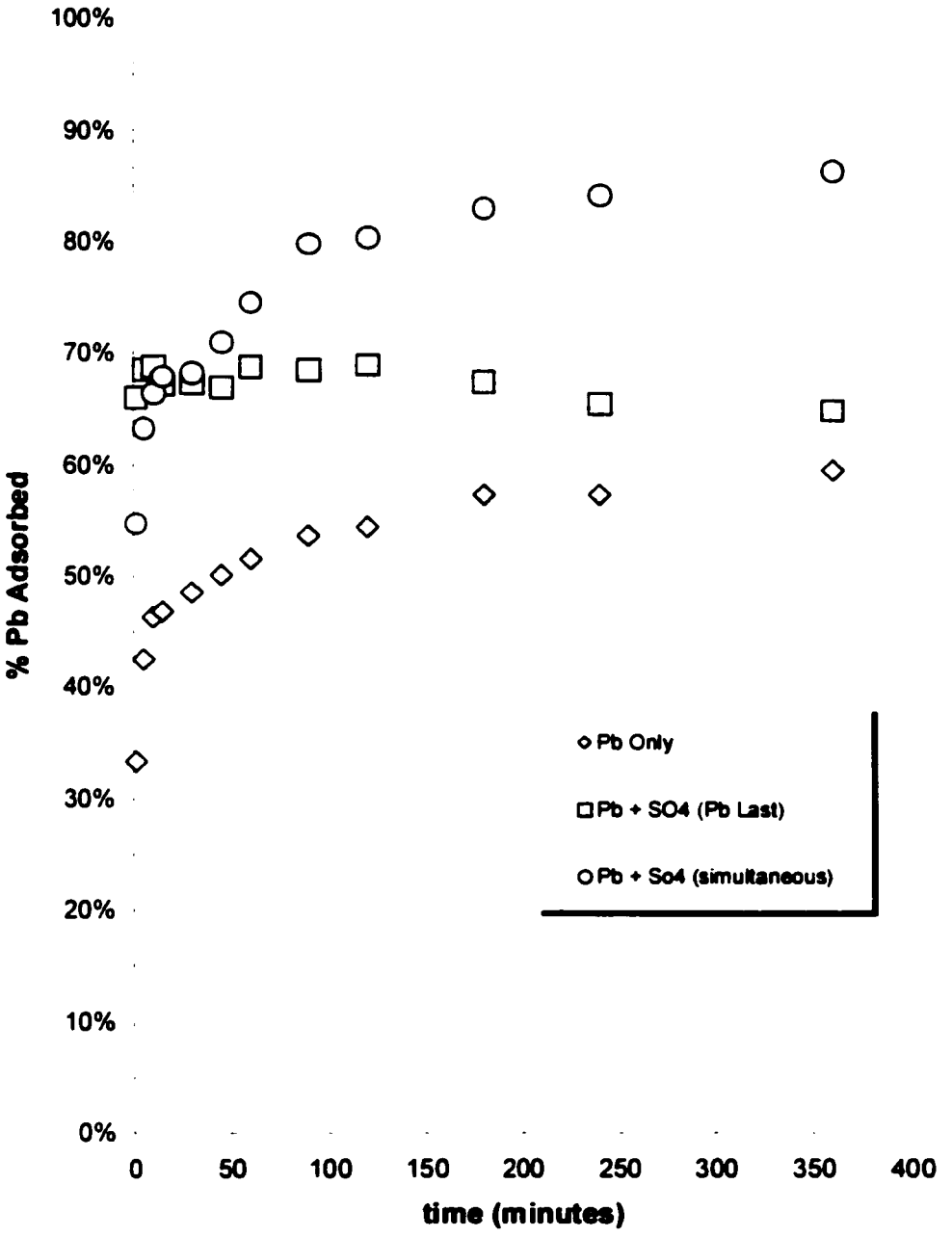

Figure 4.4 Pb adsorption kinetics conducted at pH 4.5, I = 0.01M, initial Pb concentrations of 10 μM, 0.5 g/L goethite, and either in the absence or presence of 1 mM sulfate. For the experiments with 1 mM sulfate, it was either added simultaneously with Pb, or allowed to equilibrate with goethite 24 hours prior to Pb addition.

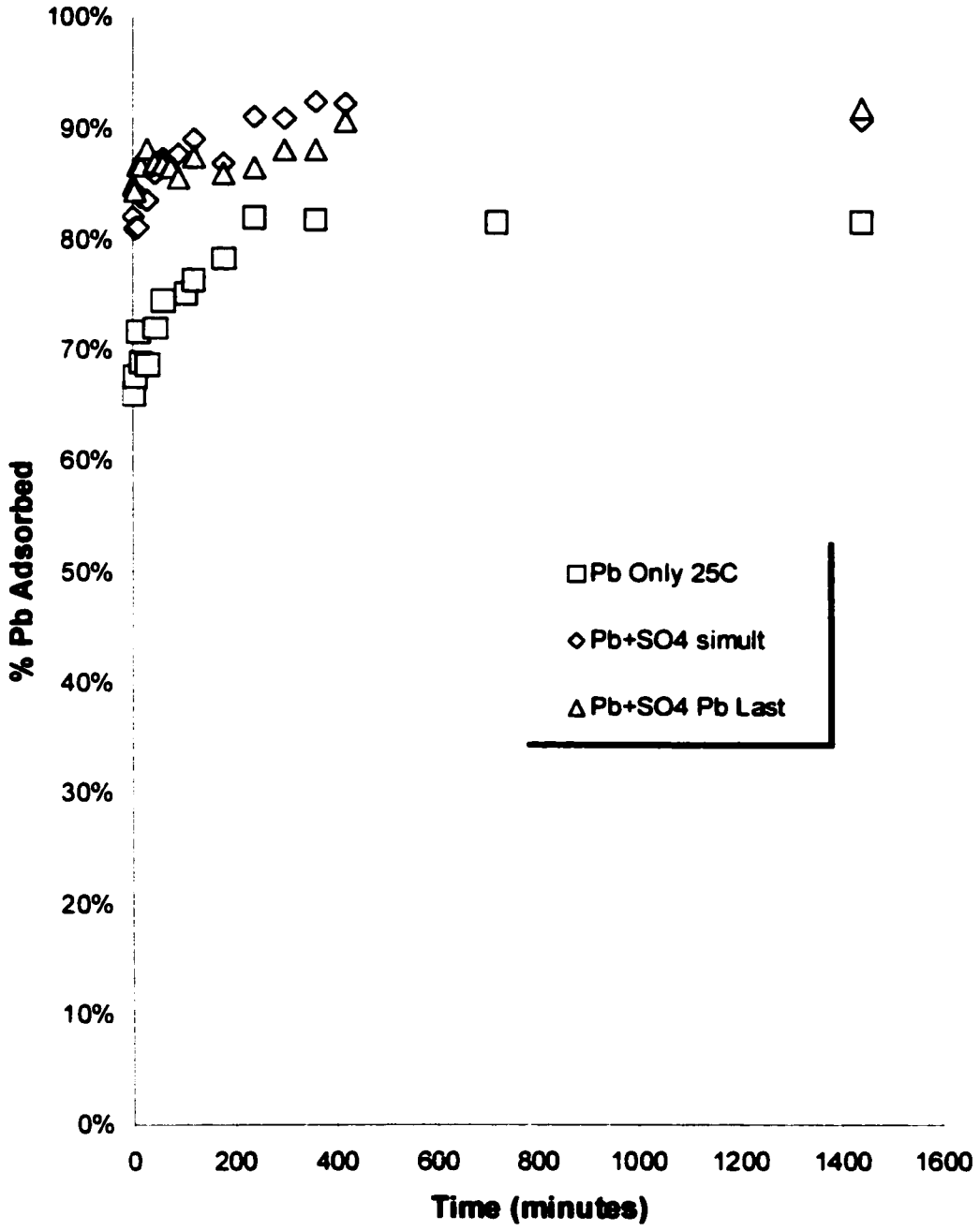

Figure 4.5. Pb adsorption kinetics conducted at pH 5.5,I = 0.01M, initial Pb concentrations of 10 μM, 0.5 g/L goethite, and either in the absence or presence of 1 mM sulfate. For the experiments with 1 mM sulfate, sulfate was either added simultaneously with Pb, or allowed to equilibrate with goethite 24 hours prior to Pb addition.

Interestingly, the final amount of adsorption is now identical regardless of sulfate addition order, although the initial rate of reaction still seems faster for the system with sulfate added first. The enhancement of Pb adsorption in the presence of sulfate is also much less pronounced than at pH 4.5.

Some conclusions about Pb/SO_4/goethite reactions can be drawn from the results of the kinetics studies. First of all, the fact that simultaneous additions of Pb and SO_4 produce reaction kinetics similar to the bare Pb ion while the addition of Pb to goethite pre-equilibrated with SO_4 resulted in much faster kinetics bears discussion. At pH 4.5, SO_4 forms inner-sphere surface complexes (Peak et al. 1999), and these complexes will decrease the positive surface charge of goethite. When Pb adsorbs to goethite in the presence of substantial amounts of inner-sphere SO_4, then adsorption kinetics might proceed more rapidly because the initial surface charge barrier to Pb^{2+} adsorption is diminished. When Pb and SO_4 are added simultaneously, the changes in surface charge might not be as pronounced because the overall surface charge would develop over time as both Pb^{2+} and SO_4^{2-} adsorb. The influence of SO_4 addition order on the final amount of Pb adsorbed is also consistent with this hypothesis. When an excess of sulfate is reacted with the surface prior to Pb adsorption, then Pb then has to compete for adsorption sites with SO_4 that is already present at the surface in an inner-sphere complex. However, in simultaneous addition of Pb^{2+} and SO_4^{2-}, lead can compete directly for unoccupied sites with unbound sulfate, so an energetic barrier

(displacement of an inner-sphere surface complex) has been removed. This also explains the observation that simultaneous addition of Pb and SO_4 results in kinetics similar to Pb-only systems because ligand exchange with a surface hydroxyl is expected to be the rate-limiting step in both cases. That can be contrasted with Pb addition to sulfate-saturated goethite where ligand exchange with an inner-sphere sulfate molecule may limit reaction rates. This is also consistent with the observation of Elzinga et al (2001) with ATR-FTIR spectroscopy that high Pb concentrations would convert SO_4 inner-sphere complexes on goethite to Pb-SO_4 ternary complexes.

At pH 5.5, the influence of addition order upon the final amount of Pb adsorbed disappears. This is also consistent with the earlier discussion about competition for sites at the surface, because at pH 5.5 there is far less inner-sphere sulfate on the goethite surface and there are far more FeOH surface sites accessible to Pb for inner-sphere complexation. A combination of these two factors would tend to decrease the importance of competition at the surface. A more rapid adsorption of lead onto sulfate-saturated goethite is still seen at pH 5.5, although the effect is not as dramatic as in the pH 4.5 experiment. This is also consistent with adsorbed sulfate enhancing the rate of adsorption by a lowering of the goethite surface charge. The effect of sulfate on surface charge is expected to be less pronounced at pH 5.5 because sulfate inner-sphere surface complexes are minor on goethite at pH above 5.0 (Peak et al. 1999). Changes in surface functional group speciation are also very important, since

there are many more FeOH surface sites available for Pb at pH 5.5 than there are at pH 4.5 when $FeOH_2^+$ is dominant. If there are many available surface sites for Pb adsorption, then the presence of SO_4 at the surface does not influence the amount of Pb adsorbed nearly as much.

Desorption studies. The results from desorption via a replenishment method are shown in Figures 4.6 and 4.7. In all desorption studies the adsorption reaction was conducted at pH 4.5 with a reaction time of 24 hours. Desorption studies with different desorbing agents were then conducted at pH 4.5 and at pH 5.5. The results from desorption studies at pH 4.5 are shown in Figure 4.6, while in Figure 4.7 desorption studies conducted at pH 3.5 are presented. Lead adsorption samples for desorption studies were produced with different sulfate addition order since a difference in the adsorption kinetics was previously observed at pH 4.5. The solutions used for desorption (0.01M NaCl and 0.007M NaCl + 1 mM SO_4) were chosen to simply remove Pb or both Pb and SO_4 from the goethite surface via mass action and dilution rather than by adding another strong competitor for surface sites. It may be somewhat surprising that a substantial quantity (25-60%) of Pb was removed by such "weak" desorbing agents. However, several studies (Strawn et al. 1998, Strawn and Sparks 2000) have shown that Pb adsorption can be rapidly reversible even when inner-sphere complexation is observed with EXAFS spectroscopy.

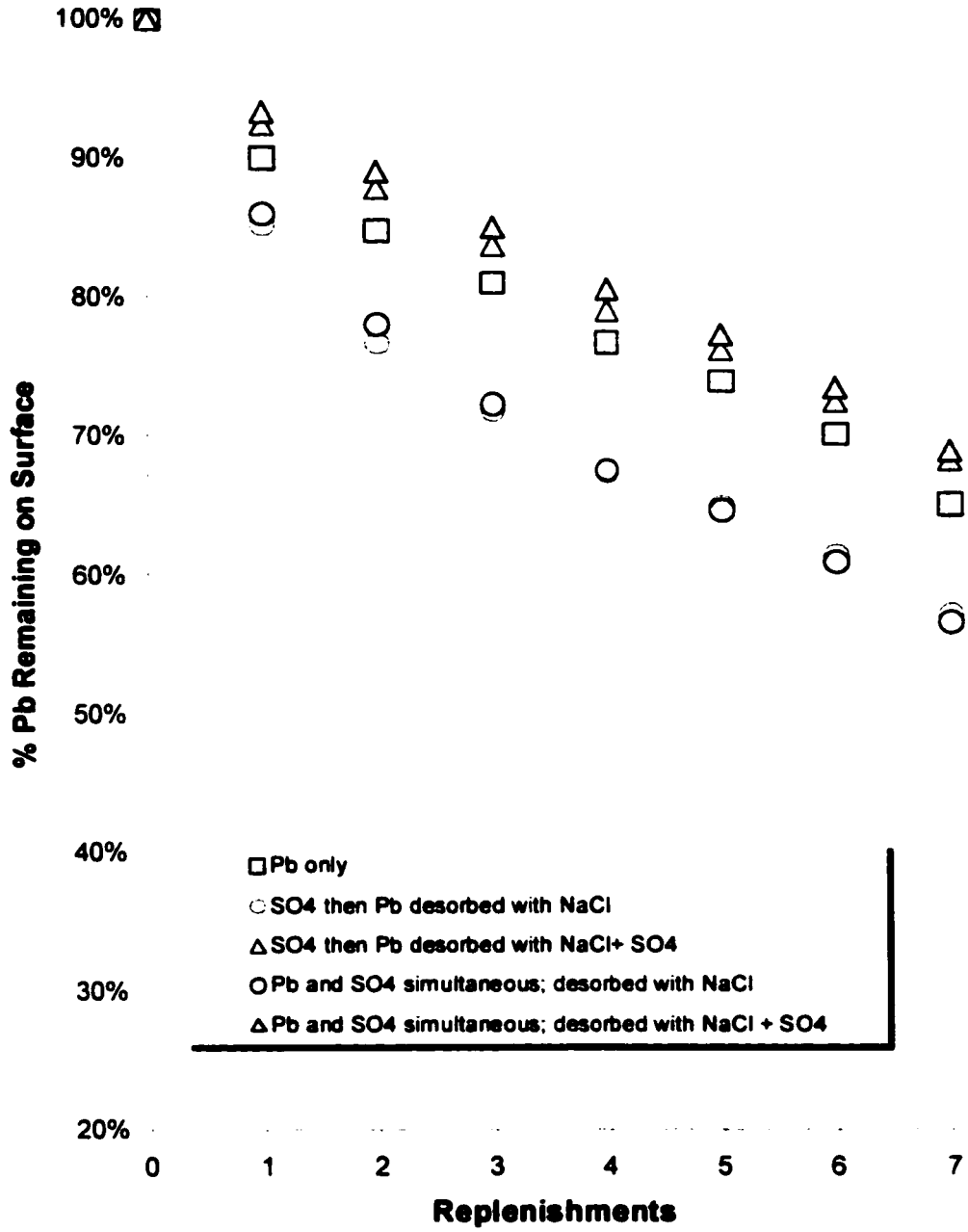

Figure 4.6 Desorption studies conducted with desorbing agents at pH 4.5.

Figure 4.6 shows the effects of different adsorption conditions and different pH 4.5 desorption agents upon the retention of Pb on goethite. For samples desorbed with NaCl, both SO_4 and Pb were removed from the surface, while for samples desorbed with NaCl and SO_4, then there should be relatively minor desorption of sulfate while Pb still is desorbed. Desorption of the sample with Pb and no sulfate by NaCl can be considered as representative of the reversibility of Pb adsorption in the absence of SO_4. It can be seen from the desorption studies conducted with 0.01M NaCl as the desorption agent that there is a greater fraction of Pb desorbed compared to the Pb only system. However, when sulfate is also present in the desorption agent, then substantially less Pb is removed than in the Pb only samples. The samples show very little variance with addition order, which may seem surprising since there were marked differences in the adsorption kinetics. However, the desorption data is normalized to the amount of sulfate initially on the surface, and so if addition order affects the initial rate and the final amount of Pb adsorbed but not the mechanism by which it is bound then one would not expect a difference in the retention behavior either. It is not possible to confirm that this is the case without further spectroscopic studies however.

In Figure 4.7, the effect of desorption at pH 3.5 with 0.01M NaCl adjusted to pH 3.5 is shown. Sulfate adsorption increases as pH is lowered, and so samples were not desorbed with NaCl + SO_4 agents since the comparisons would be affected by

changing sulfate concentrations at the surface. As in the pH 4.5 data (Figure 4.6), desorption of Pb is enhanced in the samples with sulfate present relative to the sulfate-free sample. This is to be expected as the additional Pb that adsorbs in the presence of sulfate will also desorb when sulfate is removed from the surface. Interestingly, the order of addition for Pb and SO_4 affects the amount of Pb that is desorbed. More Pb is retained from the simultaneous adsorption experiment than when Pb is added to goethite in equilibrium with sulfate. This suggests that the mechanism of either Pb or sulfate adsorption is changed by addition order. Since there was no order of addition dependence upon desorption at pH 4.5, it seems more probable that changes in sulfate are responsible. This is logical when one considers that inner-sphere sulfate surface complexes become dominant below pH 4.0; sulfate adsorbed on goethite as an outer-sphere complex at pH 4.5 may convert to an inner-sphere species and compete with Pb for surface sites. It was previously proposed that Pb and SO_4 compete directly for sites in the simultaneous addition experiment, and that less inner-sphere sulfate occurs under these reaction conditions than when sulfate is added to the goethite first and preequilibrated. This results in an overall lower sulfate loading for the simultaneous addition sample than for the sulfate-saturated goethite sample. If there is more sulfate present on the surface in the adsorption sample with Pb added to a sulfate-saturated goethite, then lowering the pH to 3.5 may result in a more pronounced competition between sulfate and lead for surface sites. This explanation runs somewhat contrary to

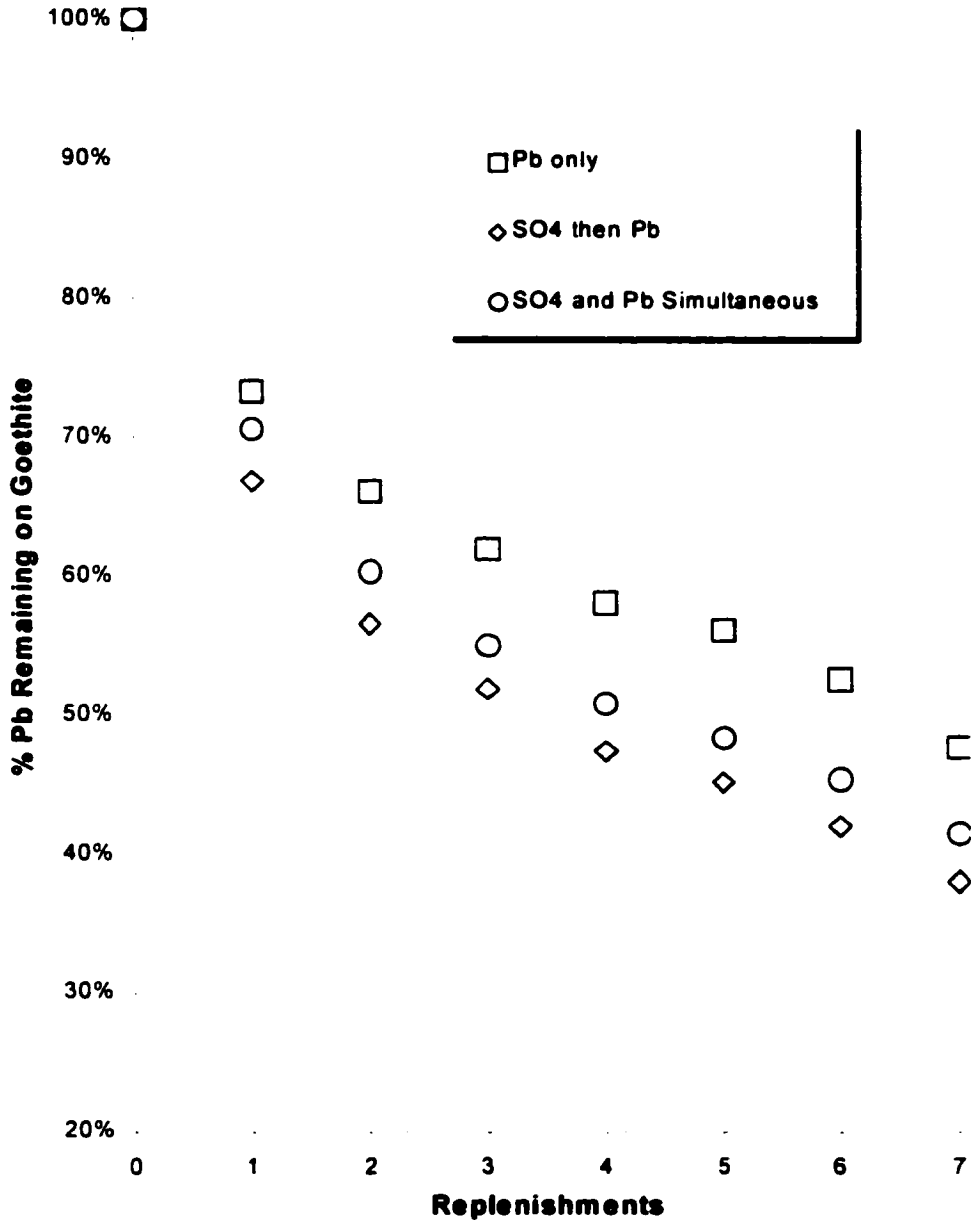

Figure 4.7 Desorption studies conducted with 0.01M NaCl at pH 3.5.

electrostatics, however, because more inner-sphere sulfate should promote Pb adsorption rather than decrease it.

Discussion

Ternary systems and the electrical double layer. From the above results, ternary complex formation with sulfate can be seen to substantially modify the rate and extent of Pb adsorption at acidic pH. Furthermore, it seems likely that not only are ternary complexes responsible but also electrostatic interactions as a result of changing surface charge upon adsorption of sulfate and Pb. This therefore has important implications for the design and refinement of surface complexation modeling. Since spectroscopy has determined that outer-sphere complexation of sulfate is important in the Pb/SO_4/goethite system, it is necessary to use a model that can describe such a reaction. This is a significant complication, as different models handle electrostatically-bound ions quite differently (or do not address them at all). Only two commonly used models have sufficient complexity to model such systems: the CD MUSIC model and the modified triple layer model. For this discussion, the Triple Layer model (TLM) will be used. The CD-MUSIC model handles distribution of charge at the surface differently (via a multiple one-pK approach) but the discussion should still be relevant.

It is beneficial to begin by considering how this surface complexation model is divided into planes. In the case of the triple layer model, potential determining ions (PDI) such as protons, hydroxyls, and specifically adsorbed ions are placed on the surface so that adsorbed ions will change the value for Ψ_0 rather than having Ψ_0 remain fixed (as in simpler Stern theory). There is another plane further from the surface (somewhat analogous to the Stern plane and also featuring a constant capacitance) called the beta plane. Electrostatically bound ions will be placed into this plane, and will further lower the potential (described by Ψ_β). Finally, there is a diffuse layer that will behave according to Guoy-Chapman theory.

For the triple layer model (TLM), inner-sphere complexation will affect the surface potential (Ψ_0) and therefore the surface charge (σ_0). The presence of an anion at the surface at pH below the PZC (where the surface is positively charged) will cause the surface charge to be less positive, and if a sufficient amount of anion is adsorbed as an inner-sphere complex then charge reversal can possibly even occur. This can result in greatly increased metal adsorption in the presence of an anion-modified surface compared to a pristine surface. However, in our experiments, charge reversal is unlikely since even at pH 4.5 (where inner-sphere complexation is known to occur) a large amount of the adsorbed sulfate remains bound electrostatically (Elzinga et al. 2001) and does not affect σ_0.

The importance of outer-sphere complexation to the overall charge and ion distribution should therefore also be addressed. At a short distance from the surface, a beta plane is defined with surface potential Ψ_β. Outer-sphere sulfate adsorbs in this plane, and will also serve to screen some of the positive surface charge.

Finally, in the diffuse layer, the positive surface charge will have the effect of increasing the amount of anions in the diffuse layer and decreasing the concentration of cations in the double layer when compared to the bulk solution concentrations.

Assuming that charge reversal doesn't occur, then this relationship between the different potentials (Ψ_0 and Ψ_β) and the concentration of cations and anions in the diffuse layer is a good explanation for why precipitation of $PbSO_{4(s)}$ has not been observed in spectroscopic studies. Since cation concentration is decreased in the diffuse layer of positively-charged colloids relative to the bulk solution, the concentration of Pb^{2+} is actually lower in the diffuse layer and in the beta plane than in bulk solution. This means that as long as the bulk solution is below an experimentally determined K_{SO} then precipitation will not occur. However, if enough sulfate is present to fully cause charge reversal then the concentration of Pb in the diffuse layer will increase relative to the bulk solution and precipitation could potentially occur. Another complication is that since the positive surface charge actually increases the concentration of hydroxyl ions (and decreases the concentration of hydronium ions) in

the double layer, the pH of the double layer and beta plane will be slightly higher than in bulk solution. The increase in pH is not substantial enough to force bulk precipitation of $Pb(OH)_{2(s)}$, and in fact may serve to increase Pb solubility because $Pb(OH)^{+}_{aq}$ concentrations will increase relative to bulk solution. However, if $Pb(OH)_{2(s)}$ precipitation does occur, then additional surface area that is potentially quite reactive will be present in the system.

The above discussion only addresses the changes upon surface charge that occur in the presence of sulfate (or any specifically adsorbing ion). Since this is a ternary system and both kinetics and equilibrium studies are being conducted, it is also important to understand how Pb can affect sulfate adsorption via changes in surface charge. Ignoring (for the moment) the possibility of direct ternary interactions, the presence of Pb on the goethite surface will still change the distribution of sulfate throughout the electrical double layer. Pb adsorbs as an inner-sphere surface complex and will make the surface potential (and hence surface charge) more positive. This will serve to increase the concentration of sulfate that can adsorb electrostatically in the beta plane. This increase in surface charge will also decrease the concentration of Pb in the beta plane and the diffuse layer, making precipitation less favorable.

To this point, only how Pb^{2+} and SO_4^{2-} can independently affect the electrical double layer (and hence the adsorption of both ions) has been considered. There is, however,

good spectroscopic evidence (Elzinga et al. 2001, Ostergren et al. 2000b) that demonstrates direct interaction between sulfate and Pb at the surface to form ternary surface complexes. Accordingly, it is important to visualize how aqueous and surface complexes of $PbSO_4$ might affect the electrical double layer as well. Incorporating aqueous $PbSO_4$ into an electrostatic model is somewhat difficult due to its neutral charge. It is generally assumed that neutral solution species are generally far less reactive than their charged counterparts, and that reactivity increases with increasing valence on the ion. However, uncharged does not actually imply inert, and neutral species may remain polar or amphoteric and may also have lowered solubility compared to their constituent ions. Recent research on arsenite adsorption on iron and aluminum oxides (Arai et al. 2001, Goldberg and Johnston 2001) and boric acid on iron oxides (Chapter 3) reveals substantial adsorption of neutral molecules on metal oxide surfaces. It is not unreasonable to assume that $PbSO_4$ aqueous complexes might behave similarly to some of these oxyanions. While $PbSO_4$ is formally neutral, the interaction between many divalent metal cations and sulfate in aqueous solutions is primarily outer-sphere in nature (Elzinga et al. 2001) and may result in a reactive complex. So the possibility of adsorption of $PbSO_4$ from solution can not be ignored. However, it is also possible that the bare metal cation adsorbs onto the goethite surface, and then ternary complex formation occurs with sulfate.

Additionally, since this aqueous $PbSO_4$ complex is neutral, it will not face the charge repulsion that Pb^{2+} must overcome to make it to the positively charged goethite surface. Another consideration is that since the thermodynamics of solution reactions are typically much faster than reactions at surfaces, then if Pb^{2+} reacts with the surface to form an inner-sphere complex, a portion of the $PbSO_4$ in the beta plane will dissociate to maintain solution equilibrium and serve as a pool of Pb^{2+} for surface reaction.

Discussion of results from this study. It was not the goal of this study to model Pb/SO_4/goethite adsorption. However, it is our hope that results from our kinetics and equilibrium studies might suggest important features of the adsorption reaction that should be described by a surface complexation model. In particular, the importance of addition order at pH 4.5 on Pb adsorption (Figure 4.4) is an observation that merits discussion. Regardless of addition order, sulfate concentrations in solution are nearly constant upon Pb addition (1.0 mM with simultaneous addition and 0.9 mM with Pb added to sulfate-saturated goethite), so the observed effect is not likely to be due to $PbSO_{4(aq)}$. The reaction kinetics are more rapid when Pb is added to a sulfate-saturated goethite even though the extent of Pb adsorption is decreased. A change in both reaction rate and extent suggests that there is a chemical change in the adsorption reaction rather than simply a change in the surface charge. EXAFS spectroscopic studies have all been conducted with Pb added to a goethite surface with sulfate

already present (Ostergren et al. 2000, Elzinga et al. 2001). In these EXAFS studies it was observed that Pb binds directly to the goethite surface. Additionally, Elzinga and coworkers (2001) found that the infrared spectra of adsorbed sulfate changed upon addition of Pb. The exact mechanism for these reactions is not known, but the ultimate formation of a direct surface hydroxyl-Pb bond and the formation of a Pb-SO_4 ternary complex have both been directly observed. It is therefore reasonable for a surface reaction to proceed via two mechanisms: either adsorbed sulfate is displaced by adsorbed Pb or Pb adsorbs on separate surface sites from SO_4, and SO_4 affects Pb adsorption by changing the surface charge of the sorbent. In both cases, ternary complex formation may occur between adsorbed Pb and SO_4.

The enhanced reaction rate when Pb is added to a sulfate-saturated goethite compared to simultaneous addition of Pb and SO_4 provides interesting insight into which mechanism is more likely. Since an additional barrier to adsorption is present if adsorbed SO_4 is displaced at the surface, it is not intuitive that the rate of reaction would be faster. Instead, one would expect the observed reaction rate to be slower if displacement of SO_4 is occurring at the surface. A better explanation for the faster rate and lower extent of adsorption is the possibility that some sites on the goethite surface are very reactive with Pb but do not form inner-sphere SO_4 surface complexes. Inner-sphere sulfate complexation on goethite occurs via ligand exchange primarily with a fully-protonated ($Fe\text{-}OH_2^+$) surface hydroxyl (Peak et al. 1999):

$$Fe\text{-}OH_2^+ + SO_4^{2-} \rightarrow Fe\text{-}OSO_3^- + H_2O$$

whereas Pb reacts more strongly with FeOH surface groups (Barger et al. 1997b):

$$Fe\text{-}OH + Pb^{2+} \rightarrow Fe\text{-}OPb^+ + H^+$$

so the adsorption upon differing sites is reasonable as long as both Fe-OH and Fe-OH_2^+ sites are both present. This would explain the kinetics results well, since the surface would be more negative in the presence of inner-sphere SO_4, Pb would have less of an electrostatic barrier to approach the surface. However, since many of the total surface sites are occupied by inner-sphere SO_4, the total amount of Pb that can adsorb is less than when Pb and SO_4 are added simultaneously. Once Pb adsorbs on the goethite surface, weakly-bound SO_4 that is present at the surface and SO_4 in the double layer then can form ternary complexes. This mechanism is also consistent with the Elzinga and coworkers (2001), who observed that conversion of SO_4 at the surface occurred at higher Pb concentrations. This would be observed over the entire concentration range if displacement of adsorbed SO_4 were the primary reaction mechanism.

Similarly, the pH 5.5 kinetics data is in good agreement with a mechanism where Pb and SO_4 adsorb to different sites and then form ternary complexes. At pH 5.5, very little of the adsorbed SO_4 is inner-sphere (Peak et al. 1999), and the dominant surface functional group is FeOH. Under these reaction conditions, it would be expected that the presence of sulfate would have less of an effect upon Pb adsorption. This is indeed

the case, and additionally there is no effect of addition order on the amount of Pb that adsorbs. At pH 5.5 it is reasonable to conclude that SO_4 primarily interacts with Pb by forming weak ternary complexes that can shield some of the Pb charge and allow for additional adsorption.

The desorption data results also provide some further insight into the nature of Pb/SO_4 interactions. When desorption is carried out at pH 4.5, then the relative amount of desorption in the SO_4 experiments has no dependence on addition order. This implies that there is no difference in the way that Pb is bound to the surface when addition order is changed. This is consistent with a Pb/SO_4 ternary complex that is of the same chemical form regardless of addition order. Interestingly, when desorption is carried out at pH 3.5, then addition order affects the amount of Pb that is desorbed from goethite. Since the same adsorption samples were used for both pH 4.5 and pH 3.5 desorption, it is reasonable to conclude that differences in desorption that result from SO_4 addition order are due to changes in SO_4 bonding at the surface. A reasonable conclusion is that the pH 3.5 NaCl desorptive agent will increase the amount of Fe-OH_2^+ surface groups and convert some outer-sphere SO_4 to inner-sphere SO_4 complexes at the goethite surface. Since more Pb was adsorbed at pH 4.5 when SO_4 and Pb were added simultaneously, more SO_4 could be adsorbed in the simultaneous samples as well. This increased concentration of SO_4 would help stabilize Pb on the surface when pH is lowered to 3.5.

Conclusions

The results of these studies indicate that interactions between sulfate and lead at the iron oxide surface may substantially affect lead retention in soils. Particularly at pH 4.5, the presence of sulfate increases Pb adsorption by 10-35% depending upon addition order. For natural systems, it is expected that different anions such as sulfate, phosphate, and carbonate will form surface complexes with metal oxides, and that oxyanions will also be ubiquitous in the soil solution. When one considers that Pb begins to precipitate above pH 6.0 as $PbSO_4$ (and $PbCO_3$ in open systems) phases, then there is a relatively narrow range of pH where binary adsorption reactions between Pb^{2+} and the goethite surface are dominant. Adsorption kinetics studies demonstrated that ternary reactions of Pb and SO_4 occur on rapid time scales. Desorption studies demonstrated that the stability of Pb adsorbed in the presence of SO_4 is variable. Under conditions where an excess of SO_4 remains in solution, Pb retention is enhanced relative to desorption of Pb in SO_4-free experiments. However, if both Pb and SO_4 are removed from solution then Pb release is greater than in the SO_4-free experiments. This makes generalizations about Pb retention difficult, as the stability of Pb-SO_4 adsorption complexes in natural systems will depend upon the composition of the soil solution.

Chapter 5

SOLID-STATE SPECIATION OF NATURAL AND ALUM AMENDED POULTRY LITTER USING XANES SPECTROSCOPY

Introduction

Phosphate is one of the most-studied of all oxyanions found in the soil environment. It is a plant macronutrient, and was first studied by soil chemists to maximize agronomic yields. An enormous amount of information about phosphate sorption on soils and soil components has been compiled over the last 50 years, with emphasis on determining empirical parameters from sorption experiments such as isotherms. An excellent overview of the early research about phosphate sorption to soils and oxides was written by R.L. Parfitt (1978). From these early studies, some important generalizations about phosphate chemistry in soils can be made. Metal oxides are the most common sorbents of phosphate in acid to neutral soils, especially iron and aluminum oxides. This is due to their high surface area and positive surface charge below pH 7. In alkaline and calcareous soils, precipitation of calcium phosphate also becomes important in describing phosphate reactivity. Phosphate sorption is usually described as biphasic, with an extremely rapid initial uptake followed by a much slower continued sorption. This has been explained by a fast adsorption reaction

followed by either a slow diffusion to internal sites or by a precipitation reaction with cations in the soil such as aluminum, iron, or calcium.

In the last three decades, phosphate research has shifted its emphasis from agricultural productivity to that of environmental protection. Repeated over application of inorganic fertilizers and organic wastes such as biosolids and manure high in phosphate has led to extremely high levels of phosphate in soils of the Mid-Atlantic region of the United States (Sims 1997).

This phosphate is commonly in an extremely soluble form, and makes its way to waterways via erosion and surface flow (Sims and Wolf 1994, Sharpley et al. 1994), and even leaching though the soil to the drainage and groundwaters in some cases (Sims et al. 1998). This poses a serious environmental threat for several reasons. First of all, contamination of drinking water has occurred in some instances. An even more serious threat to the environment comes from eutrophication. Phosphorus is a limiting nutrient in many aquatic systems, and anthropogenic inputs of excessive phosphate can often lead to algal blooms and fish kills when the respiration depletes the available oxygen. Finally, there are emerging human health concerns, as phosphate levels have been linked to *Pfiesteria piscicida* growth (Faith and Miller 2000). *Pfiesteria* is a toxic dinoflagellate that can cause neuro-physiological effects such as memory loss in humans.

The major contributor to excessive phosphorus levels in Delaware soils and waters is poultry manure. Approximately 750,000 tons of poultry manure is produced per year, and this presents an incredible challenge to those trying to minimize environmental effects of over application. Several possible solutions have been proposed, including: (i) genetic modification of feed grain to make phosphorus in corn more digestible to poultry by reducing levels of phytic acid and alleviating the need for large quantities of supplemental phosphate in feeds (Ertl et al. 1998), (ii) dietary supplements of phytase to increase phosphate uptake from grain and minimize additional inorganic phosphate supplements in feed (Huff et al. 1998), and (iii) application of water treatment chemicals such as coagulants to immobilize phosphate in the poultry litter (Moore and Miller 1994, Shreve et al. 1995). As an immediate solution, the use of coagulants has gained favor by researchers and farmers for its low cost, ease of use, and effectiveness at lowering levels of water soluble P in poultry litter.

Coagulants containing aluminum appear to be the most useful for Delaware soils because ferric-based coagulants will tend to be reduced to iron (II) in anaerobic conditions, which will negatively influence phosphate sorption (Vadas and Sims 1999). In particular, there has been research (Moore and Miller 1994, Shreve et al. 1995) on the use of alum (aluminum sulfate) to reduce water-soluble phosphate levels in poultry litter. Shreve and coworkers (1995) determined that alum not only lowers water-soluble P concentrations in poultry litter, but also continues to be effective at

lowering P levels in runoff once the litter is applied to soils. It has been proposed (Moore and Miller 1994) that the following chemical reaction occurs between alum and phosphate:

$$Al_2(SO_4)_3 \cdot 14H_2O_{(s)} + 2PO_4^{3-}{}_{(aq)} \rightarrow 2\ AlPO_{4(s)} + 3SO_4^{2-}{}_{(aq)} + 14\ H_2O_{(l)}$$

whereby alum reacts with aqueous phosphate in the litter to form an aluminum phosphate. However, it is important to consider that many environmental variables are affecting any chemical reactions that occur between phosphate and alum in the poultry litter. First of all, the animal waste (and therefore PO_4) is being produced continuously; while the alum is applied only at the beginning of each flock of birds. This means that an initial pH of 4-5 occurs due to acidification caused by alum solubilization. The pH then slowly increases to roughly pH 7 over the time the flock is in the house (Moore and Miller 1994). Reactions may also be affected by the fact that mixing only occurs by the movement of birds in the houses, which is sporadic and imperfect. There are also fluctuations in water content and in temperature that could affect the pathway by which reactions proceed. Extrapolation of aluminum/phosphate reaction mechanisms elucidated in controlled laboratory conditions to explain alum/litter reactions under such variable conditions is tenuous at best. Therefore, studies which monitor alum/litter reactions under conditions similar to the field are

required to determine the mechanisms that are occurring and also whether reaction products change with residence time.

Understanding how alum reacts with litter to reduce levels of water-soluble P requires the use of molecular-scale spectroscopic techniques, as macroscopic techniques such as extractions cannot conclusively determine reaction mechanisms (Sparks 1995). For these molecular-scale techniques to be of predictive value, the studies should be conducted in conditions as close to the field environment as possible, with normal amounts of water present and at ambient pressures to avoid possible artifacts that can be caused by sample preparation. Researchers have successfully employed *in situ* Attenuated Total Reflectance Fourier Transform Infrared (ATR-FTIR) spectroscopy to determine the adsorption mechanisms of phosphate on goethite (Tejedor-Tejedor and Anderson 1990) and ferrihydrite (Arai and Sparks 2001). These studies provided detailed information about complexation mechanisms of phosphate on iron oxides, but conducting similar ATR-FTIR spectroscopic studies to determine phosphate bonding in poultry litter would be impractical due to overlapping infrared bands of different phosphate species as well as interferences from organic spectral features of the poultry litter. The complicated composition of the poultry litter and the high probability that any aluminum phosphates that form are amorphous make bulk X-ray diffraction also extremely difficult in this system. Several other techniques that are commonly used in studies of heavy metals (XPS, DRS) are also of less utility when investigating lighter

elements such as Al and P. Fortunately, X-ray Absorption Spectroscopy (XAS) spectroscopy provides a molecular scale method to probe the local chemical environment of P in the litter samples. Extended X-ray Absorption Fine Structure (EXAFS) spectroscopic studies of the effects of phosphate on iron oxy-hydroxide precipitation have shown that P k-edge EXAFS are possible (Rose et al. 1997), but the studies required considerable sample modification and were not composed of such a complex mixture of phosphate species as the litter samples in this study. Furthermore, iron is a much heavier backscatterer and makes the fitting of P EXAFS data much easier than dealing with aluminum, calcium, and carbon (the likely nearest neighbors to phosphate in poultry litter samples). On the other hand, X-ray Absorption Near Edge Structure (XANES) spectroscopy provides a method to probe the speciation of phosphate in poultry litter with minimal sample modification and much simpler data reduction. Unlike many other routine spectroscopic tools, XANES can be employed with heterogeneous samples (e.g., soils and poultry litter) and one can analyze samples *in situ* (normal amounts of water at room temperature and pressure). Useful and unique chemical information can be obtained from XANES such as oxidation state and approximate concentration (if calibrated). One of the most powerful aspects of EXAFS is the ability to utilize software code to fit theoretical scattering paths to experimental spectra and extract parameters such as nearest neighbor identity, nearest coordination number, and bond distances (Zabinsky et al. 1995). Unfortunately, XANES spectra are dominated by multiple scattering contributions and *ab initio* fitting

of XANES spectra for lighter elements such as phosphorus is not yet commonplace. Nonetheless, qualitative structural information about the average local chemical environment can also be elucidated via XANES spectroscopy by employing a fingerprinting technique, meaning that unknown samples are compared with a library of reference compounds to find similarities (Fendorf and Sparks 1996).

The overall objective of this study is to perform direct speciation of poultry litter using XANES spectropscopy. Of particular interest are what mineral phases form in both unamended and alum-amended poultry litter, and how the amount of alum added affects the speciation of phosphate.

Materials and Methods

Sample Collection and Preparation. Poultry litter samples were obtained from J.T. Sims that had been air-dried and homogenized. These samples were part of an extensive field study involving 200 poultry houses in southern Delaware that have similar history and operating practices. One hundred of these houses received alum application (with varying rates ranging from 0.6 and 1.1 aluminum/phosphate ratios in the final litter), and one hundred houses received no alum addition. The chemical analysis of these samples had also been performed in Dr. Sims' lab prior to XANES analysis. The chemical analysis of these samples is summarized in Table 1. The EPA 3050 method was utilized for total elemental analysis of the litter samples, and water

soluble elements were extracted via shaking a 100 gL^{-1} slurry of poultry litter and deionized water for one hour, filtering with a 0.45μm filter, and analyzing the filtrate with ICP-AES. All values are in mg kg^{-1}. Some generalizations about the effects of alum on poultry litter chemistry can be made from the chemical analysis. Total phosphorus concentrations in all samples are around 20,000 mg kg^{-1} litter (2%wt.) regardless of whether alum is added or not. To understand how pH and alum/P ratio are affecting water soluble P, the water soluble P was divided by the total P to determine the percent of phosphate in the litter that is water soluble (labeled % soluble in Table 5.1). For the unamended samples, there is surprisingly no clear variation in the percentage of P that is water soluble with pH. However, a strong correlation between aluminum/phosphate ratios and water soluble phosphate is observed. Water soluble P levels in the litter decrease markedly upon alum addition when compared to the control houses. This occurs with an increase in levels of water-soluble Al. Interestingly, the observed concentrations of Al are above solubility limits, and so some colloidal aluminum (either hydroxide phases or aluminum-organic complexes) are likely passing through the filters used. With the exception of house 182, all of the alum amended houses fall in the 1-3% water soluble P range, while the control houses range from 7-13% water soluble P. Also bearing discussion is the fact that Al/P ratios, when presented as a molar ratio rather than by weight are all reasonably close to 1.0, which may indicate $AlPO_{4(s)}$ precipitation in amended samples.

Table 5.1. Chemical analysis of poultry litter samples used in XANES spectroscopic studies. Numbers are all expressed as mg/kg litter.

Control Houses

House	Total P (mg/kg)	Water Sol P (mg/kg)	% Soluble	Al/P Ratio (wt%)	Al/P Ratio (molar)	Water Sol Al (mg/kg)	Final pH
536	20712	2679	12.9	0.04	0.05	3.8	7.91
504	20160	2225	11.0	0.04	0.05	4.8	7.81
509	19888	2222	11.2	0.04	0.05	4.4	7.74
519	21498	1557	7.2	0.04	0.05	5.4	7.95
507	21174	1910	9.0	0.05	0.05	2	7.42
592	21843	1672	7.7	0.05	0.06	5.4	7.38
541	19590	1308	6.7	0.05	0.06	6.1	8.23

Alum Amended Houses

House	Total P (mg/kg)	Water Sol P (mg/kg)	% Soluble	Al/P Ratio (wt%)	Al/P Ratio (molar)	Water Sol Al (mg/kg)	Final pH
131	21052	492	2.3	0.65	0.75	20.7	7.3
117	21867	732	3.3	0.66	0.76	23.3	7.36
181	20080	973	4.8	0.71	0.82	20.5	7.15
182	19410	1167	6.0	0.84	0.97	19.5	7.03
125	19696	332	1.7	0.90	1.04	18.9	7.23
184	19629	421	2.1	1.00	1.16	21.1	6.62
191	19132	542	2.8	1.13	1.31	18.8	6.89

However, there is a sizeable fraction of the total P that is present as organic phosphate (as much as 20-50% depending upon sources and diet) that is not expected to react with aluminum. This makes using macroscopic information such as molar ratios unreliable. If one considers water soluble phosphate levels from the unamended houses to be typical (1300-2700 mg/kg litter), then a crude estimate of the phosphate associated with aluminum can be made by subtracting the water soluble phosphate in the alum amended samples (300-1200 mg/kg litter) from an average of the control houses (1940 mg/kg litter on average). If this estimate for the amount of water soluble phosphate removed from the litter by alum is compared to the aluminum added, then molar ratios of Al/P are much higher (10-20 to 1), and show a consistent trend. In houses where alum was most effective at lowering water soluble phosphorus, then the Al/P ratio is low. For houses where more water soluble phosphate remained after alum addition, the Al/P ratio is larger. This is in contrast with the ratios obtained from total Al and P, which showed no consistent trend and reported molar ratios near 1. The results of this analysis are compiled in Table 5.2. The difficulty in interpreting the macroscopic data highlights the need for direct speciation of the poultry litter.

Table 5.2. Chemical analysis of alum amended poultry litter samples reanalyzed to compare the reduction in water soluble phosphate to the amount of alum added. Numbers are all expressed as mg/kg litter.

House	Sol P Decrease (mg/kg)	Al Added (mg/kg)	Al/P Ratio (wt%)	Al/P Ratio (molar)
131	1447	13705	9.47	10.94
117	1207	14345	11.88	13.73
181	966	14176	14.68	16.96
182	772	16285	21.09	24.38
125	1607	17707	11.02	12.73
184	1518	19708	12.98	15.00
191	1397	21638	15.49	17.90

Reference minerals and sorbent synthesis. Variscite, wavelite, and monetite (dicalcium phosphate) reference minerals and XANES spectra were supplied by Dr. Y.A. Arai. Hydroxylapatite, calcium sulfate, aluminum sulfate, ammonium sulfate, calcium chloride, and phytic acid reagent grade chemicals were all purchased commercially, ground with a mortar and pestle, and used without further modification. Taranakite was synthesized according to the method of Zhou et al. (2000), and amorphous aluminum phosphate was synthesized by titrating a solution containing 0.1M $Al(Cl)_3$ and 0.1M NaH_2PO_4 to pH 4.5 and incubating at 25C for 48 hours. Gibbsite sorbent was provided by Dr. N. Yamaguchi, and had a specific surface area of 96 m^2g^{-1}. Amorphous aluminum hydroxide was produced by titration of a 1M $AlCl_3$ solution to pH 5 with 4M KOH, followed by repeated washing with centrifugation (five times with deionized water) to remove residual Al and Cl. For adsorption onto aluminum hydroxides, the reaction conditions were a reaction time of 24 hours, pH 5, ionic strength of 0.1M ($NaNO_3$), and 20 mM PO_4 added. Synthetic adsorption and amorphous precipitates were filtered at the beamline's laboratory space with a vacuum pump, the filtrate was washed with 100 mL of deionized water, and the product was estimated to contain approximately 10% water.

X-Ray Absorption Near Edge Structure (XANES) Spectroscopy. All XANES spectroscopic studies were conducted at beamline X19-A of the National Synchrotron Light Source at Brookhaven National Laboratory in Upton NY. Samples were covered

with a thin mylar film and placed inside a helium-purged sample compartment. Samples of reference salts were analyzed as ground powders, and all mineral phases and litter samples were analyzed as moist pastes. Water content of the litter samples was estimated to be approximated 20-30%. A solid state PIPS detector collected spectra in fluorescence mode. XANES spectra were collected from 10 eV below the P k edge until 50 eV beyond the edge, which encompasses the near edge region. Limitations of the beamline prohibited going further below the P edge, making background subtraction sometimes a challenge for more dilute samples. For S and Ca k edge XANES studies, samples were collected from 100 eV below the edge to 50 eV above the edge to improve background subtraction. Multiple scans of each sample were collected and averaged together to improve the signal to noise ratio. Data reduction was done with WinXAS 2.1. The background was removed with a linear fit, and the spectra were all normalized to e_0 of 2158.51 eV.

Results and Discussion

To understand phosphate speciation in natural samples, it is necessary to determine how different chemical environments affect the XANES spectra of phosphate. This is particularly important in our studies since we are using a fingerprinting technique to compare poultry litter samples to references. The two cations that are most likely to interact with phosphate in the poultry litter are calcium and aluminum since their concentrations are much higher than any other ions in the litter. When the litter is in

an unamended state, calcium is anticipated to be the dominant cation, while when alum is added to the poultry houses then both aluminum and calcium may potentially react with phosphate.

A portion of the total phosphorus in the poultry litter is present as organic phosphates. The exact amount is not known, but it can be assumed to be relatively constant in both alum amended and non amended samples. Figure 5.1 shows the XANES spectra of phytic acid (innositol phosphate) as an aqueous species (50%wt) and as a calcium salt. In both cases, the observed XANES spectra are devoid of features that readily distinguish them from aqueous phosphate. Therefore, quantitatively distinguishing between free inorganic P, very weakly bound phosphate (associated with organic matter), and organic P in the poultry litter samples is very difficult. However, there are some differences that are more qualitative in nature. Careful comparison reveals that organic phosphate spectra possess some broadening of the white line peak (2158.5eV) as well as an increase in the post edge spectral height compared to aqueous phosphate. Neither of these differences is suitable for separating a mixture of organic and aqueous phosphates into individual components. However, it may be reasonable to assume that the primary source of organic phosphate in the litter is the animal waste itself and that formation of organic phosphate in the litter is relatively minor. This implies that the fraction of organic P is relatively constant in both control and amended samples while the fraction of weakly bound and aqueous phosphate is

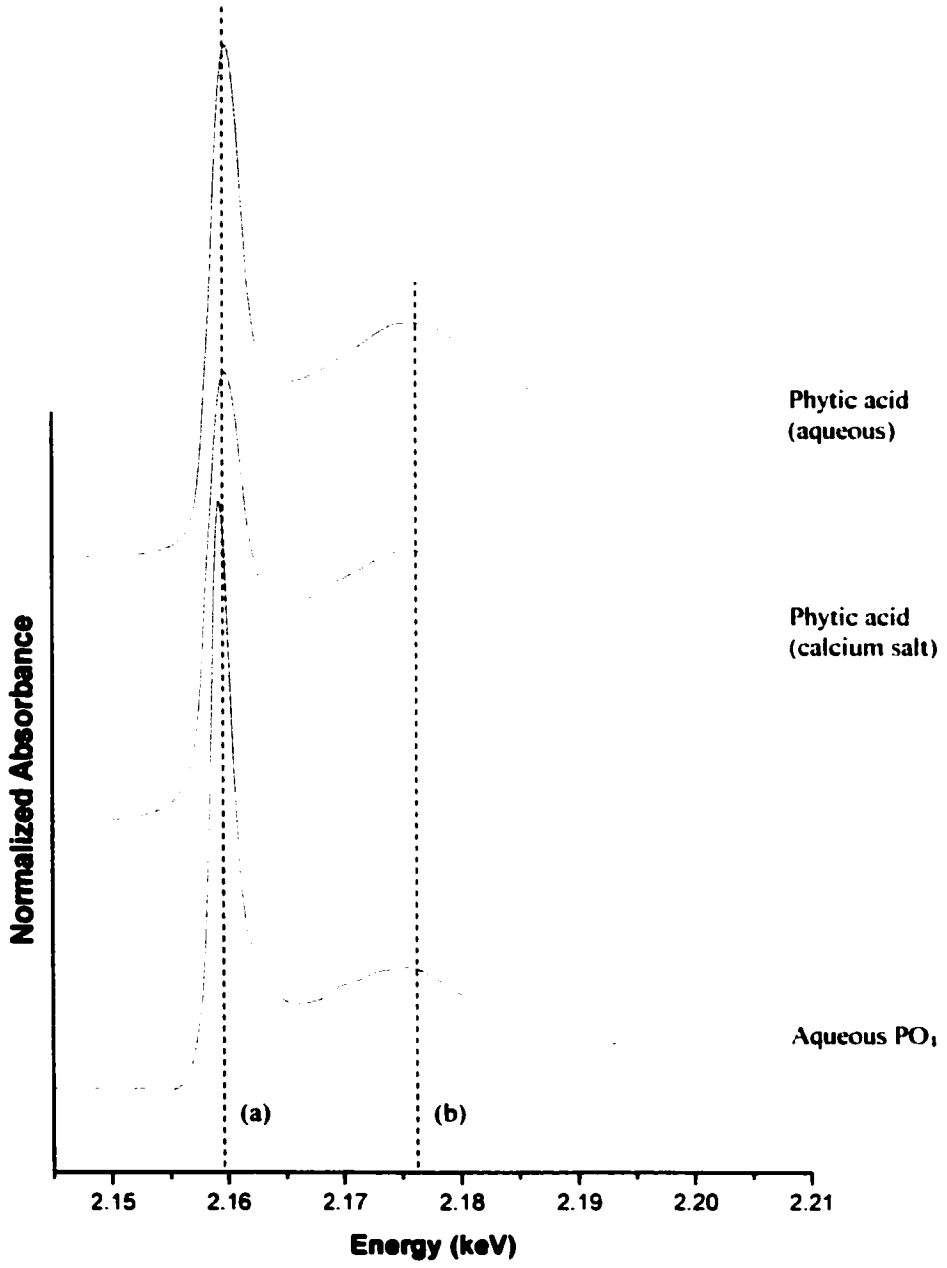

Figure 5.1. P k-edge XANES spectra of different organic phosphate reference materials. Phytic acid (inositol phosphate) was chosen as it is a major form of organic P in poultry feed, and aqueous phosphate was included for comparison. The dashed lines indicate different spectral features of importance, and are labeled as follows: (a) absorption edge (white line energy) for P(V) (b) Oxygen oscillation

variable that any changes in the importance of spectral features that can be attributed to either compound is due to differences in the amount of free or weakly bound phosphate in the litter.

For calcium phosphate references, samples were analyzed that encompass sorption onto calcium carbonates and also precipitation of both amorphous and crystalline calcium phosphates. The XANES spectra of these references can be seen in Figure 5.2. Whether sorbed onto amorphous calcium carbonate or precipitated as calcium phosphate minerals, phosphate bound to calcium displays several features in the XANES region. The first and most important feature is the presence of a shoulder past the edge at 2160-2165 eV. This feature is seen in all calcium phosphate references regardless of structure or cystallinity. There is a second peak that occurs at approximately 2170 eV in all references with a structure similar to apatite ($Ca_2(OH)PO_4$). This feature is present in the phosphate on $CaCO_3$ sample as well, suggesting that precipitation is likely occurring along with adsorption in that system. Finally, some calcium phosphate minerals have a $CaHPO_4$ structure, such as brushite (dicalcium phosphate dehydrate) and monetite (dicalcium phosphate). Dicalcium phosphates lack the peak at 2170 eV seen in apatite-type minerals.

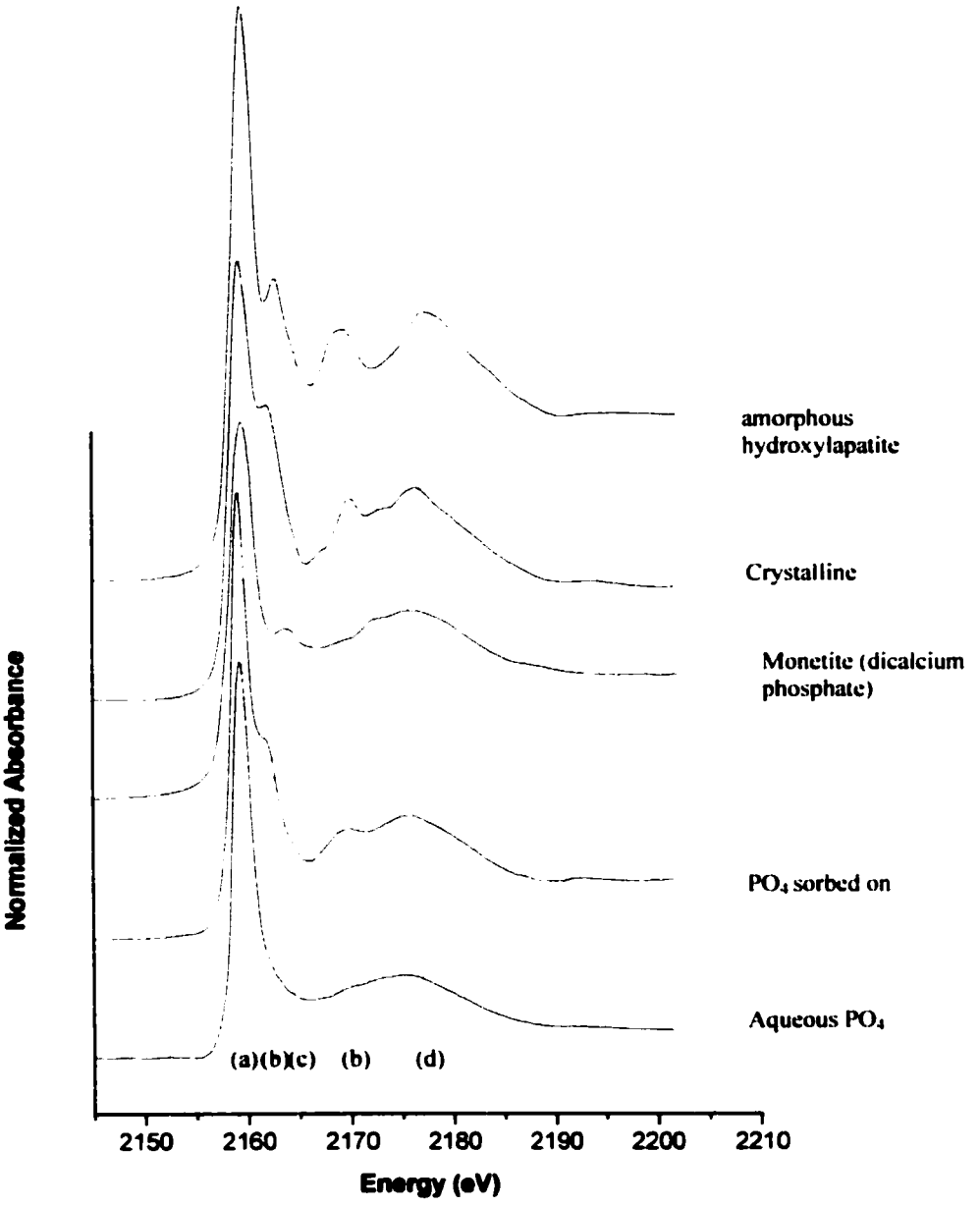

Figure 5.2. P K-edge XANES spectra of different calcium phosphate reference materials. Crystalline and amorphous mineral phases and sorption samples are included, with aqueous phosphate for comparison. The dashed lines indicate different spectral features of importance, and are labeled as follows: (a) absorption edge (white line energy) for P(V) (b) unique spectral feature of hydroxylapatite type calcium phosphates (c) Unique spectral features of dicalcium phosphate type phases (d) Oxygen oscillation

For aluminum phosphate references, samples were chosen that encompassed a range of aluminum-phosphate bonding environments: adsorption onto amorphous and crystalline aluminum oxides and precipitation of amorphous and crystalline aluminum phosphates. The XANES spectra of these reference samples can be seen in Figure 5.3. The differences between spectra of phosphate adsorbed on aluminum oxides and $PO_{4(aq)}$ are fairly subtle. Careful inspection of the spectra reveals a loss of the slight shoulder seen in $PO_{4(aq)}$ past the edge jump (2160-2165 eV) and a shift in the position and shape of the oxygen oscillation at 2175 eV when phosphate is adsorbed on aluminum oxides. This means that it is possible to distinguish adsorbed phosphate from $PO_{4(aq)}$. As the spectra of aluminum phosphate precipitates are examined, one notices an additional peak at 2165-2170 eV. This feature is broad in amorphous $AlPO_4$ and taranakite ($AlNH_4PO_4$) and becomes sharper and better defined in crystalline aluminum phosphates (wavelite and variscite). In all cases, the precipitation of phosphate with aluminum results in distinctive features in the XANES spectra.

Fortunately, the distinctive peaks for the aluminum and calcium phosphate minerals are at different energies and so it is possible to distinguish calcium and aluminum phosphates in litter samples. It is also possible to distinguish between phosphate adsorbed on aluminum oxides and precipitated aluminum phosphate due to subtle differences in the XANES region.

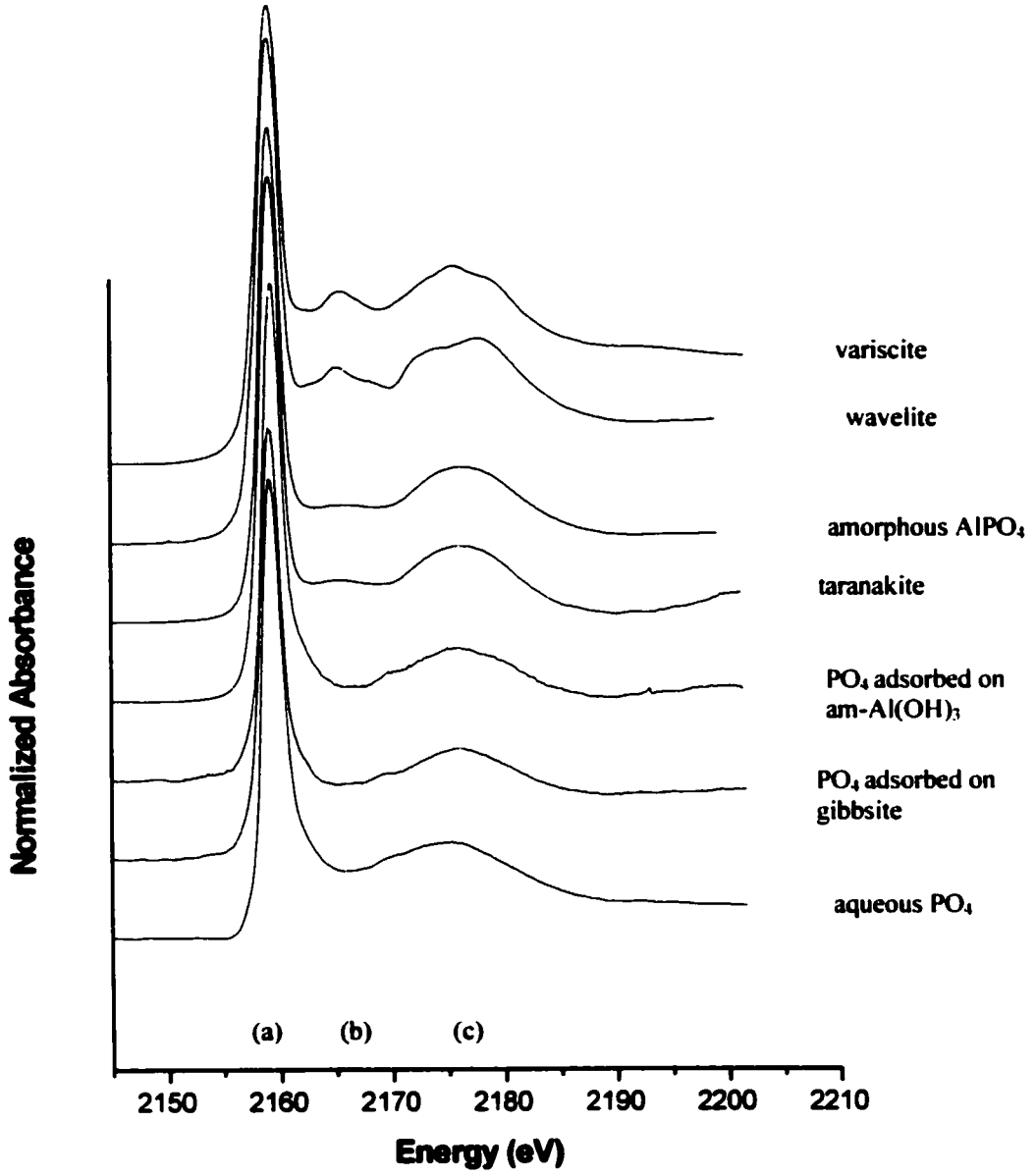

Figure 5.3. P K-edge XANES spectra of different aluminum-phosphate reference materials such as minerals and sorption samples. Amorphous and crystalline aluminum phosphates are shown along with phosphate adsorbed on both amorphous and crystalline aluminum oxides. Aqueous phosphate is also included for comparison. The dashed lines indicate different spectral features of importance, and are labeled as follows: (a) absorption edge (white line energy) for P(V) (b) unique spectral feature of aluminum phosphates not observed in litter samples (c) Oxygen oscillation

XANES spectra of poultry litter samples from southern Delaware poultry houses are shown in Figures 5.4 and 5.5. Samples numbered 504-592 are from houses where alum was not used (Figure 5.4), while samples numbered 117-191 were obtained from houses where alum was applied at different aluminum/phosphorus ratios (Figure 5.5). All of the litter samples in Figures 5.4 and 5.5 were analyzed "as is" without drying to remove water present and without grinding to homogenize the sample. Unless otherwise noted, all samples analyzed were of a fine particle size (20μm and less) as the majority of phosphate was in this fraction.

The spectra of several unamended samples are seen in Figure 5.4. The dashed spectra at the top of the graph are references that could potentially match the samples. It is clear that all of the litter spectra are similar, and that they all lack most of the features of phosphate found in aluminum phosphates (Figure 5.2) and apatite-type calcium phosphate minerals (Figure 5.1). The spectra most closely resemble aqueous phosphate and phytic acid, but the shoulder at 2160-2165 eV is much more pronounced than that of either reference compound. The position of this shoulder is consistent with the presence of a small amount of dicalcium phosphate type minerals in the samples. All of the samples appear essentially identical, suggesting that phosphate speciation is fairly consistent among all of the houses in the absence of alum.

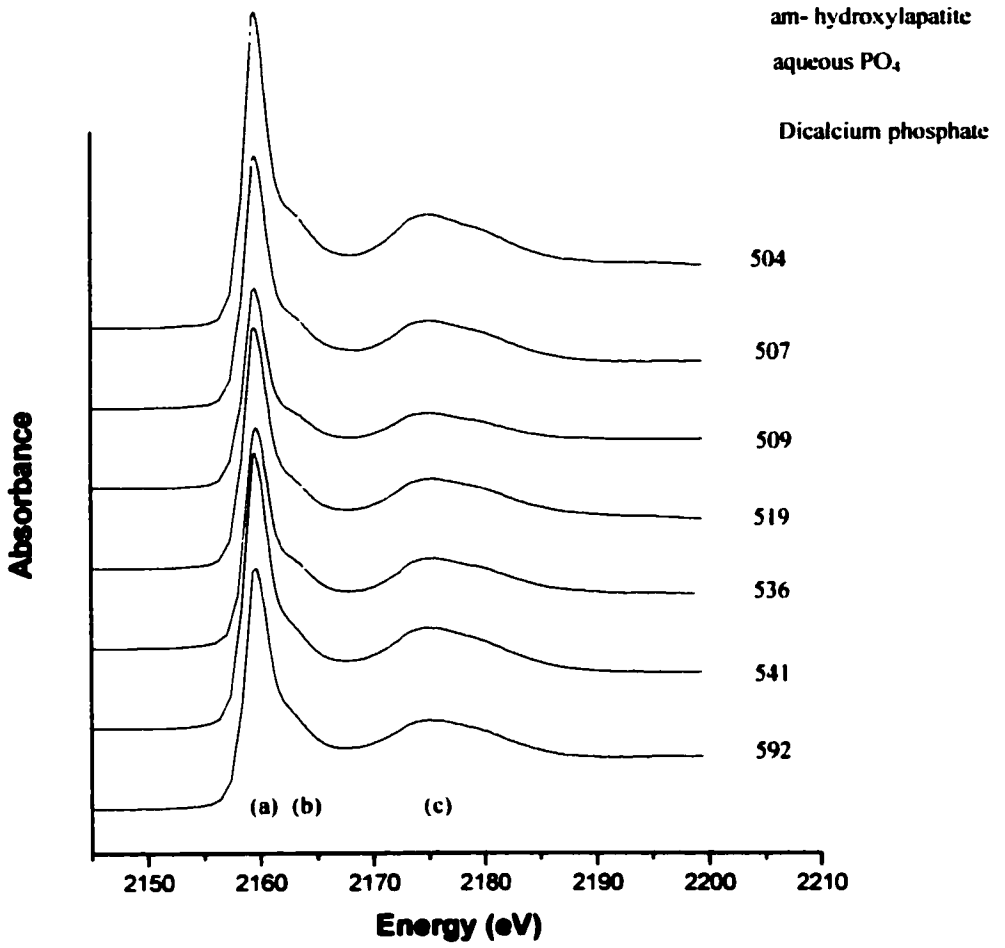

Figure 5.4. P K-edge XANES spectra of poultry litter samples from the control houses (no alum added). The spectra of aqueous phosphate, dicalcium phosphate, and amorphous hydroxyapatite are shown for reference. The litter samples are labeled according to the house from which they were taken, as in Table 1. The dashed lines indicate different spectral features of importance, and are labeled as follows: (a) absorption edge (white line energy) for P(V) (b) unique spectral feature of dicalcium phosphate and also present in litter samples (c) Oxygen oscillation

Since the poultry litter has a final pH of approximately 8, it is not surprising that calcium phosphates are observed with XANES. However, the absence of more thermodynamically stable calcium phosphates such as hydroxylapatite in the unamended litter deserves further discussion. Brushite (dicalcium phosphate) and monetite (dicalcium phosphate dihydrate) have a similar structure and are common calcium phosphates in soils under supersaturated conditions (Grossl and Inskeep 1991). However, in the absence of organic matter, these more soluble dicalcium phosphate phases rapidly convert to hydroxylapatite, the stable endpoint of the calcium phosphate system in aqueous environments at neutral or slightly basic pH values (Lindsey 1979, Stumm and Morgan 1996). In the presence of organic matter, however, the crystallization and transformations of calcium phosphates is far more complex. Inskeep and Silvertooth (1988) and Grossl and coworkers (Grossl and Inskeep 1991, 1992) studied the effects that organic acids have on the precipitation rates of dicalcium phosphate dihydrate (brushite), octacalcium phosphate, and hydroxyapatite. Their studies employed a suite of organic acids with different sizes and functional groups, and the precipitation reaction was followed by adding seed crystals of the appropriate mineral to a slightly supersaturated solution. The principal findings of these studies were that large molecular weight organic acids decrease the rate of precipitation for all three calcium phosphates by sorbing onto the minerals and coating the crystal growth sites. However, the precipitation of dicalcium phosphate continues via overgrowth of dicalcium phosphate on the organic-coated seed crystal

whereas octacalcium phosphate and apatite do not (Grossl and Inskeep 1991). Our XANES spectroscopic studies are consistent with the work of Grossl and Inskeep, since in poultry litter there is a huge quantity of organic matter that could coat any small calcium phosphate particles that form and inhibit crystal growth. In this chemical environment, brushite or monetite type calcium phosphates that are intimately associated with organic matter seem more favorable to form than other calcium phosphates that may be more thermodynamically stable in the absence of organic matter.

In the alum-amended samples (Figure 5.5) there are changes that can be observed as the Al:P ratio (the amount of alum added to the litter) is increased in the samples. At an Al:P ratio of 0.6, the spectra closely resemble those of unamended samples, suggesting that organic phosphate, weakly bound phosphate, and dicalcium phosphates are present. As aluminum content increases, however, the shoulder at 2160-2165 eV disappears, and the shape of the edge narrows while the oxygen oscillation at 2175 eV shifts slightly and becomes more rounded and symmetrical. These changes are consistent with the phosphate adsorbed on aluminum oxide references. The two samples with highest Al: P ratios appear to contain only phosphate adsorbed onto aluminum oxides and possibly some organic phosphate (there are no clearly distinguishing features to separate these references other than a broadening of the

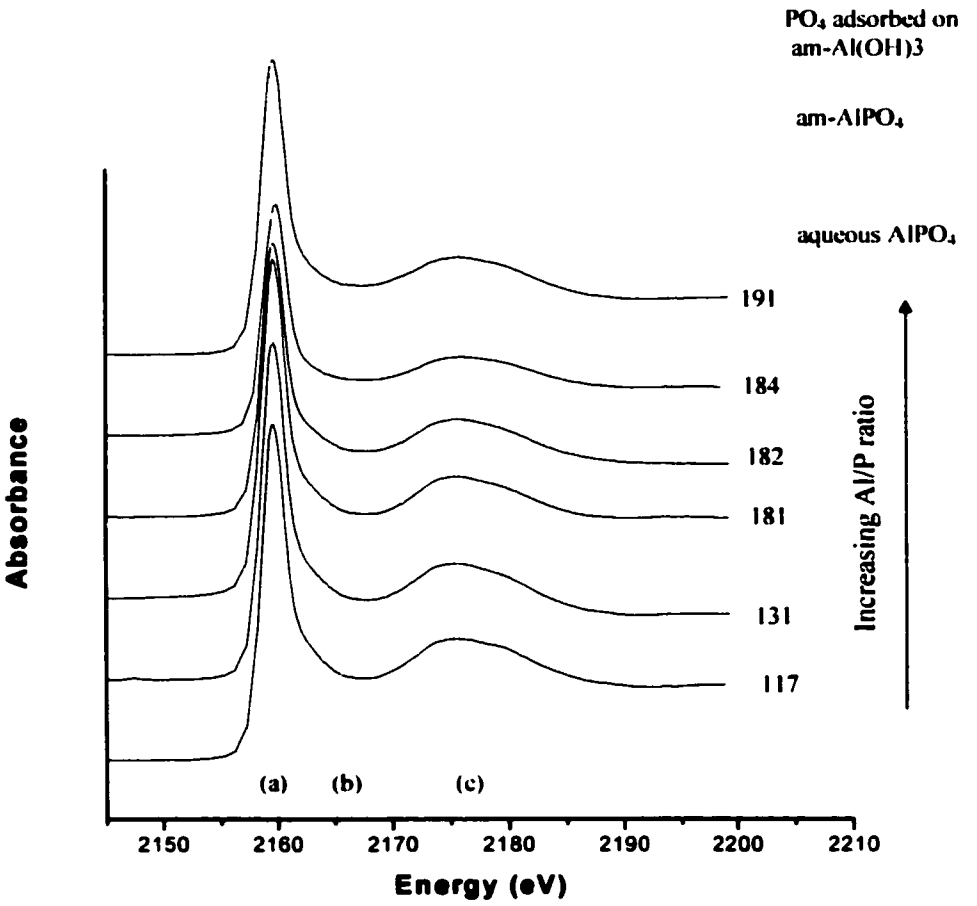

Figure 5.5. P k-edge XANES spectra of poultry litter samples from houses with alum added. The spectra of aqueous phosphate, phosphate adsorbed on amorphous aluminum hydroxide, and amorphous aluminum phosphate are shown for reference. The litter samples are labeled according to the house from which they were taken, as in Table 1. The dashed lines indicate different spectral features of importance, and are labeled as follows: (a) absorption edge (white line energy) for P(V) (b) unique spectral feature of aluminum phosphates not observed in litter samples (c) Oxygen oscillation

white line peak in organic P). No aluminum phosphate precipitate phases were observed in any of the samples.

Similarly to the unamended samples, the speciation of phosphate in the alum-amended litter at first appears to be quite different than one would predict from thermodynamic stability constants for aluminum phosphates. There are several reasons that aluminum phosphates might not occur in alum amended litter, however. First of all, the litter's pH initially drops to approximately pH 5 upon alum addition, and then gradually increases to wround pH 7 when the flock is removed from the house. As the pH gradually increases above 5, aluminum phosphate stability decreases greatly. It is possible that aluminum phosphate precipitation occurs that is followed by dissolution as time (and pH) increases. Alternatively, the reactivity of aluminum and phosphate could be kinetically controlled rather than dictated by thermodynamics. If the precipitation rates of aluminum hydroxides are much faster than aluminum phosphate precipitation rates then the sorption of phosphate on aluminum hydroxides could be expected to dominate the system. Furthermore, the presence of large quantities of organic matter may affect the precipitation rate of aluminum phosphates more than it does the precipitation of aluminum hydroxides.

One other issue regarding the alum amended samples bears noting. The XANES data indicates that some dicalcium phosphate is present in the 0.75-0.85 molar Al/P ratio

samples, but not in the higher Al/P ratio samples. Another interesting observation is that the water soluble phosphate amounts are not necessarily higher in these samples than in samples with higher total Al/P ratios where only phosphate sorbed on aluminum hydroxides is observed with XANES. This may possibly be explained by considering how phosphate enters the litter (from chicken feces) and hypothesizing about how it may interact chemically with alum in the litter. It is plausible that not all of the initial $CaHPO_4$ fed to the chickens as a dietary supplement dissolves, and so the chicken feces contains $CaHPO_4$, Ca^{2+}, and HPO_4^{2-}. The $CaHPO_4$ is not completely water soluble at the neutral to slightly basic pH of the poultry litter. Alum addition results in precipitating out $Al(OH)_3$ which adsorbs aqueous and weakly bound HPO_4^{2-} added to the litter by the feces.

Aluminum hydroxide precipitation is favored over $AlPO_4$ precipitation if the water soluble P (~2000 mg/kg litter) is the only pool readily available for reaction with Al. Alum addition will lower the litter pH, which decreases $CaHPO_4$ stability. When this occurs, further phosphate adsorption on aluminum hydroxides is expected. However, this relationship is complex, and so choosing the "optimum" Al/P ratio isn't clear cut. External factors such as feed formulation and chicken breed will affect the $Ca^{2+}/HPO_4^{-}/CaHPO_4$ distribution in the feces, and water content of the litter may substantially affect alum performance.

This hypothesis is consistent with the observation that $CaHPO_4$ spectral features can weakly be observed in the alum amended houses with Al/P (total) ratios of ~ 0.6. Lower total additions of alum will not decrease the pH as much and so they may not completely dissolve the $CaHPO_4$ present in the feces. It also is a reasonable explanation for why some samples have higher Al/P ratios but not lower water soluble P. No more $CaHPO_4$ is observed in the XANES for the high Al/P ratio samples and so presumably the conversion from calcium phosphates is complete. In some cases, however, the aluminum hydroxide/phosphate sorption complex may not as effective a sink for the phosphate as was the original $CaHPO_4$ solid phase.

Since XANES is an average local environment, and poultry litter is highly heterogeneous, experiments were also conducted to test the variability of the XANES spectra in the samples. Figure 5.6 shows a sample from house 182 prepared either as a dried, ground, and sieved powder, as an unconsolidated "as is" sample packed into a sample holder, and two separate samples prepared by selecting for the fine fraction by sieving the "as is" samples. The spectrum of the dried sample seems different and contains more free inorganic phosphate than the "as is" samples. The unconsolidated sample appears to have slightly more monetite-like calcium phosphate than the samples selected from the fine fraction. There is no difference in sample replicates taken from the fine fraction, and even the differences discussed above are very slight.

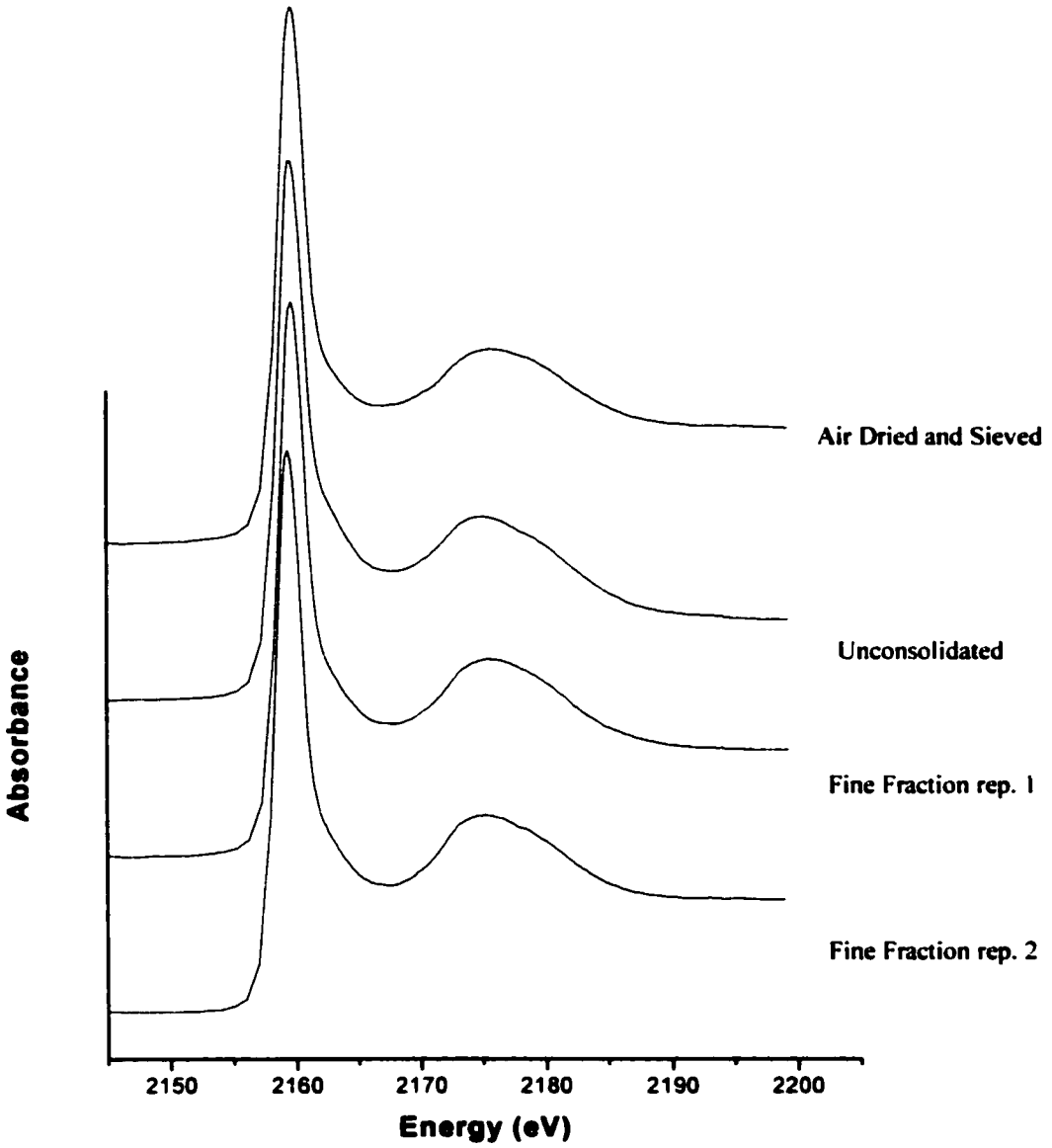

Figure 5.6. P K-edge XANES spectra of a sample from house 182 prepared in several different ways. The two fine fraction spectra result from spreading the as is sample on scotch tape prior to sample collection to select for finer particles in the litter. The unconsolidated spectrum is the result of packing the entire litter sample into a holder. The dried and ground spectrum is the result of more intensive sample modification. All samples appear similar in local bonding environment of P.

In general, XANES spectroscopy seems able to capture spectra that are representative of the samples as a whole.

While the results from P XANES spectroscopy are consistent with dicalcium phosphate formation in the unamended samples and with phosphate adsorbed on aluminum hydroxides in the alum-amended samples, the differences in spectra are all relatively subtle. This makes conclusive phosphate speciation difficult. Furthermore, it is possible that other reference compounds not analyzed may have similar spectral features to the poultry litter samples. To verify that interpretation of P XANES spectra was correct and to obtain additional chemical information about litter samples, both Ca and S k-edge XANES was also conducted.

Since dicalcium phosphate was observed at the P edge with XANES, one would expect that features consistent with dicalcium phosphate would also be present at the Ca edge.

Results from studies at the Ca k edge are presented in Figure 5.7. In the control houses, the observed Ca XANES spectrum is consistent with aqueous/weakly bound Ca^{2+} and some dicalcium phosphate. The contributions of dicalcium phosphate to the control sample can be seen by the peak at 4060 eV. This peak does not overlap with that of hydroxylapatite, and furthermore the shape and position of the white line peak is not consistent with hydroxylapatite. In the alum amended sample, there are notable

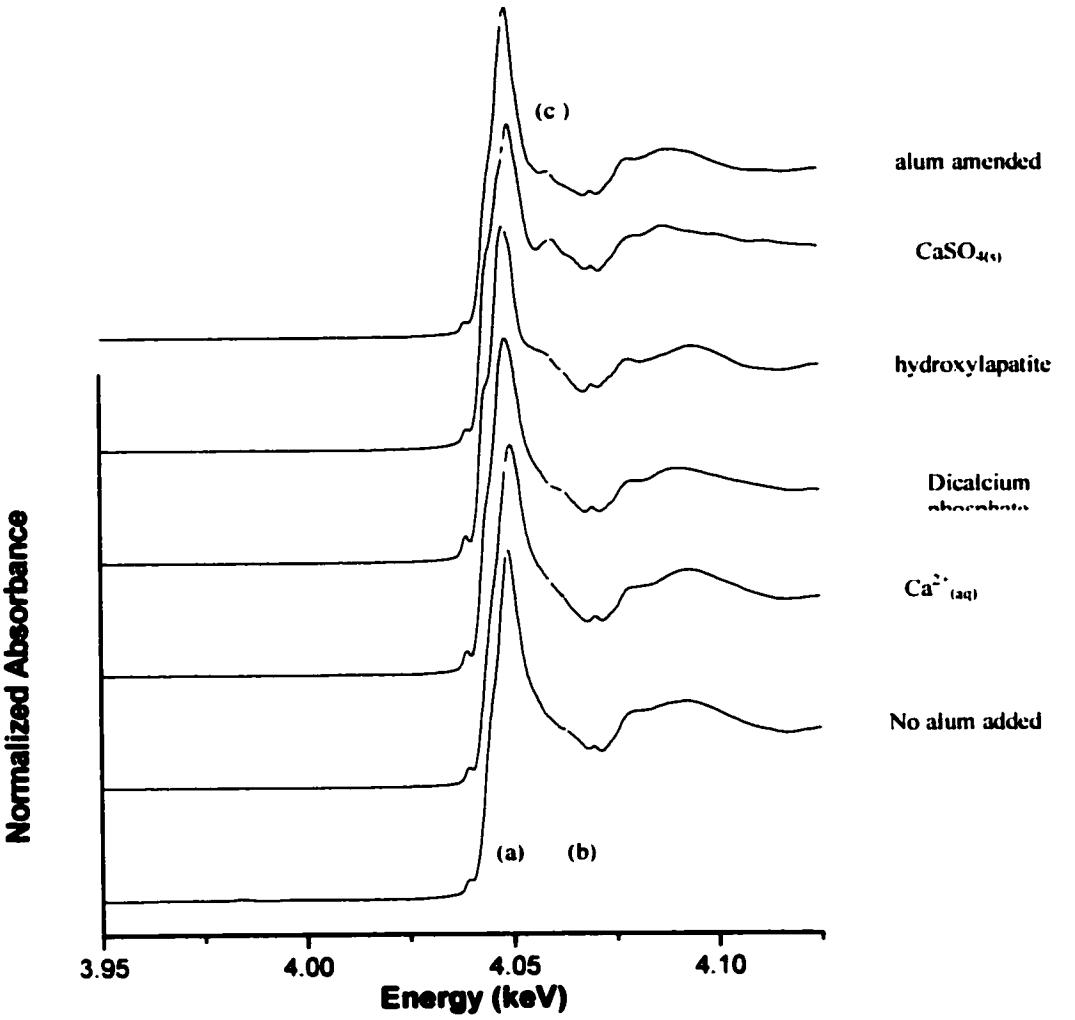

Figure 5.7. Ca K-edge XANES spectra of poultry litter samples with and without alum amendments compared to many calcium standards. It can clearly be seen that upon alum amendment that the XANES spectra of the litter samples shifts from that of a mixture of aqueous (weakly bound) calcium and dicalcium phosphate to that of calcium sulfate. The dashed lines indicate different spectral features of importance, and are labeled as follows: (a) absorption edge (white line energy) for Ca(II) (b) unique spectral feature of dicalcium phosphate (c) unique spectral feature of calcium sulfate

differences from the unamended spectra. The features attributed to dicalcium phosphate disappear, and new peaks appear in positions consistent with calcium sulfate. These results confirm the P XANES interpretation that in unamended soils dicalcium phosphate is present while in alum amended soils it is not observed. The Ca XANES results also suggest that amendment of litter with alum results in an increase in the amount of $CaSO_4$ in the samples. This is reasonable, since alum addition would result in huge inputs of sulfate to the system. To further investigate sulfate speciation in the litter, S k-edge XANES was also utilized.

Figure 5.8 shows the S k-edge XANES spectra of an unamended and an alum amended litter sample compared to aqueous sulfate, alum, ammonium sulfate, and gypsum ($CaSO_4$). In both litter samples, S occurs primarily with an oxidation state of +6, with some neutral and sulfur (I) present. The lower oxidation state sulfur is likely due to amino acids with cysteine linkages and methionine present in the organic matter of the litter. In the alum amended sample, the amount of S(VI) increases substantially (which is expected with the huge input of sulfate from the alum). For both amended and control houses, the XANES spectra suggest that the dominant S(VI) species is $CaSO_4$. A second sulfate species is present, but the features, designated as (d) in Figure 5.8, are not particularly well resolved from those of $CaSO_4$. It can be said that they do not arise from aluminum sulfate or from aqueous sulfate, and that they are consistent with ammonium sulfate. One of the other benefits of alum addition noted

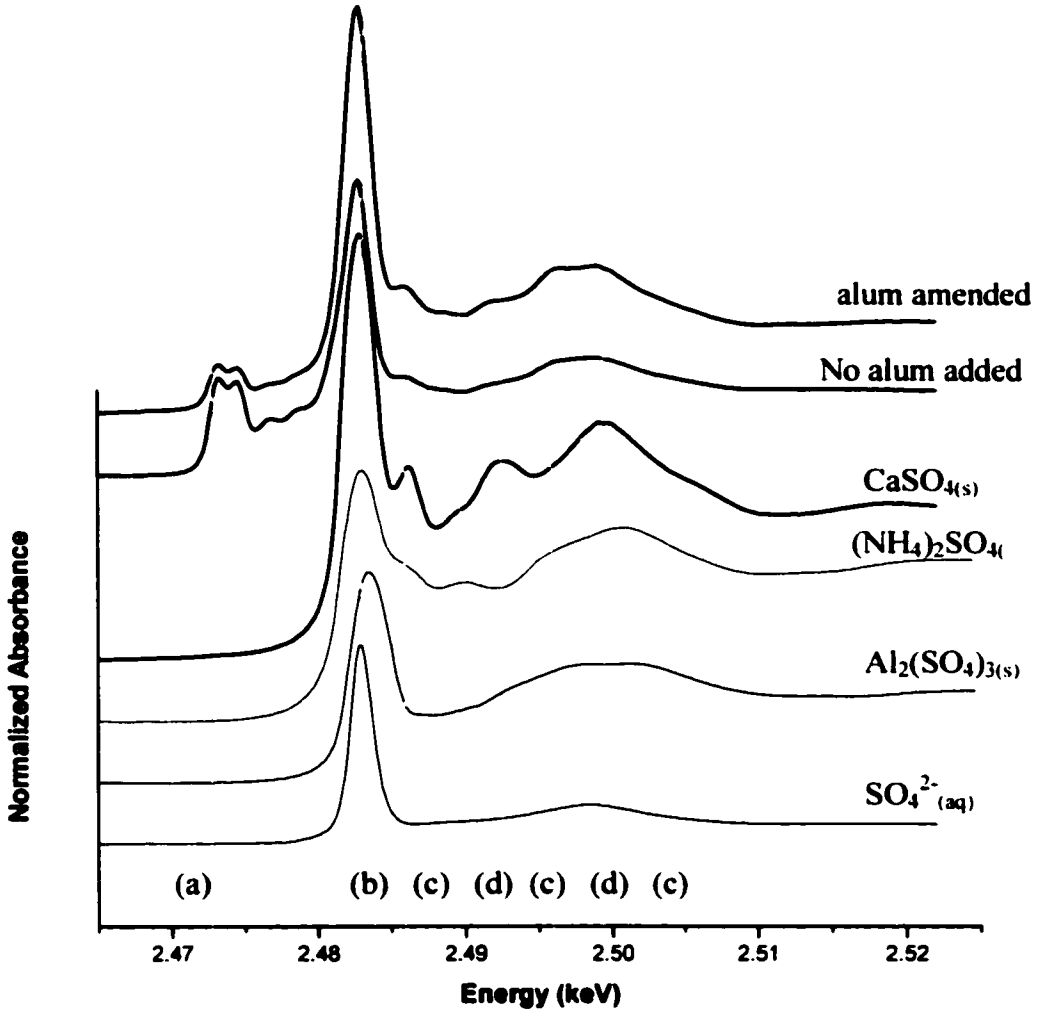

Figure 5.8. S K-edge XANES spectra of poultry litter samples with and without alum amendments compared to various sulfate references. The dashed lines indicate different spectral features of importance, and are labeled as follows: (a) absorption edge (white line energy) for S(0) (b)) absorption edge (white line energy) for S(VI) (c) unique spectral features of calcium sulfate seen in samples and references (d) spectral features consistent with ammonium sulfate seen in samples and references

by researchers is a reduction in ammonia emissions from the litter. Formation of ammonium sulfate solid phases has been proposed as an explanation for this decrease in volatile ammonia, and the XANES spectra are consistent with this hypothesis.

When the P, Ca, and S XANES results are considered together, then the overall speciation of mineral phases in poultry litter becomes much clearer. The overall reactions consistent with the XANES spectroscopy are summarized in Figure 5.9. Initially, chickens are fed a diet of grain supplemented with calcium phosphate because the digestive tract of chickens is unable to extract sufficient phosphorous from phytic acid. Once the dietary calcium phosphate is inside the chicken's gastrointestinal tract, pH becomes acidic and some of the calcium phosphate dissociates to Ca^{2+} and aqueous phosphate. These ions may associate with organic materials or remain dissolved in solution. This organic matrix high in calcium and both inorganic and organic phosphate (primarily phytic acid) is then excreted as waste. The waste ages over time in the house as the chickens are raised, with continuous addition of fresh waste and mixing from movement of the birds. In the control houses, calcium and inorganic phosphate react to form dicalcium phosphates. Transformation to more stable hydroxylapatite phases is retarded by the large amount of high molecular weight organic material in the litter. Aluminum sulfate (alum) addition produces an amorphous aluminum hydroxide and aqueous sulfate. Sulfate reacts with calcium to form calcium sulfate, and the inorganic phosphate then reacts

a) Unamended Poultry Houses

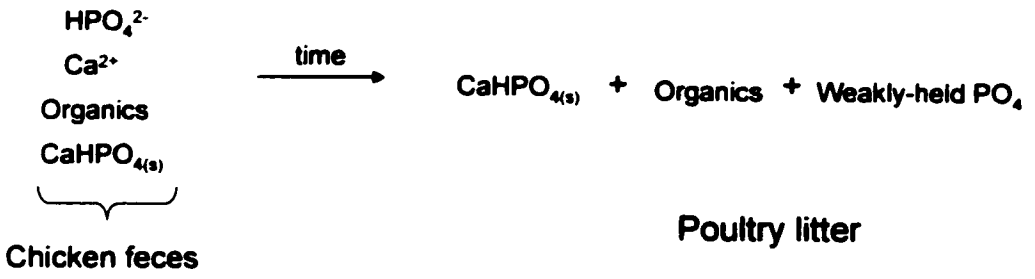

b) Alum-amended Poultry Houses

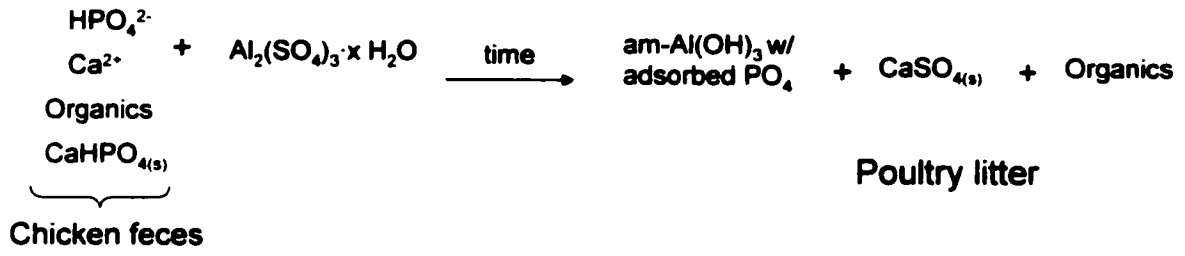

Figure 5.9. Summary of the reactions proposed to explain the P, Ca, and S XANES results. Figure 5.9a contains reactions important in the control houses, while 5.9b shows how addition of alum affects speciation.

with aluminum hydroxides via adsorption. No evidence of aluminum phosphate solid phases was seen with XANES spectroscopy.

Conclusions

The results of this XANES spectroscopic study demonstrate that phosphate chemistry in unamended poultry litter is dominated by dicalcium phosphate dihydrate chemistry, and by adsorption onto aluminum hydroxides in alum-amended litters. This means that the environmental fate of phosphate in alum-amended litter is determined primarily by the stability of phosphate adsorption complexes on aluminum hydroxides. Accordingly, there are many unanswered questions about phosphate chemistry in soils amended with poultry litter. Further research is needed to understand the long term dynamics of phosphate desorption from alum-amended litter after it has been applied to soils. It is not known whether adsorbed phosphate will slowly convert to aluminum phosphate solid phases after incorporation in soils, or if the slow crystallization of amorphous aluminum hydroxides will result in a lowered surface area and phosphate release. Environmental effects such as mineralization of the litter and wetting/drying cycles of the sun may also affect phosphate stability, but are not understood at this time. More controlled laboratory experiments where reaction variables such as pH, water content, Al:P ratio, and time are controlled should be conducted to provide insight into how management practices such as multiple small applications of alum and more rigorous pH controls may affect phosphate solubility. Fundamental studies

on the comparative kinetics of aluminum phosphate and aluminum hydroxide precipitation in the presence of organic matter are also needed.

OVERALL CONCLUSIONS

Molecular-scale spectroscopic studies can provide detailed information about reactions of oxyanions in the soil environment. However, instead of producing a simplified and general description of soil chemical processes, it is apparent that sorption processes at the mineral-water interface are quite complex. However, the research in this dissertation provides a wealth of useful information regarding specific sorption reactions of sulfate, selenate, boric acid, and phosphate on common soil components.

Sulfate and selenate react similarly with iron oxides and hydroxides. This is not unexpected, since both S and Se are Group VI metals, and the hydrated radius and acidity constants of sulfate and selenate are similar as well. To study sulfate adsorption on iron oxides, Attenuated Total Reflectance Fourier Transform Infrared (ATR-FTIR) spectroscopy was employed, and selenate adsorption reactions with iron oxides was monitored with both ATR-FTIR and Extended X-ray Absorption Fine Structure (EXAFS) spectroscopy. The types of surface complexes that sulfate and selenate form is dependent upon pH (pH 3.5-pH 8.0 were studied), ionic strength (0.005M-1.0M were studied), equilibrium solution concentrations (5 μM- 1mM were studied), and iron oxide sorbent (hematite, goethite, and amorphous iron oxide were studied). Sulfate and selenate react to form inner-sphere monodentate surface complexes on hematite over all pH and ionic strength. On goethite, however, sulfate and selenate form outer-sphere surface complexes at pH 6.0 and above, and a mixture of outer- and inner-sphere surface complexes between pH 3.5 and 6. The relative amount of outer-sphere to inner-sphere adsorption is affected by pH, ionic strength and

equilibrium concentration of oxyanion in solution. Inner-sphere complexation is favored by lowering pH, increasing ionic strength, and by increasing the solution concentration of sulfate or selenate. Sulfate and selenate adsorption reactions on amorphous iron hydroxides are similar to those on goethite. However, far more outer-sphere complexation is observed on amorphous iron oxides and inner-sphere complexation is of relatively minor importance.

In another research project, boric acid adsorption on amorphous iron oxide was studied using ATR-FTIR spectroscopy. Boric acid adsorption on amorphous iron hydroxides is primarily dependent upon pH. At pH 6.5, some outer-sphere boric acid is observed. This is not typically predicted with electrostatic models because boric acid is a neutral molecule. However, boric acid is a Lewis acid, and so the B metal center may attract some electron density from O atoms of the iron oxide surface hydroxyls. In addition to outer-sphere boric acid, boric acid also adsorbs via ligand exchange to form inner-sphere surface complexes. At pH 6.5, the majority of inner-sphere complexes remain trigonal, but some tetrahedral boric acid complexes are also observed. At pH 9.3 and 10.4, outer-sphere complexation is no longer observed, but trigonal and tetrahedral inner-sphere complexes are both present at the surface. As pH increases from pH 6.5 to 10.4, tetrahedral boron at the iron oxide surface increases dramatically. When the results are considered as a whole, it is reasonable to conclude that the trigonal boric acid is the primary adsorbate, and that it forms either trigonal or tetrahedral inner-sphere complexes at the surface of amorphous iron hydroxide. These reactions lead to a speciation at the surface that is very different than in solution: tetrahedral borate is

not found in solution at pH 6.5, and trigonal boric acid is a minor component in solution at pH 10.5.

The above studies were all conducted with model components and a single oxyanion in suspensions with sodium chloride as an electrolyte. In natural systems, many other ions such as metals, other oxyanions, organic ligands are present that may interact with oxyanions at the mineral/water interface. It has previously been determined with spectroscopic studies that lead and sulfate form ternary complexes on the goethite surface, but the stability and importance of these ternary complexes has not been investigated. The effects that sulfate has on lead adsorption and desorption on goethite was studied to better understand how oxyanion chemistry may affect metal reactivity in natural systems. The overall findings were that ternary complex formation between lead and sulfate can significantly change the amount, rate, and stability of lead adsorption onto an iron oxide surface. It was found that the presence of sulfate increases the extent of lead adsorption by approximately 20% between pH 4 and 6. Additionally, it was found that the order of sulfate addition also affected the rate and extent of lead adsorption at pH 4.5, with simultaneous addition of lead and sulfate resulting in slower adsorption kinetics but a greater amount of lead adsorption. When lead was added after goethite reacted with sulfate at pH 4.5, the kinetics were far more rapid but less lead was adsorbed. When kinetics experiments were repeated at pH 5.5, addition order of sulfate had only a minor effect on the rate of adsorption but no effect on the amount of lead that ultimately adsorbed. This can be explained by competition for a limited number of Fe-OH surface sites at pH 4.5 between inner-sphere sulfate and lead, which is alleviated by an increase in the amount of available adsorption sites

for lead and a decrease in the amount of inner-sphere sulfate at the surface as pH is raised to 5.5. Desorption studies provided important insight into the stability of lead that adsorbs in the presence of sulfate. When sulfate remains in the soil solution, the additional lead is retained by the goethite surface, but if desorption removes lead and sulfate from solution then lead adsorbed in the presence of sulfate is very labile.

My dissertation research primarily utilized pure systems in the laboratory to better control reaction conditions. Important reaction variables (pH, ionic strength, reactant concentration) were systematically varied to understand how they affect adsorption mechanisms. This physico-chemical approach to fundamental research allows one to develop a clear understanding of the often complex reactions of oxyanions at mineral surfaces. However, understanding the chemistry of oxyanions in natural systems is one of the ultimate goals of fundamental research, and many reactions in the field scale are not tightly controlled. Molecular scale studies in such cases are often used to perform speciation of natural systems and determine the phases that control oxyanion availability and toxicity. One such example of this is the chemistry of phosphate in poultry litter, and how speciation of phosphate is affected by the addition of aluminum sulfate.

X-ray Absorption Near Edge Structure (XANES) spectroscopy at the P, S, and Ca K-edge was employed to directly speciate poultry litter samples with and without alum additions. It was learned that in unamended poultry litter samples, phosphate is present as dicalcium phosphate organic phosphates, and weakly bound phosphate. Calcium is present as both weakly bound and dicalcium phosphate, and sulfur is

present as reduced organic sulfur as well as some calcium sulfate. When alum is added to the litter, phosphate is present as organic phosphate and phosphate sorbed onto aluminum hydroxides, while calcium is present primarily as calcium sulfate. Sulfur is present as reduced organic sulfur, calcium sulfate, and a small amount of ammonium sulfate. These results suggest that since phosphate sorbed on aluminum hydroxides is the dominant phase, and adsorbed phosphate remains fairly labile, then treatment of alum may not be a permanent solution for lowering phosphate levels in areas where litter is applied to soils.

When one compares the results from sulfate, selenate, boric acid, and phosphate studies, it is clear that it is impossible to make sweeping generalizations about oxyanion reactivity. Much like transition metal chemistry, steric hindrances, molecule size, electronegativity, Lewis acidity, and other chemical properties affect the surface chemistry of oxyanions substantially. However, there are some recurring trends and themes in my research that bear discussion. First and most importantly, reactions typically involve a continuum of co-occurring surface complexes. Outer-sphere and inner-sphere complexation often occur simultaneously, and more than one inner-sphere complex sometimes occur together. Changes in the relative importance of different surface complexes occur as reaction variables such as pH, ionic strength, and concentration are changed. Therefore, to adequately characterize oxyanion reactivity with molecular-scale techniques, it is necessarily to conduct studies with a wide range of reaction conditions. This physico-chemical approach to spectroscopic studies will produce a far clearer picture of how oxyanions will react under ever-changing conditions in the natural world.

When moving from binary systems to more complicated systems such as ternary metal-oxyanion complexation and speciation of oxyanions in natural samples, the importance of conducting complementary spectroscopic studies for different elements of interest cannot be stressed enough. Lead EXAFS combined with sulfate FTIR studies proved capable of detecting relatively subtle changes in complexation mechanisms, and then carefully designed macroscopic studies (adsorption kinetics and desorption studies) could determine the actual importance of molecular scale changes to the availability of lead. In the case of speciation of poultry litter, conducting XANES at multiple edges (P, S, and Ca) allowed much greater detail about the chemistry of alum amendments to be determined. The overall confidence in the speciation was considerably improved by probing the system from the standpoints of multiple elements. As the questions that soil chemists probe with spectroscopy become more complex, such a multi-faceted approach will become increasingly necessary.

Research often raises many new questions as it resolves old ones, and my dissertation research is no different. While sulfate, selenate, and boric acid reactions with iron oxides are well-characterized in chapters 1-3, it is not known how the presence of competing ligands and anions might affect the continuum of outer- and inner-sphere complexes that occur in binary systems. Carbonate is of special interest, as it is ubiquitous in soils, and may substantially change surface charge and compete with oxyanions for complexation sites. Ternary adsorption reactions of lead and sulfate were studied in chapter 4, but the studies were limited to pH and concentrations where only adsorption occurs. Future research that considered precipitation reactions and the

effects of competition between adsorption and precipitation on lead adsorption kinetics would be of great interest. Another interesting project that remains to be done is modeling ternary complex formation at the goethite surface using the data from Chapter 4.

The study of phosphate speciation in poultry litter is a complicated and contentious research topic, and there are many research questions that remain. Since it was observed that phosphate adsorption on aluminum oxides is the primary reason for a decrease in water soluble phosphate in the presence of alum, it is important to fully understand aluminum hydroxide/phosphate chemistry. Long term aging and desorption studies of phosphate adsorbed on amorphous aluminum hydroxides would provide vital information to soil scientists interested in the long term stability of this alum-amended litter. Such studies would need to address the effects of organic material, both high molecular weight and dissolved organic acids. Another important question is how the stability of aluminum hydroxides and the phosphate adsorbed onto them will be affected by microbial degradation of litter material.

REFERENCES

Ahlrichs, J.S. and Hossner, L.R. *J. Environ. Qual.* **1987**, *16 (2):* 95-98.

Ainsworth, C.C., Pilon, J.L., Gassman, P.L., and van der Sluys, W.G. "Cobalt, cadmium, and lead sorption to hydrous ferric oxide: residence time effect." *Soil Sci. Soc. Am. J.* **1994,** *58*:1615.

Ali, M. A. and D. A. Dzombak. "Competitive sorption of simple organic acids and sulfate on goethite." *Environ. Sci. Technol.* **1996a**, *30*(4): 1061-1071.

Ali, M.A. and Dzombak, D.A. *Geochim. Cosmochim. Acta.* **1996b**, *60*:5045

Alvarez, R. and D. L. Sparks "Polymerization of silicate anions in solutions at low concentrations." *Nature* **1985**, *318*: 649-651.

Arai, Y.A. and Sparks, D.L. *J. Colloid Interface Sci.* **2001**, *241*, 317.

Arai Y.A., Elzinga E.J., and Sparks D.L. *J. Colloid Interface Sci.* **2001**, *235*, 80-88.

Bar-Yosef, B. and Meek, D. *Soil Science.* **1987**, *144 (1):* 11-19.

Bargar, J.R., Towle, S.N., Brown, G.E. Jr., and Parks, G.A. Geochim. Cosmochim. Acta. **1996**, 60, 3541-3547.

Bargar, J.R., Brown, G.E. Jr., and Parks, G.A. *Geochim. Cosmochim. Acta.* **1997a**, 61, 2617.

Bargar J.R., Brown Jr. G.E. Parks G.A. *Geochim. Cosmochim. Acta* **1997b,** *61*, 2639-2652.

Bargar J.R., Persson, P., and Brown Jr. G.E. *J. Phys. IV* **1997c,** *7*, 825-826.

Bargar J.R., Brown Jr. G.E. Parks G.A. *Geochim. Cosmochim. Acta* **1998**, *62*, 193-207.

Benjamin, M.M. and Leckie, J.O. *Environ. Sci. Technol.* **1981**, *15*: 1050-1057.

Benjamin, M.M. and Leckie, J.O. *Environ. Sci. Technol.* **1981**, *16*: 162-170.

Beyrouty, C. A., G. E. v. Scoyoc, et al. "Evidence supporting specific adsorption of boron on synthetic aluminum hydroxides." *Soil Sci. Soc. Am. J.* **1984**, *48*: 284-287.

Bigham, J. M., Schwertmann, U., Carlson, L., Murad, E. *Geochim. Cosmochim. Acta* **1990**, *54*, 2743.

Boyle-Wright, E.J., Katz, L.E., and Hayes, K.F. *Environ. Sci. Technol.* **2002a**, *36*, 1212

Boyle-Wright, E.J., Katz, L.E., and Hayes, K.F. *Environ. Sci. Technol.* **2002b** , *36*, 1219.

Bunzl, K., Schmidt, W., and Sansoni, B. "Kinetics of ion exchange in soil organic matter IV. Adsorption and desorption of Pb^{2+}, Cu^{2+}, Cd^{2+}, Zn^{2+}, and Ca^{2+} by peat. *J. Soil Sci.* **1976**, *27*, 32-41.

Charlet, L., N. Dise, and W. Stumm. "Sulfate adsorption on a variable charge soil and on reference minerals." *Agriculture, Ecosystems, and Environment* **1993**, *47*: 87-102.

Cotton, F. A. and G. Wilkinson. **Advanced Inorganic Chemistry**. New York, John Wiley and Sons. **1980.**

Criscenti L. J. & Sverjensky, D. A. "The role of electrolyte anions in divalent metal adsorption on oxide and hydroxide surfaces in salt solutions." *Am. J. Science* . **1999**, *299*: 828-899.

Davis, J. A. and J. O. Leckie. "Surface ionization and complexation at the oxide/water interface. 3. Adsorption of anions." *J. Colloid Interface Sci.* **1980**, *74*: 32-43.

Degenhardt, J. and A. J. McQuillan. "*In situ* ATR-FTIR spectroscopic study of adsorption of perchlorate, sulfate, and thiosulfate ions onto chromium(III) oxide hydroxide thin films." *Langmuir* **1999**, *15*: 4595-4602.

Eggleston, C. M., S. Hug, W. Stumm, B. Sulzberger, M. Dos Santos Alfonso. "Surface Complexation of Sulfate by Hematite Surfaces: FTIR and STM Observations." *Geochim. Cosmochim. Acta* **1998**, *62*(4): 585-593.

Eick, M.J., J.D. Peak, P.V. Brady, and J.D. Pesek. "Kinetics of lead adsorption/desorption on goethite: Residence time effects." *Soil Science.* **1998**, *164*: (1) 28-39.

Elzinga, E. J. and D. L. Sparks. "Reaction condition effects on nickel sorption mechanisms in illite-water suspensions." *Soil Sci. Soc. Am. J.* **2000**, *65*:94-101..

Elzinga E.J., Peak D., and Sparks D.L. "Spectroscopic studies of Pb(II)-sulfate interactions at the goethite-water interface." *Geochim. Cosmochim. Acta* **2001**, *65*, 2219-2230.

Ertl D.S., Young, K.A., and Raboy, V. *J. Environ. Qual.* **1998**, *27(2)*, 299.

Faith S.A. and Miller C.A. *Vet. Hum. Toxicol.* **2000**. *42 (1)*, 26-29

Fendorf, S.E. and Sparks, D.L. in **Methods of Soil Analysis: Part 3, Chemical Methods.** D.L. Sparks, A.L. Page, P.A. Helmke, R.H.Loeppert, P.N. Soltanpour, M.A. Tabatabai, C.T. Johnson, and M.E. Sumner (eds.). Soil Science Society of America, Madison WI. **1996.**

Geelhoed, J. S., T. Hiemstra, W.H. van Riemsdijk. *Geochim. Cosmochim. Acta* **1997**, *61*, 2389-2396.

Goldberg, S., H. S. Forster, et al. *Soil Sci. Soc. Am. J.* . **1993**, *57*: 704-708.

Goldberg S. and Johnston C.T. *J. Colloid Interface Sci.* **2001**, *234*, 204-216.

Grossl, P.R. and Inskeep, W.P. *Soil Sci. Soc. Am. J.*, **1991**, *55*, 670.

Grossl, P.R. and Inskeep, W.P. *Geochim. Cosmochim. Acta*, **1992**, *56*, 1955.

Harrison J.B. and V.E. Berkheiser. *Clays Clay Miner.* **1982**, *30*: 97-102.

Harter, R.D. *In* **Rates of soil chemical processes** ; D.L. Sparks and D.L. Suarez (ed.) Soil Science Society of America : Madison, WI, **1991**; volume 27 pp 135-149

Hayes, K.F. and Leckie, J.O. *In* **Geochemical processes at mineral surfaces** ; J.A. Davis and K.F. Hayes (ed.) American Chemical Society, Washington, D.C. **1986** ; vol 323.

Hayes, K. F., Roe A. L., Brown G.E., Hodgen K.O., Leckie J.O., and Parks G.A. *Science* **1987**, *238*: 783-786.

He, L. M., L. W. Zelazny, V. C. Baligar, K.D. Ritchey, and D.C. Martens. "Hydroxyl-sulfate exchange stoichiometry on γ-Al_2O_3 and kaolinite." *Soil Sci. Soc. Am. J* **1996**, *60*: 442-452.

He, L. M., L. W. Zelazny, V. C. Baligar, K.D. Ritchey, and D.C. Martens. "Ionic strength effects on sulfate and phosphate adsorption on γ - alumina and kaolinite: Triple layer model." *Soil Sci. Soc. Am. J* **1997**, *61*: 784-793.

Hodges, S. C. and G. C. Johnson. "Kinetics of sulfate adsorption and desorption by Cecil soil using miscible displacement." *Soil Sci. Soc. Am. J.* **1987**, *51*: 323-331.

Huff, W.E., Moore, P.A., Waldroup, P.W., Waldroup, A.L., Balog, J.M., Huff, G.R., Rath, N.C., Daniel, T.C., and Raboy, V. *Poultry Sci.* **1998,** *77(12)*, 1899.

Hug, S. J. "*In Situ* Fourier Transfom Infrared measurements of sulfate adsorption on hematite in aqueous solutions." *J. Coll. Interface Sci.* **1997**, *188*: 415-422.

Inskeep, W.P. and Silvertooth, J.C. *Soil Sci. Soc. Am. J.*, **1988**, *52*, 941.

Johnston, C.T.; and Sposito, G. Disorder and early sorrow. Progress in the chemical speciation of the soil solution. p. 89-100. *In* Future developments in soil science research, L.L. Boersma (ed.), Soil Sci. Soc. of Am. Publications, Madison, WI., **1987.**

Keren, R. and G. A. O'Conner. "Effect of exchangeable ions and ionic strength on boron adsorption by montmorillonite and illite." *Clays Clay Miner.* **1982**, *30*: 341-346.

Keren, R. and F. T. Bigham . Boron in water, soils, and plants. **Advances in Soil Science**. New York, Springer-Verlag, Inc. **1985**.

Keren, R. and D. L. Sparks. "Effect of pH and ionic strength on boron adsorption by pyrophyllite." *Soil Sci. Soc. Am. J.* **1994**, *58*: 1095-1100.

Lindsey, W.L. Chemical Equilibria in Soils. John Wiley and Sons, New York; **1979**.

Manceau, A. and Charlet L. *J. Colloid Interface Sci.* **1994**, *168*: 87-93.

Manceau, A., Bosset, M.-C., Sarret, G., Hazemann, J.-L., Mench, M., Cambier, P., and Prost, R. (1996). "Direct determination of lead speciation in contaminated soils by EXAFS spectroscopy." *Environ. Sci. Technol.* **30**(5), 1540.

Moore, P.A. Jr. and Miller, D.M. *J. Environ. Qual.* **1994**, *23*, 325.

Nakamoto, K., **Infrared and Raman Spectra of Inorganic and Coordination Compounds**. John Wiley and Sons, New York, **1986**.

Neal, R.H. and Sposito, G.S. *Soil Sci. Soc. Am. J.* **1989**, *53*: 70-74.

Ostergren, J.D., Trainor, T.P., Bargar, J.R., Brown, G.E. Jr., Parks, G.A. *J. Colloid Interface Sci.* **2000a**, *225*,466.

Ostergren, J.D., Brown, G.E. Jr., Parks, G.A., Persson, P. *J. Colloid Interface Sci.* **2000b**, *225*, 483.

Parfitt, R. L. and R. S. C. Smart. "Mechanism of sulfate adsorption on iron oxides." *Soil Sci. Soc. Am. J.* **1978**, *42*(1): 48-50.

Parfitt, R.L. *Advances in Agronomy*. **1978**, *30*, 1.

Peak, D., R. G. Ford, and D.L. Sparks.. "An *in situ* ATR-FTR investigation of sulfate bonding mechanisms on goethite." *J. Colloid Interface Sci.* **1999**, *218*: 289-299.

Peak D., Elzinga E.J., and Sparks D.L in **Heavy Metals Release in Soils**, H.M. Selim and D.L. Sparks, eds. Lewis Publishers New York, NY. **2001**

Perrson, P., P. Nordin, J. Rosenqvist, L. Lövgren, L. Öhman, and S. Sjöberg.. "Comparison of the adsorption of *o*-phthalate on boehmite, aged γ-Al_2O_3, and goethite." *J Colloid Interface Sci.* **1998**, *206*: 252-266.

Persson, P. and L. Lovgren. "Potentiometric and spectroscopic studies of sulfate complexation at the goethite-water interface." *Geochim. Cosmochim. Acta* **1996**, *60*(15): 2789-2800.

Ridley, M.K., D.J. Wesolowski, D.A. Palmer, P. Benezeth, and R.M. Kettler. "Effect of sulfate on the release rate of Al^{3+} from gibbsite in low-temperature acidic waters." *Environ. Sci. Technol.* **1997**, *31*: 1922-1925.

Rietra, R. P. J. J., T. Hiemstra, W.H. van Riemsdijk.. "Sulfate adsorption on goethite." *J. Colloid Interface Sci.* **1999, *218***: 511-521.

Rose J, Flank AM, Masion A, Bottero JY, Elmerich P. *Langmuir*. **1997**, *13: (6)* 1827

Ross, S.D. "Chapter 11: Borates" in **The Infrared Spectra of Minerals**, V.C. Farmer ed. Mineralogical Society, London England. **1974.**

Schwertmann, U., P. Cambier, and E. Murad. "Properties of goethites of varying crystallinity." *Clays and Clay Minerals* **1985**, *33*(5): 369-378.

Schwertmann, U. and R. M. Cornell. Iron Oxides in the Laboratory; Preparation and Characterization. New York, NY, Weinheim. **1991**

Sharpley, A.N., Chapra, S.C., Wedopohl, R., Sims, J.T., Daniel, T.C., and Reddy, K.R. *J. Environ. Qual.* **1994**, *23*, 437

Shreve, B.R., Moore, P.A., Daniel, T.C., Edwards, D.R., and Miller, D.M. *J. Environ. Qual.* **1995**, *24*, 106.

Shriver, D. F., Atkins P.A., Langford C.H. **Inorganic Chemistry**. W.H. Freeman and Company. New York,N.Y. **1994.**

Sims, J.T. and Wolf D.C. *Adv. Agron.* **1994**, *52*, 1.

Sims, J.T. (in J. Rechigl (ed.) *Uses of by-products and wastes in agriculture*; Am. Chem. Soc., Washington D.C. 72. **1997**

Sims JT, Simard RR, Joern BC. *J Environ. Qual.* **1998**, *27 (2)*, 277.

Sparks, D. L. **Environmental Soil Chemistry**. San Diego CA, Academic Press. **1995**

Sposito, G. A. **The Surface Chemistry of Soils**. New York, Oxford University Press. **1984**

Strawn, D.G., Sheidegger, A.M., and Sparks, D.L. *Environ. Sci. Technol.* **1998**, *32*, 2596.

Strawn, D.G. and Sparks, D.L. "The use of XAFS to distinguish between inner- and outer-sphere lead adsorption complexes on montmorillonite." *J. Colloid Interface Sci.* **1999**, *2216*: 257-269.

Strawn, D.G. and Sparks, D.L. "Effects of soil organic matter on the kinetics and mechanisms of Pb(II) sorption and desorption in soil." *Soil Sci. Soc. Am. J.* **2000**, *64*, 144.

Stumm, W. and J. J. Morgan. **Aquatic Chemistry**. New York, John Wiley and Sons. **1996**

Su, C. and D. L. Suarez. "Coordination of adsorbed boron: A FTIR spectroscopic study." *Environ. Sci. Technol.* **1995**, *29*: 302-311.

Su, C. and D. L. Suarez. "Boron sorption and release by allophane." *Soil Sci. Soc. Am. J.* **1997**, *61*: 69-77.

Su, C. and D.L. Suarez. *Soil Sci. Soc. Am. J.* **2000**, *64*: 101-111.

Suarez, D. L., S. Goldberg, and Su, C.. "Evaluation of oxyanion adsorption mechanisms on oxides using FTIR spectroscopy and electrophoretic mobility." In **Mineral-Water Interfacial Reactions: Kinetics and Mechanisms**. D. L. Sparks and T. J. Grundl. New York, Oxford University Press. **1998**

Sugimoto, T. and Y. Wang. "Mechanism of the shape and structure control of monodispersed a-$Fe2O_3$ particles by sulfate ions." *J. Colloid Interface Sci.* **1998**, *207*(1): 137-149.

Tejedor-Tejedor, M.I. and Anderson, M.A., *Langmuir* **1990**, *6*, 602

Turner, I. J. and J. R. Kramer. "Sulfate ion bonding on goethite and hematite." *Soil Science* **1991**, *152*(3): 227-230.

Vadas, P.A. and Sims, J.T. *J. Environ. Qual.* **1999**, *28 (6)*, 1870.

Venema, P., T. Hiemstra, Peter Weidler, and W.H. van Riemsdijk.. "Intrinsic Proton Affinity of Reactive Surface Groups of Metal (Hydr)oxides: Application to Iron (Hydr)oxides." *J. Colloid Interface Sci.* ***1998***, *198*(2): 282-295.

Waychunas, G.A., N. Xu, C.C. Fuller, J.A. Davis, J.M. Bigham. *Physica B* **1995**, *208&209*, 481-483.

Wijnja, H. and C.P. Schulthess. "Vibrational spectroscopy study of selenate and sulfate adsorption mechanisms on Fe and Al (hydr)oxide surfaces." *J. Colloid Interface Sci.* **2000**, *229*: 286-297.

Yamaguchi, N. U., M. Okazaki, and T. Hashitani. (1999). "Volume changes due to SO_4^{2-}, SeO_4^{2-}, and $H_2PO_4^-$ adsorption on amorphous iron (III) hydroxide in an aqueous suspension." *J. Colloid Interface Sci.* **209**: 386-391.

Yasunaga, T. and Ikeda, T.. "Adsorption-desorption kinetics at the metal oxide-solution interface as studied by relaxation kinetics." In J.A. Davis and K.F. Hayes (ed.) Geochemical processes at mineral surfaces. Vol 323. American Chemical Society, Washington, D.C. **1986**

Yates, D. E. and T. N. Healy (1975). "Mechanism of anion adsorption at the ferric and chromic oxide/water interfaces." *J. Colloid Interface Sci.* **52**: 222-228.

Zabinsky, S.I., J.J. Rehr, A. Ankudinov, R.C. Albers and M.J. Eller, "Multiple Scattering Calculations of X-ray Absorption Spectra", *Phys. Rev. B.* **1995**, *52*, 2995.

Zhang, P. C. and D. L. Sparks. "Kinetics and mechanisms of sulfate adsorption/desorption on goethite using pressure-jump relaxation." *Soil Sci. Soc. Am. J.* **1990a** *54*: 1266-1273.

Zhang, P. C. and Sparks D. L.. *Environ. Sci. Technol.* **1990**, *24*: 1848-1856.

Zhou, J.M., Liu, C., and Huang, P.M. "Perturbation of Taranakite Formation by Ferrous and Ferric Iron under Acidic Conditions" *Soil Sci. Soc. Am. J.* **2000**, *64*, 885-892.